UNIVERSITY OF OKLAHOMA

GRADUATE COLLEGE

THE UNCOUPLED SURFACE LAYER AT THE CROSSTIMBER MICRONET

A Dissertation

SUBMITTED TO THE GRADUATE FACULTY

in partial fulfillment of the requirements for the

degree of

Doctor of Philosophy

By

Matthew James Haugland
Norman, Oklahoma
2006

THE UNCOUPLED SURFACE LAYER AT THE CROSSTIMBER MICRONET

A DISSERTATION APPROVED FOR THE

SCHOOL OF METEOROLOGY

BY

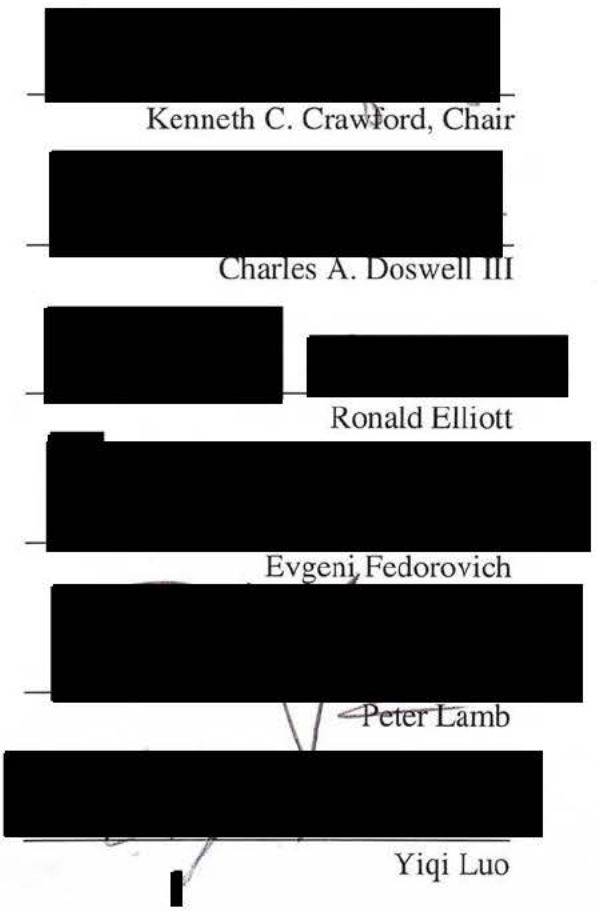

Acknowledgements

This work was funded by a graduate fellowship from the National Science foundation. Funding for the Crosstimber Micronet was provided by a graduate fellowship from the American Meteorological Society, sponsored by NASA's Earth Science Enterprise. Additional support for the Micronet was provided by the University of Oklahoma, Oklahoma Climatological Survey, and WeatherPages.com.

Very special thanks are due Ken Crawford, my advisor and committee chair. This work would not have been possible without his generous help. He has been a great role model to me both as a scientist and as a person. He taught me much of what I know about meteorology, was instrumental in making the Crosstimber Micronet a reality, and has greatly improved this dissertation in many ways. I cannot thank Dr. Crawford enough for his mentorship and friendship over the past 5 years. [I'll even forgive him for being a Texas Longhorns fan, and congratulate his football team for slipping past OU and winning the national championship this year.]

Special thanks also are due my Ph.D. committee: Chuck Doswell, Ron Elliott, Evgeni Fedorovich, Pete Lamb, and Yiqi Luo. Specifically, I thank Dr. Doswell for his excellent advice and challenging, thought-provoking discussions. He has helped me to be more rounded as a scientist and to think beyond this dissertation. And now that I look back, I forgive and even thank him for persuading me to take AME 5803 and MATH 5163. Dr. Elliott helped me see the important need for applications of my research, especially outside the field of meteorology. Many of the applied aspects (and, in my opinion, strongest points) of this dissertation were inspired by his suggestions.

I thank Dr. Fedorovich for teaching me most of what I know about the planetary boundary layer. He helped me see the wisdom of not making bold claims without first investigating what others in the field have found. His suggestions (which focused on the physics that underpin this work) have greatly improved this dissertation. Dr. Lamb helped me understand the 'big picture' and how to maximize the contribution of my research to the field of meteorology. His suggestions helped me focus more on the major concepts of this work, which has improved the coherence of this dissertation. I thank Dr. Luo for teaching me about the role of plants in this study and for teaching me almost everything I know about CO_2, which became an important part of the physical arguments in this dissertation. His suggestions from a non-meteorologist perspective have improved the readability and applicability of this work to other fields.

Several others made this dissertation possible by their help with the Crosstimber Micronet. Many thanks are due the staff of the Oklahoma Climatological Survey, especially David Grimsley. The Micronet would not exist in present form without David's help. He acquired and installed most of the instruments at the Micronet, and taught me almost everything I know about its operation. I thank him for his generosity, hard work, and friendship.

Much help with the Micronet also was generously given by Megan Ferris. She assisted with installation and maintenance of sensors and helped tremendously in maintaining the Micronet during my 5 months in the UK. She also was a great friend and provided valuable encouragement throughout my years as a Ph.D. student.

Two of the towers used at the Micronet, as well as 5 sonic anemometers, were generously lent by Petra Klein. Assistance with installation of the towers was provided

(or attempted) by Evgeni Fedorovich, Petra Klein, Alan Shapiro, and my dad (Jim Haugland) and brothers (TJ and Torrey Haugland).

The building near CR14 which facilitated automated data collection was built by my dad (Jim Haugland) with help from my mom (Holly Haugland) and brothers (TJ and Torrey). Without it, data collection would have been very tedious, and would have been nearly impossible during my months in the UK. Observations from those months, which provided verification for the model forecasts, were perhaps the most important of this dissertation.

I thank those who help me receive the AMS and NSF fellowships that helped fund the Micronet and this work. They include (but are not limited to) Fred Carr, Ken Crawford, Chuck Doswell, Kelvin Droegemeier, and Jeff Kimpel.

I probably would still be an undergraduate without the help of the OU School of Meteorology staff, especially Celia Jones. I seem to have difficulties filling out forms and turning them in on time. But Celia has always come to my rescue whenever I was told that I couldn't enroll, couldn't graduate, or couldn't take the general exam. I thank her for her patience, diligence, and forgiveness.

Thanks are due Renee McPherson, who unknowingly contributed greatly to this dissertation. By making me believe I had less time to finish than I did, she helped me make rapid progress during the summer and fall, which gave me extra time to make major improvements to the USL model during the first months of 2006.

I thank the California Department of Water Resources for providing free, high quality data that were an important part of this work.

Thanks also are due my friends in the UK for encouraging me during development of the USL model, the most difficult and frustrating part of this work. I thank the Meteorology Department at the University of Reading, especially Stephen Belcher and Janet Barlow for their help with my research, and Ross Reynolds for facilitating my studies there. I also thank First Great Western Trains and Virgin Trains for providing a quiet, comfortable environment for working on much of this dissertation.

I also thank others who helped via discussions of the science that relates to this work. These include (but are not limited to) Jeff Basara, Jerry Brotzge, Claude Duchon, Howard Johnson, Hans Peter Schmid, and several National Weather Service SOOs from around the country who attended the COMET Planetary Boundary Layer Symposia.

Many thanks are due my friends at OU who have helped and encouraged me in more ways than I can mention. In particular, I thank Andy Taylor who gave me tremendous encouragement and helped materially by teaching me much of what I know about MOS and its limitations.

Most of all, I thank my parents Jim and Holly Haugland. It would double the length of this dissertation to mention half of the ways they have helped me throughout the years. Most of what I have done in my life, including this dissertation, would not have been possible without their love, support, example, and generosity.

Finally, I thank my God and Lord Jesus Christ, without whom this fascinating world would not exist, nor would I be here to study it.

Table of Contents

Abstract

One of the greatest challenges faced by weather forecasters is the large spatial variability of temperature that occurs at small scales, particularly on clear nights with light wind. The physical processes that create this variability were analyzed using 3 years of meteorological observations from the Crosstimber Micronet, an automated microscale surface observation network in central Oklahoma.

The observations revealed extreme microscale temperature gradients across the Micronet (i.e., > 10°C across less than 200 m of land). These gradients were shown to be created by the unique surface energy balance within a turbulence-free layer of air that sometimes develops near the ground. This layer is called the uncoupled surface layer (USL).

Based on the surface energy budget and parameterizations derived from observations of the USL at the Micronet, the Uncoupled Surface Layer forecast model (USL model) was developed to predict near-surface temperatures on clear nights. The USL model represents a new approach to temperature forecasting that, heretofore, has not been documented in the scientific literature.

Nine diverse locations across central Oklahoma, central California, and southern California were selected for verification of forecasts by the USL model on clear nights from June-December 2005. These forecasts were compared with concurrent forecasts by operational Model Output Statistics (MOS), a well-respected forecasting technique used operationally for decades.

Forecasts by the USL model were 0.5-4.1°C (21-72%) more accurate than those by MOS. The largest improvements over MOS were observed at the Crosstimber Micronet (72%) and Cuyama, California (67%). Both are located in sheltered valleys that are considered very favorable for development of the USL. The USL model also substantially outperformed MOS at locations that are considered less favorable for USL development (e.g., urban areas along the Pacific Coast).

The accuracy of the USL model confirms that the uncoupled surface layer is an important feature of the near-surface nocturnal boundary layer at a variety of locations. The results also suggest that the USL model could lead to significant improvements in nighttime temperature forecasting.

1. Introduction

Meteorological parameters near the earth's surface at night are difficult to predict accurately. One of the most challenging problems is the large spatial and temporal variability that exists at small scales, particularly on clear nights with light wind. In this paper, nighttime (i.e., between sunset and sunrise) meteorological conditions near the ground surface are analyzed using three years of observations from the Crosstimber Micronet, an automated microscale surface observation network in central Oklahoma. This analysis provides the foundation for a simple forecast model designed to improve temperature forecasts in wind-sheltered areas on clear nights.

It is estimated that over 40% of the U.S. economy is in some way sensitive to weather and climate (NRC 1998). Most of that sensitivity is to meteorological conditions near the ground. Approximately half is dependent on nighttime weather and climate.

One of the most sensitive industries to nighttime weather and climate, particularly the impact of radiational cooling on clear nights, is the citrus industry. During 1983, a severe freeze across central and northern Florida caused approximately two billion dollars in damage to Florida's citrus industry. In California's San Joaquin Valley, the freeze of 1998 caused approximately $700 million in damage to crops and an estimated $2 billion in indirect damage to the local economy.

The importance of nighttime temperature forecasts to the citrus industry is illustrated by the case of *Grossman v. Citrus Associates of the New York Cotton Exchange*. A trading advisor in the frozen concentrated orange juice market and his clients filed suit against a private weather forecasting firm for disseminating erroneous

forecasts of low temperatures for orange groves with intent to manipulate the market. The intent to manipulate the market could not be proven, but it was acknowledged that nighttime temperature forecasts play a crucial role in the market (Klein and Pielke 2002).

Frost can be detrimental to many other types of crops. Though steps can be taken to mitigate potential frost damage, they rely on accurate forecasts of the temperature during the night. If unexpected freezing temperatures occur, the crops may suffer unnecessary damage. If freezing temperatures are predicted but do not occur, unnecessary costs may be incurred.

Accurate forecasts of nighttime temperatures also are important in managing energy resources. Inaccurate forecasts lead to inaccurate estimates of future energy use, which can be very costly to the energy industry. Hobbs et al. (1999) estimated that a 1% reduction of forecast error could save a single utility up to $1.6 million annually.

According to Tribble (2003), temperature is the most important weather variable to energy load forecasting. Sharp increases in energy usage are observed during the morning when the temperature is lowest. Thus, an improvement in minimum temperature forecasts would play a key role in improving management of energy resources.

Radiation fog is a hazardous by-product of nighttime cooling. Approximately 700 highway deaths per year in America are related to fog, approximately 10 times the number of annual deaths from tornadoes (Whiffen et al. 2002). One of the most dangerous aspects of fog is that it forms under clear and otherwise benign meteorological conditions, when weather hazards generally are not expected. Improved prediction of nighttime temperatures, particularly in low-lying fog prone areas, would lead to better prediction of fog formation and could potentially help save lives.

The Crosstimber Micronet is a 5-acre outdoor laboratory designed for the study of microscale near-surface meteorological phenomena in an area of complex vegetation and terrain. It is ideally located in a sheltered, low-lying area where some of the most damaging conditions (i.e., freezing temperatures, heavy frost, and fog) and large microscale anomalies frequently are observed to occur.

The Micronet lies near the center of the Oklahoma Mesonet, a mesoscale network of 117 stations across the state of Oklahoma (Brock et al. 1995). In this study, observations from five sites within the Crosstimber Micronet are compared with those from five nearby Mesonet sites. On clear nights, differences in meteorological conditions between the Crosstimber Micronet and the five surrounding Mesonet sites can be substantial. They often are as large as synoptic scale variations across the southern plains.

One of the most striking anomalies occurs with observations of air temperature. The lowest sites above MSL at the Micronet often are 10°C cooler than the surrounding Mesonet sites. Even horizontal temperature differences across the 5-acre Micronet can be almost unbelievably large. At 1.5 meters above the ground, temperature differences of up to 10°C have been observed across a distance of less than 200 meters. Vertical temperature gradients also can be anomalously large at the Micronet (e.g., greater than 1°C per meter).

The purpose of paper is to document cool nighttime temperature anomalies that occur at the Micronet, analyze the physical processes that create the anomalies, and develop a model to predict nighttime temperatures at the Micronet. Based on the general understanding of the nighttime planetary boundary layer gained by analysis of Micronet

observations, the model will be extended to predict nighttime temperatures at other locations outside the Micronet.

The following propositions will be tested:

1) At the Crosstimber Micronet, a sub-layer that is uncoupled from the ambient nocturnal boundary layer develops near the ground on clear nights. This sub-layer is called the uncoupled surface layer (USL).

2) Nighttime temperature anomalies at the Micronet are created by the unique energy balance within the USL, a feature that generally does not develop at the surrounding Mesonet sites.

3) The presence and depth of the USL at the Micronet are determined by the wind speed across central Oklahoma.

4) The USL impacts other near-surface atmospheric parameters such as dewpoint and carbon dioxide concentration by trapping air near the ground.

5) A simple surface energy balance model, constructed to predict the presence, depth, and energy balance of the USL, can predict nighttime near-surface temperatures in sheltered areas (e.g., the Crosstimber Micronet) more accurately than operational model output statistics (MOS) forecasts interpolated to the Micronet's location.

The model, based on Micronet observations from 2004, will be tested and verified using an independent set of Micronet observations from June 2005-January 2006. Its forecasts of the nighttime temperature at 1.5 m above ground level will be compared with

MOS, a forecasting technique that has been used with considerable success for decades (Taylor and Leslie 2005). Adjustments will be made to the model to allow it to forecast for two other locations outside the Micronet: El Reno, Oklahoma and Madera, California. El Reno was chosen because it is another location in central Oklahoma where cool nighttime temperature anomalies are known to occur (Hunt et al. 2005). Madera was chosen for its low-lying location in the San Joaquin Valley, a region where fog and freeze damage to citrus crops are major problems. These forecasts also will be compared with MOS forecasts. Verification is provided by Mesonet and California Irrigation Management Information System (CIMIS; CIMIS 2005) observations at El Reno and Madera, respectively.

Chapter 2 of this manuscript will review the scientific literature that underpins this work. In Chapter 3, the data and analysis methodology are discussed. Observational data analysis results are presented in Chapter 4. A description of the model and modeling results are contained in chapters 5 and 6, respectively.

2. Scientific Background

2.1. Anomalous Nighttime Temperatures

Numerous recent studies have shown that low-lying areas experience anomalously cool temperatures on clear nights with light wind (Table 2.1). Most of these studies were based on observations from short-term field campaigns. They focused on the impact of mesoscale land features such as valleys and basins. However, relatively few studies have focused on small valleys (i.e., less than 1 km across; Wong et al. 1987).

Name	Location	Avg. Horiz. Resolution	Domain Size (km)	Terrain Range (m)	Nights studied
CASES-97, LeMone et al. (2003)	Kansas	11 km	30 x 55	150	30
Simonsen (2001)	Oklahoma	5 km	20 x 45	180	30
Acevedo and Fitzjarrald (2001)	New York	4 km	15 x 27	130	60
Laughlin and Kalma (1987, 1990)	Australia	2 km	11 x 11	300	24, 100
Gustavsson et al. (1998)	Sweden	0.6 km	22 x 0.2	75	16
CASES-99, Poulos et al. (2002)	Kansas	0.6 km	3 x 3	150	30
Elsner et al. (1996)	Florida	160 m	0.8 x 0.2	25	72
Clements et al. (2003)	Utah	150 m	1 x 0.5	150	5
This study	**Oklahoma**	**50 m**	**0.18 x 0.05**	**12 / 70***	**900**

* indicates the terrain range of the surrounding 3 km x 3 km area

Table 2.1. Recent studies that observed large nocturnal temperature anomalies. Average horizontal resolution is the average spacing between sensor stations. Terrain range is the elevation difference between the highest and lowest stations.

Simonsen (2001) and Fiebrich and Crawford (2001) studied observations from the ARS Micronet, a mesoscale observation network located in Oklahoma's Little Washita Watershed. The watershed is located in southwest Oklahoma, 60 km southwest of the Crosstimber Micronet. They observed horizontal temperature differences of up to 10°C across distances of less than 30 km. Studies in other areas found similar temperature gradients across mesoscale domains.

Strong nighttime near-surface temperature gradients have been attributed to various causes that generally fall into one of two categories: cold air drainage and in-situ cooling. Cold air drainage is a process whereby relatively cold, dense air flows down sloped terrain and replaces warmer air at lower elevations (Fleagle 1950). This drainage occurs on clear nights with calm to very light wind. The process requires an upslope source of relatively cool air. Cold air drainage has been shown to be a significant cooling mechanism in mountainous regions (Maki et al. 1986; Kondo et al. 1989). Mahrt et al. (2001) suggested that most land surfaces experience nocturnal drainage flows under clear skies and weak synoptic flow. During the CASES-99 field campaign, performed in south-central Kansas during October 1999, five sonic anemometers observed wind components across a small gully. The anemometers detected flows that were toward the downslope direction by night, which the authors concluded was evidence of drainage flow. However, Thompson (1986) showed that cold air drainage is not necessary for cold pools to develop. He observed that katabatic flows usually follow the formation of strong temperature inversions and spatial gradients, rather than precede them. Clements et al. (2003) likewise found that downslope cold air flows occurred only after the formation of cold pools.

Cold pools that do not exhibit characteristics of cold air drainage usually are attributed to in-situ cooling (Simonsen 2001). Broadly defined, in-situ cooling is a process where the properties of a surface in one area allow it to cool more effectively than in surrounding areas by altering the local surface energy balance. Factors that can affect components of the nocturnal surface energy balance include terrain, vegetation, and thermal properties of the soil.

In-situ cooling is believed to occur at the Tallahassee Regional Airport (TLH). Elsner et al. (1996) analyzed observations at TLH from 1984-1992. The analysis showed that TLH was consistently cooler than other nearby airports on clear nights. Six temperature sensors were installed around the airport during the cool seasons of 1992-1993 and 1993-1994. The observations revealed that all six locations were cooler than the main TLH site on clear nights, while the main TLH site was cooler than the other nearby airports.

Cold air drainage was ruled out as a cause, because TLH is not located in an area where cold air could pool. The terrain is higher toward the north but lower toward the south. Another reason why cold air drainage was ruled out was that the phenomenon was less dramatic later in the night and during the moist warm season months. The high nighttime relative humidity during the warm season limits radiational losses but has a relatively small impact on cold air drainage. Thus, the authors concluded that cold air drainage was not an important factor.

Elsner et al. (1996) concluded that the cool anomaly was created by sandy soils and the lack of trees at the airport. Sandy soils emit radiation more effectively than do the wet, loamy soils of the surrounding region. Their presence allowed the surface at TLH to cool more rapidly. Furthermore, the airport is relatively free from trees, which capture outgoing longwave radiation. Though this enhanced sky view factor (i.e., the fraction of the sky that is visible from the ground) also existed at other airports in the region, it was a more important factor at TLH because of the sandy soil there. Using information about the local soil types, Kara et al. (1998) modeled the area surrounding TLH. Their model predicted nighttime temperatures at TLH with reasonable accuracy. The results led them

to conclude that soil properties (as well as roughness length) are an important factor in the nighttime temperature anomaly observed at TLH.

Gustavsson et al. (1998) performed a study in a hilly region of southwestern Sweden during the winter of 1994. The terrain across the area varied from 165 to 240 m above sea level, a range similar to that of the area surrounding the Crosstimber Micronet. They used observations from 13 fixed sites along a 22 km stretch of road. Continuous observations from a car driving along the same stretch of road were used to supplement the fixed observations. Sixteen clear nights were studied. On those nights, horizontal temperature differences of up to 15°C were observed along the path.

The development of the cool anomalies occurred quickly. On one night, a strong cold pool, 7.8°C cooler than a nearby station, developed during the first hour after sunset. The cold pool was considered too large and had developed too quickly to be created by cold air drainage. Furthermore, the cooling rates across the region were not dependent on the size of the valley, another indication that cold air drainage did not create the cold pools.

Unlike the Tallahassee case, the sky view factor and soil properties were not considered to be significant factors. The sky view factor, which can range from 0 to 1, was 0.6-0.8 along the path. These values are large enough that sky obstruction did not substantially limit outgoing longwave radiation. The observation period included a night with a snow depth of 0.3 m or greater across the path. Thus, the surface radiating properties were nearly uniform on that night. But the temperature pattern was similar to that of the nights with no snow cover. Thus, variation in soil properties also could be ruled out as an important causal factor.

The topography at two of the coolest sites provided a clue about the cause of the cool anomalies. One site was located at the bottom of a valley, but the other was located on gently sloping terrain surrounded by trees. The authors concluded that the trees reduced turbulent mixing of relatively cool air near the surface and warmer air aloft. In other words, the trees reduced the flux of sensible heat between the surface and the air aloft. With the reduced sensible heat flux, the net outgoing radiation was not balanced by the surface heat fluxes. To maintain the conservation of energy, rapid cooling occurred across the sheltered areas.

Rapid nighttime cooling associated with the absence of turbulent mixing has been documented for many years. However, the phenomenon is not well-represented by numerical weather prediction (NWP) models. Louis (1979) demonstrated that near-zero sensible heat flux values, which resulted from decoupling of the near-surface nocturnal boundary layer, occurred in models but caused them to produce unrealistically low near-surface temperature forecasts. Though this result is physically realistic, it is not necessarily representative of an area as large as a single grid cell in a mesoscale model. To compensate for the rapid cooling, empirical parameterizations are used. These parameterizations produce forecasts that are consistent with turbulent conditions, even though conditions in part of the grid cell may not be turbulent.

The sensitivity of nighttime temperatures to sensible heat flux was demonstrated by Derbyshire (1994). He observed nighttime conditions in Bedfordshire, England on two clear nights: one with light wind (initially 6 m s^{-1}) and the other with stronger wind (initially 10 m s^{-1}). On the first night, the observed sensible heat flux values were near zero. For the same time period, the model he used predicted a sensible heat flux of 20-

30W/m^2, which led to a significant overestimation of the predicted temperature. On the night with stronger wind, observed sensible heat flux values were higher and the model agreed well with the observed temperature. Derbyshire concluded that it is very difficult to predict whether sensible heat fluxes values on clear nights will be near 30 W/m^2 or near zero. This difficulty creates significant uncertainty in nighttime temperature forecasts. To forecast temperatures more accurately on clear nights, more must be known about the dynamics of the stable boundary layer when turbulence is weak.

2.2. Structure of the Stable Nocturnal Boundary Layer

The nocturnal planetary boundary layer is generally considered to be a single stable layer, approximately 100 m deep, in contact with the earth's surface (Garratt 1992, 164-171). But rapid cooling of the ground surface can create three distinct sub-layers within the nocturnal planetary boundary layer. Clements et al. (2003) studied these layers at Peter Sinks near Logan Utah, a location known for extreme low temperatures.

Peter Sinks was an ideal location because the along-valley wind component there is not significant. While advection, reduction of radiational cooling by the along-valley wind, and valley circulations were important factors in other studies (Whiteman et al. 1996), such was not the case at Peter Sinks. Instruments were installed across a 1-km oval-shaped limestone sinkhole, which was surrounded by terrain with elevations approximately 150 m higher than the center of the sinkhole. The sinkhole was completely enclosed to a height of 35 m above the center.

At the bottom of the sinkhole, observed nighttime sensible heat flux values were near zero except during periods when winds aloft penetrated into the basin. These observations were consistent with those performed in other basins (Whiteman et al. 1990, 1996; Kondo et al. 1989). Shortly after sunset, rapid cooling was observed at the bottom of the sinkhole. The rapid cooling is consistent with the absence of sensible heat flux.

The rapid near-surface cooling altered the structure of the nocturnal boundary layer over the sinkhole. Clements et al. (2003) noted two distinct sub-layers that formed shortly after sunset. The lowest layer was characterized by negligible sensible heat flux and a significantly lower temperature than the surrounding area. Hence, this layer was identified as the "cold pool stable layer" (CPSL). Located above the CPSL was a capping inversion layer (CIL), which separated the CPSL from the "free atmosphere". In this case, the "free atmosphere" refers to the ambient stable boundary layer (ASBL). The vertical temperature profile was bluff-like (as in Fig. 2.1) rather than linear or logarithmic. The temperature increased rapidly with height in the middle layer (the CIL), but less so in the CPSL and in the free atmosphere (ASBL). Strong horizontal temperature gradients were observed in the CPSL, but horizontal temperature gradients were nearly zero in the ASBL.

Downslope flows were reported, but only within the CPSL. The authors did not find any evidence that mass from above the CPSL was transferred down into the CPSL. The downslope flows were reported only after the CPSL had developed, which indicated that they did not create the cold pool.

The results suggest that the most important factor was the sheltering from the ambient wind by the side walls of the sinkhole. The lack of turbulent mixing created an

imbalance between net outgoing longwave radiation and surface energy fluxes, which required rapid cooling to maintain conservation of energy. Mechanical mixing brought relatively warm air from the ASBL down to the top of the CIL, but the high density of air at the bottom of the CIL prevented the warmer air from reaching the CPSL. Likewise, cool air in the CPSL was trapped under the CIL. Thus, the CPSL was uncoupled from the ASBL. On one night when the wind speed near the top of the sinkhole reached 4 m s^{-1}, warmer air from the ASBL penetrated the capping inversion and the CPSL deteriorated rapidly. During those periods, the CPSL was not detectable.

This framework of understanding the structure of the nocturnal near-surface boundary layer in terms of three distinct layers can be expanded beyond sinkholes. As Gustavsson et al. (1998) suggested, trees and other physical barriers could create similar "cold pools". Furthermore, the characteristics of the CPSL may exist over much larger areas when the meso-synoptic scale pressure gradient is weak. The essential features of the CPSL are its lack of turbulence and its detachment from the ambient stable boundary layer. Hence, any layer that shares the characteristics of the CPSL is hereafter called an uncoupled surface layer (USL).

The USL can be defined as a stable layer in contact with the surface where turbulence is negligible. It is consistent with the traditional definition of the (coupled) surface layer; namely, that it is in contact with the surface and fluxes of latent and sensible heat within the layer can be considered constant with height (i.e., zero in this case). The more common term "decoupled" was not used because it implies that the layer once was coupled and later became uncoupled through a process of decoupling. This is not necessarily true of the USL.

The depth of the USL is analogous to the roughness length, the depth over which the wind speed is zero (Monin and Obukhov 1954). This depth is generally lower than the vegetation height (Garratt 1992, p. 87), but may exceed the vegetation height under very calm conditions. Though local near-surface flows may develop within the USL (e.g. downslope cold air flows), they are independent of the flow aloft in the ASBL.

Uncoupled surface layers have been shown to develop in wind tunnels as well as in the atmosphere. Ohya et al. (1996) used a wind tunnel to simulate atmospheric flow over a relatively cool surface. The airflow in the tunnel was heated to a temperature of 50°C, while the surface was cooled to 3°C. The air near the surface quickly decoupled from the main flow. Fluxes of momentum and heat became nearly zero in the uncoupled layer, much like the conditions observed in the CPSL/USL at Peter Sinks.

The absence of turbulent fluxes within the USL creates a unique energy balance that does not exist elsewhere in the nocturnal planetary boundary layer. The energy balance within the USL can be represented as a balance between net radiation and ground heat flux.

$$R_{net} + G = 0, \tag{2.1}$$

where R_{net} is net radiation and G is ground heat flux. Positive values indicate transfer of energy toward the surface. Negative values indicate transfer of energy away from the surface.

When discussing net heating or cooling of the surface, it is helpful to consider the surface as a volume (i.e., an interface layer) rather than an infinitesimally thin interface as in Equation 2.1. The interface layer may include soil, vegetation, and air near the ground.

This introduces a new term, ΔQ, which represents the flux of heat stored (i.e., heating or cooling) within the interface layer. Equation 2.1 becomes:

$$R_{net} + G + \Delta Q = 0, \tag{2.2}$$

where ΔQ is the net heat storage $z \cdot \rho c_p \cdot dT/dt$, z is the layer depth (including air), ρ is the average density of air in the layer, c_p is the average specific heat of the layer at constant pressure, and dT/dt is the time rate of change of the average temperature within the layer.

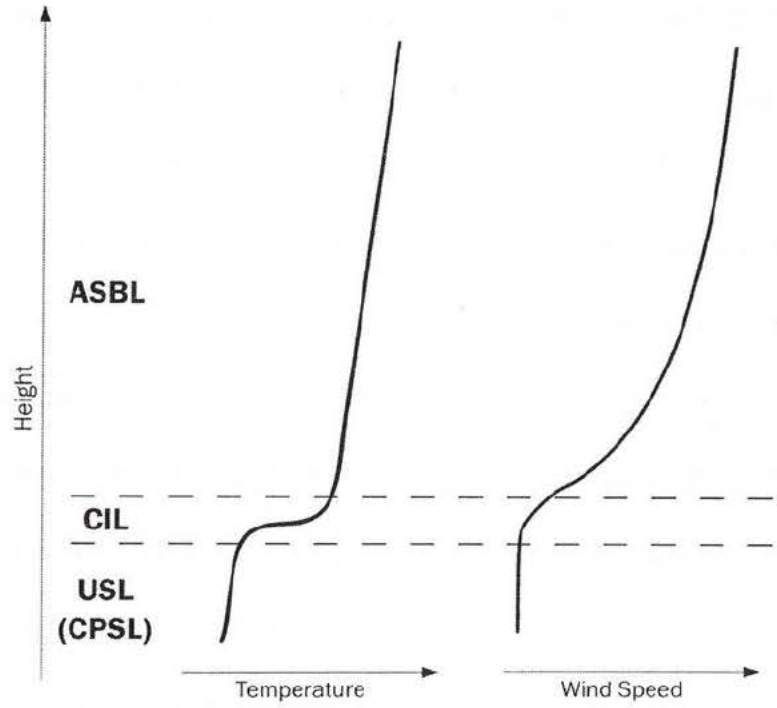

Figure 2.1. Diagram of the near-surface nocturnal boundary layer with idealized profiles of temperature and wind speed.

Shortly after sunset on clear evenings, when outgoing longwave radiative flux is greater than the ground heat flux, high cooling rates occur within the USL. Overnight, the surface becomes cooler than the underlying soil and the air aloft. Ground heat flux begins to balance net radiation, and the cooling rate decreases. By that time, the USL is

substantially cooler than the ASBL. This unique energy balance is responsible for the anomalously low nighttime temperatures observed in sheltered areas such as Peter Sinks.

The ASBL can be defined as a stable layer where turbulent fluxes are significant compared to the outgoing radiative flux. Within this layer, wind shear and buoyancy create small-scale perturbations to the mean flow (i.e., turbulence). Turbulent fluxes within the ASBL include those of momentum, sensible heat, and latent heat.

The ASBL is the highest vertically of the three layers, but may approach the surface, particularly at well-exposed locations where turbulent mixing is stronger. The ASBL can be up to 200 m deep and is characterized by weak stable stratification and negative turbulent heat fluxes (Stull 1988). The flow within the ASBL primarily depends on the meso-synoptic scale pressure gradient. At the synoptic scale, this layer can be considered equivalent to the nocturnal planetary boundary layer.

Within the ASBL, net radiation is balanced by sensible heat flux, latent heat flux, ground heat flux (if the ASBL is in contact with the ground), and net heat storage within the interface layer (Oke 1978, p. 34).

$$R_{net} + H + LE + G + \Delta Q = 0, \tag{2.3}$$

where R_{net} is net radiation, H is sensible heat flux, LE is latent heat flux, G is ground heat flux, and ΔQ is the net heat storage described earlier.

Sensible and latent heat fluxes are significant compared to net outgoing radiation. Thus, the net heat storage term is small, and cooling rates within the ASBL are much lower than in the USL. In exposed areas where the ASBL approaches the surface, nighttime temperatures are substantially higher than in sheltered areas where the ASBL is located well above the surface (Fig. 2.2).

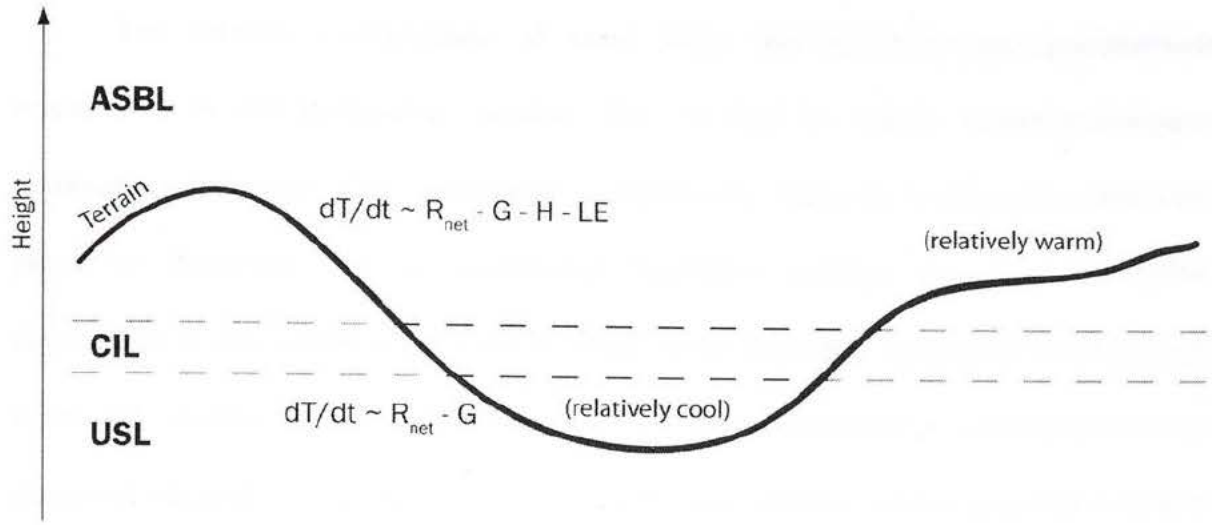

Figure 2.2. Idealized cross-section of the near-surface nocturnal boundary layer in an area of complex terrain.

The capping inversion layer (CIL) also can be generalized. It is defined as the interface between the USL and ASBL. It shares some characteristics with both the USL and ASBL because it contains entrained air from both layers. But the CIL is distinguished by strong vertical and horizontal gradients of temperature and wind speed. The strong vertical temperature gradient across the CIL restricts transport of air from the ASBL to the USL, which allows the USL to remain relatively cool. As a result, the CIL also can trap water vapor, carbon dioxide, and other gasses in the USL.

The CIL separates a layer of nearly nonexistent wind from a layer of relatively strong wind. Thus, vertical wind shear across the CIL can be strong. Strong wind shear in a stable layer can generate turbulent eddies. If the shear is sufficient, these eddies can transport air from the ASBL into the USL. This process creates dramatic changes in temperature and other meteorological parameters within a short period of time (Clements et al. 2003).

The relative contributions of wind shear and buoyancy are quantitatively represented by the Richardson number (Ri). At high Ri values, negative buoyancy dominates wind shear. Thus, turbulence is suppressed. When Ri is near zero, turbulence plays an important role in modulating nighttime cooling. Lyons et al. (1964) demonstrated that turbulence begins to break down nighttime inversions when Ri falls below 0.5. Webb (1970) and Businger et al. (1971) found that mean velocity profiles are disturbed when Ri approached the critical Richardson number, which generally is held to be 0.2. Webb (1970) noted that temperature fluctuations in the stable boundary layer almost disappeared when Ri was sufficiently higher than 0.2. It is likely that the development of the USL is closely related to this critical value. When Ri falls below the critical value, turbulence begins to destroy the USL.

Kondo et al. (1978) measured turbulent fluctuations over a flat paddy field near Sendai, Japan. They studied observations from clear nights with light wind during 1974-1975. They found that meteorological conditions were relatively steady when sufficient turbulence existed (i.e., when Ri was less than 0.2). But when Ri was between 0.24-0.5, they observed intermittent turbulence and temperature fluctuations. When Ri was above 0.5, the fluctuations became much weaker. Turbulence virtually ceased when Ri exceeded 2.

Van de Wiel et al. (2002a, 2002b, & 2003) studied intermittent turbulence using observations from the CASES-99 field campaign in south-central Kansas (Poulos et al. 2002). During clear nights in October 1999, they observed intermittent periods of large negative heat fluxes and quiet periods with almost no heat flux. The observations were consistent with those of Kondo et al. (1978).

According to Van de Wiel et al. (2003), knowledge of the physical mechanisms that generate intermittent turbulence is very limited because of the difficulty in measuring fluxes when turbulence is weak. They could not conclude with certainty whether the intermittency was generated by local shear effects, by instability on the scale of the entire surface inversion layer, or by turbulence aloft diffusing to the surface. However, they believed that wind shear, which dynamically created small-scale eddies, was the primary mechanism. According to their hypothesis, the surface cooled quickly by radiational cooling, which allowed air near the ground to decouple from the flow aloft. In other words, a USL developed near the surface. Eventually, because of the horizontal pressure gradient, the shear became strong enough to create turbulence which penetrated the USL and mixed warmer air from the ASBL down to the surface.

The authors suggested that intermittent turbulence can be expected on clear nights with moderate to rather small pressure gradients. They emphasized the importance of a vegetation layer. Vegetation has a lower heat capacity than does air and soil. Thus, the vegetation temperature can change more quickly. The rapid changes in surface (vegetation) temperature create a feedback mechanism, which perpetuates the intermittent turbulence.

This process was modeled by Van de Wiel et al. (2002a). Their model, which was based on a previous model by Revelle (1993), consisted of a coupled system of three nonlinear differential equations. The model parameterized a low vegetation layer and assumed that all fluxes were zero at the top of the stable boundary layer. This simple model captured the essential elements of the mechanism that generated intermittent turbulence. By using an intermittency parameter based on pressure gradient, the model

was able to predict whether intermittent turbulence would occur. However, the usefulness of the model is limited by its high sensitivity to the local estimations of the intermittency parameters. Thus, they emphasized a strong need for experimental research on the occurrence of intermittent turbulence in stable boundary layers.

Van de Wiel et al. (2003) classified clear nights into three regimes: turbulent, intermittent, and radiative. Other studies have classified the nocturnal planetary boundary layer itself into multiple regimes. Those regimes generally are based on static stability. Some classifications include two categories: very stable and weakly stable (Malhi 1995; Oyha et al. 1997; Mahrt et al. 1998). Others include three or more categories (Mahrt et al. 1998; Smedman 1988; Derbyshire 1990; Holtslag and Nieuwstadt 1986).

Mahrt et al. (1998) defined the regimes according to sensible heat flux and scaled height z/L (i.e., height above the surface divided by the Monin-Obukhov length) from similarity theory (Monin and Obukhov 1954). The classification included the following regimes: very stable, weakly stable, and transition. The division between the weakly stable and transition regimes was given as the scaled height at which the downward sensible heat flux is a maximum. However, this value is not universal (Mahrt et al. 1998; Malhi 1995); more importantly, the classification scheme requires flux measurements that are not available at most meteorological stations.

The recognition of distinct sub-layers within the stable boundary layer suggests a simpler way of classifying the nocturnal near-surface boundary layer - by the presence and height of each sublayer. This simple framework (i.e., understanding the nocturnal boundary layer in terms of three sub-layers) can help interpret some of the results that surprised authors of previous studies.

For example, in their study of nighttime temperatures in limestone sinkholes of various sizes and shapes, Whiteman et al. (2004) were surprised to find that the drainage area of the sinkhole did not appear to affect the temperature. Their initial expectation was based on the assumption that cold air drainage was an important factor. But their results are consistent with the development of a USL in the sinkholes. Unlike cold air drainage, USL development is not dependent on the drainage area.

Acevedo and Fitzgerald (2001) studied nighttime temperatures near Albany, New York. They uncovered a strong linear relationship between a station's temperature relative to the domain average temperature and the station's height relative to the surrounding 3 km x 3 km area (i.e., cool anomalies occurred at low elevations and warm anomalies occurred at high elevations). But the relationship was less significant between the temperature and absolute station elevation. Thus, the linear relationship was stronger on the 3km x 3km scale than across the entire domain.

Their results are consistent with the development of a USL, which implies that local sheltering is more important than cold air drainage or mesoscale variations in soil properties. The station's height relative to the surrounding 3km x 3km area is more representative of the sheltering of the site than is the absolute station elevation.

Studies have shown seemingly conflicting results regarding the impact of trees on nighttime temperatures. Kalma et al (1986) documented that trees generally increase the nighttime temperature by 1.3-1.5°C. Gross (1987) concluded that the nighttime temperature in a valley would be lower after deforestation. Their arguments were primarily based on the impact of the sky view factor on net radiation, with less attention given to the trees' impact on sensible heat flux. On the other hand, Gustavsson et al.

(1998) concluded that trees tend to reduce the nighttime temperature by reducing the sensible heat flux.

These results can be harmonized by considering the density of the trees, leaf area, and the relative importance of net radiation and sensible heat flux. On calm nights when sensible heat flux is minimal in forested and non-forested areas (because vertical mixing is minimal), the sky view factor may be most important and lead to anomalously high temperatures in forested areas. But on windier nights, the reduction of sensible heat flux (i.e., reduction of vertical mixing) by trees may be more important. On windy nights, relatively low temperatures may occur across the forested areas compared to non-forested areas. Furthermore, if the canopy is very dense, the reduction of outgoing radiation may dominate on most nights, creating warm anomalies in densely canopied areas. But in woodland or under open canopies (i.e., canopies under which a significant portion of the sky is visible), the reduction of sensible heat flux may be more important than the reduced sky view factor. In summary, the impact of trees on nocturnal temperatures is variable. It depends on the synoptic conditions and the density of the canopy.

Much attention in previous studies has been given to the time at which the strongest horizontal temperature gradients occur. In-situ cooling can occur more rapidly than cold air drainage (Gustavsson et al. 1998). Thus, when the strongest gradient occurs shortly after sunset, it usually is attributed to in-situ cooling. But when the strongest horizontal temperature gradient is observed later during the night, it often is attributed to cold air drainage (Simonsen 2001).

Rather than using the time of strongest temperature gradient to determine the cooling mechanism, the timing of USL development may offer a better explanation of

why the strongest gradient occurs at different times of the night in different cases. It will be shown that the strongest horizontal temperature gradients occur when the USL exists at one measurement location while not at another nearby location.

On nights with weak but increasing wind, the USL initially may be present over a large area. The strongest gradient may occur several hours after sunset, when the CIL or ASBL reach the surface over part of the area. But on nights with slightly stronger wind, the USL may initially be present in some areas and erode as the wind speed increases. On those nights, the maximum gradient is expected to occur earlier (i.e., less than two hours after sunset). These possibilities emphasize the value of a high-quality, long-term (i.e., multi-year) dataset of near-surface meteorological observations.

In summary, the scientific literature offers the following support to the results presented later:

1) On clear nights, significant cool temperature anomalies can occur in low-lying areas without cold air drainage. Similar anomalies are observed in areas where trees reduce the near-surface wind speed.

2) When the near-surface wind is sufficiently weak, a layer of air near the ground can decouple from the ambient stable boundary layer (ASBL), to form an uncoupled surface layer (USL; although the literature does not use the term 'USL', it refers to features that conform to what is defined in this study as the USL).

3) Observations have demonstrated that turbulence within the USL is negligible, and that the lack of turbulence allows enhanced radiational cooling to occur within the USL.

4) When vertical wind shear is sufficient to create turbulence, relatively warm air from the ASBL can mix down into the USL. Sometimes this process occurs intermittently throughout the night.

3. Data and Analysis

This dissertation focuses on meteorological conditions across a portion of central Oklahoma and across a 200 m x 100 m parcel of land known as the Crosstimber Micronet. The study domain is approximately 50 km x 50 km and is centered approximately 40 km southeast of Oklahoma City (Fig. 3.1). The Crosstimber Micronet is located near the center of the domain.

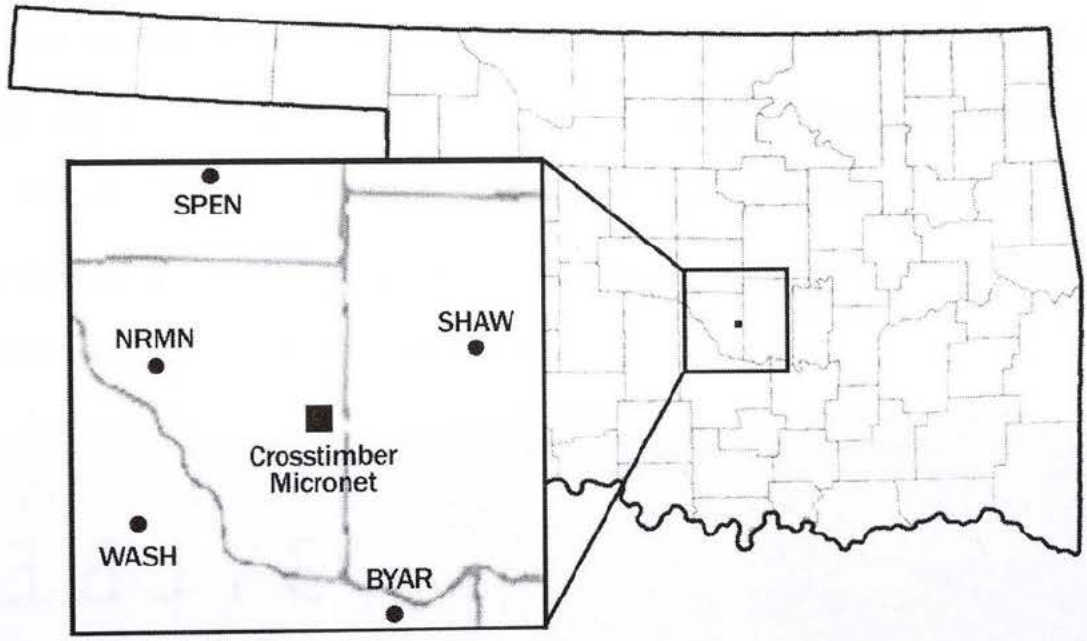

Figure 3.1. Study domain showing the location of the Crosstimber Micronet and surrounding Oklahoma Mesonet sites.

The region is covered by gently rolling hills and relatively flat plains. The mean elevation ranges from near 300 m above sea level in the southeast corner of the study domain to 400 m in the northwest corner. Across most of the domain, the hills do not rise more than 20 meters above the mean elevation. Thus, the terrain is relatively flat

compared to that in similar studies where large horizontal temperature gradients were observed.

The dominant vegetation type of central Oklahoma is tallgrass prairie. Common grasses in the tallgrass prairie include little bluestem, silver bluestem, buffalograss, and hairy gramma. These are C4 (warm-season) grasses, which grow during April-October and are dormant during November-March.

Five Oklahoma Mesonet sites represent mesoscale meteorological conditions across the domain: Norman (NRMN), Spencer (SPEN), Shawnee (SHAW), Byars (BYAR), and Washington (WASH; Brock et al. 1995). Each of these sites is located in a grassy field (Fig. 3.2). The terrain around each Mesonet site is relatively flat compared to the terrain near the center of the domain. The center of the domain is hilly and is etched by creeks and rivers, which form narrow valleys.

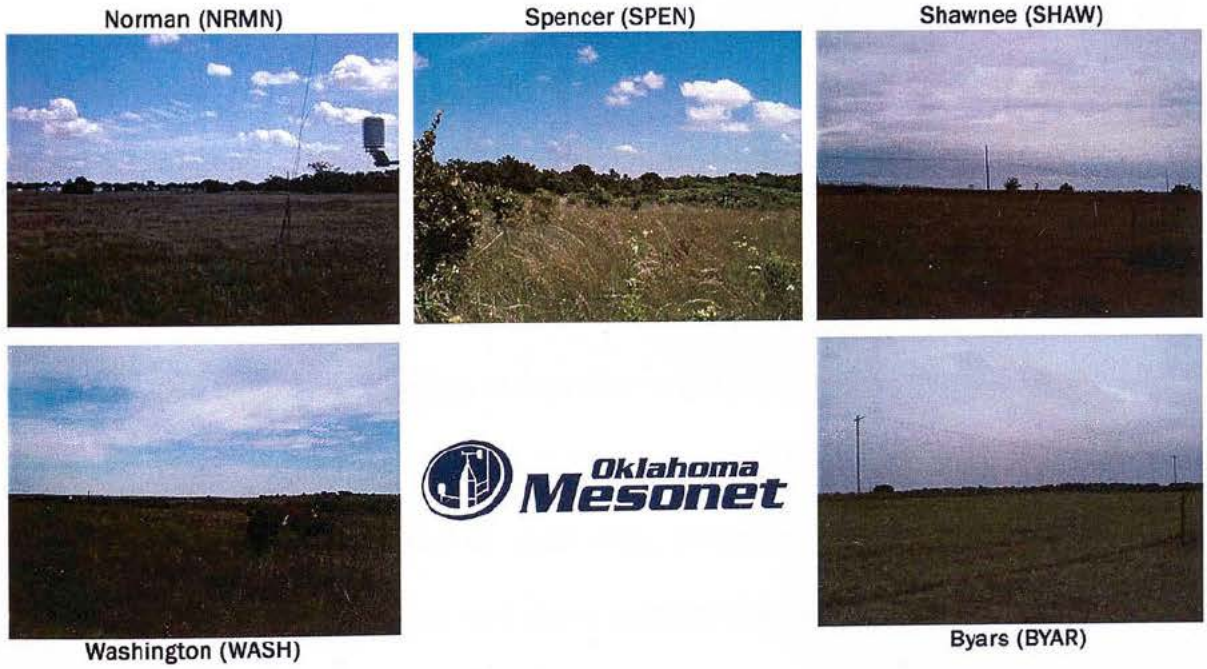

Figure 3.2. Photos at the five Oklahoma Mesonet sites in the study domain; the view in each image is toward the southeast, the prevailing nighttime wind direction.

Trees are more numerous toward the eastern part of the domain, but are most numerous near the center. A strip of oak woodland stretches across the eastern two-thirds of the domain (Fig. 3.3). This strip is known as the Crosstimbers ecoregion, also called the "Cross Timber".

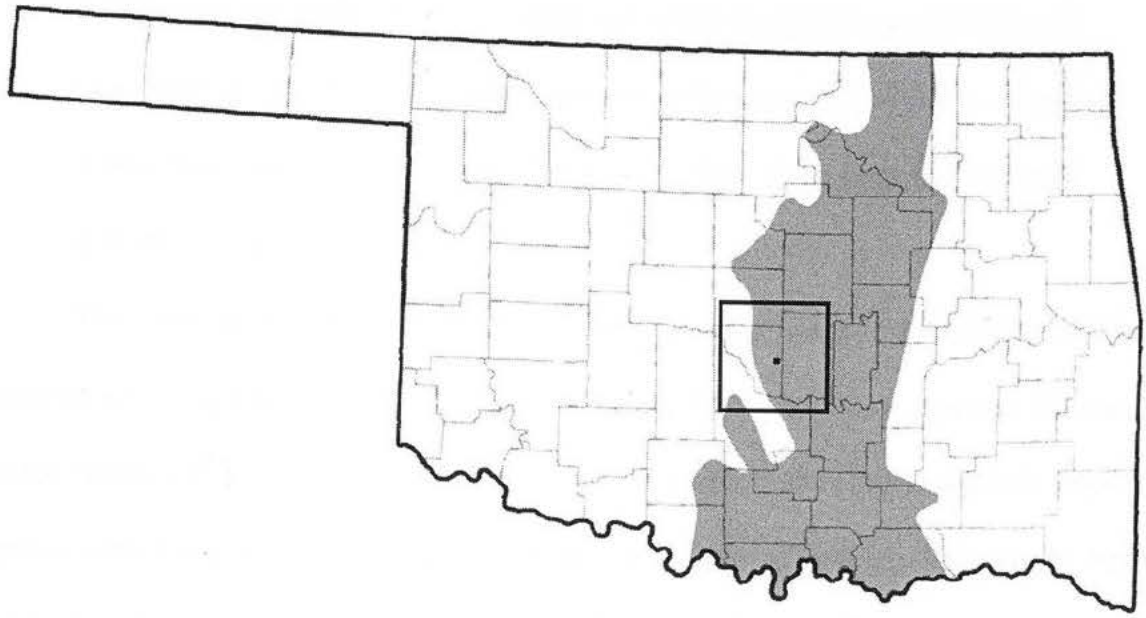

Figure 3.3. Map of Oklahoma showing the domain and the Crosstimbers ecoregion.

The Cross Timber extends from southeastern Kansas to central Texas. It is a transition zone between the prairie toward the west and eastern hardwood forests toward the east. Thus, the Cross Timber shares characteristics with both regions. It is distinguished by the dominance of short oaks, primarily post oak and blackjack oak. These oaks are uniquely ragged and dense compared to other trees in Oklahoma. The "Cross Timber" was named for the difficulty faced by early settlers who attempted to cross it. Washington Irving described this difficulty in 1835:

> "The Cross Timber is about forty miles in breadth and stretches over a rough country of rolling hills, covered with scattered tracts of post-oak and black-jack; with some intervening valleys, which at proper seasons, would afford good pasturage. It is very much cut up by deep ravines, which in the rainy seasons, are the beds of temporary streams, tributary to the main rivers... I shall not easily forget the mortal toil and vexations of the flesh and spirit, that we underwent occasionally, in our wanderings through the Cross Timber. It was like struggling through forests of cast iron."

The "cast iron" trees of the Cross Timber were not ideal for lumber production. Consequently, the Cross Timber is one of the least disturbed forest types in the eastern United States (The Ancient Cross Timbers Consortium 2003). Many ancient oaks still survive, especially in areas that are too steep for grazing or farming. The unique terrain and undisturbed vegetation of the Cross Timber makes it an excellent region for the study of land-atmosphere interactions.

The Crosstimber Micronet is located on a 200 m x 100 m tract of land in a relatively undisturbed part of the Cross Timber. The tract was selected because it stretched across a hill and a small valley. Thus, it was considered an ideal location for micrometeorological research. The southern edge of the tract is located near the center of a small valley (Fig. 3.4). Toward the south, 300 m south of the Micronet's southern edge, a ridge rises 40 m above the valley floor. A small creek is located on the southern edge of the Micronet, and a larger creek is located 500 m west of the Micronet. A ridge rises 50 m above the west bank of the larger creek, approximately 700 m west of the Micronet.

Toward the east, the terrain gently slopes upward to a ridge that is 20 m above the lowest point at the Micronet. That ridge is located approximately 700 m east of the Micronet's eastern edge.

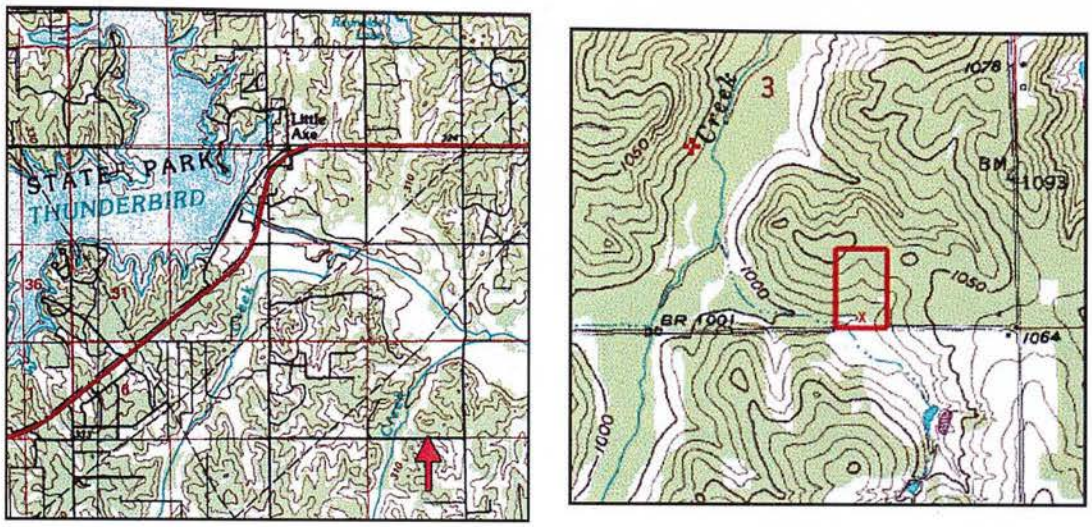

Figure 3.4. Topographic map of the Crosstimber Micronet and surrounding area.

The northern 80% of the Micronet lies on the southern slope of hill that rises 15 m above the valley floor. A dense canopy of post oak, blackjack oak, and black hickory trees, which are 5-15 m tall, covers the slope. The southern 20% of the Micronet is flat and is covered by little bluestem and silver bluestem grasses.

Six permanent meteorological stations are located at the Crosstimber Micronet: CR14, CR15, CR16b, CR17, CR18, and CR19 (Fig. 3.5; Fig. 3.6). Five additional stations, S1-S5, are located between CR18 and CR16b. CR18 and CR19 are co-located in the valley at the southern end of the Micronet. CR15 is located at the top of a ridge on the northern edge of the Micronet. CR14 and CR17 are co-located 50 m south of CR15. CR16b is located on the slope, between CR18/19 and CR14/17. From 2002-2004, CR16a

was located 50 m north of CR18. During April 2004, it was moved to the top of a 15 m tower approximately 30 m northeast of its previous location and was renamed 'CR16b'.

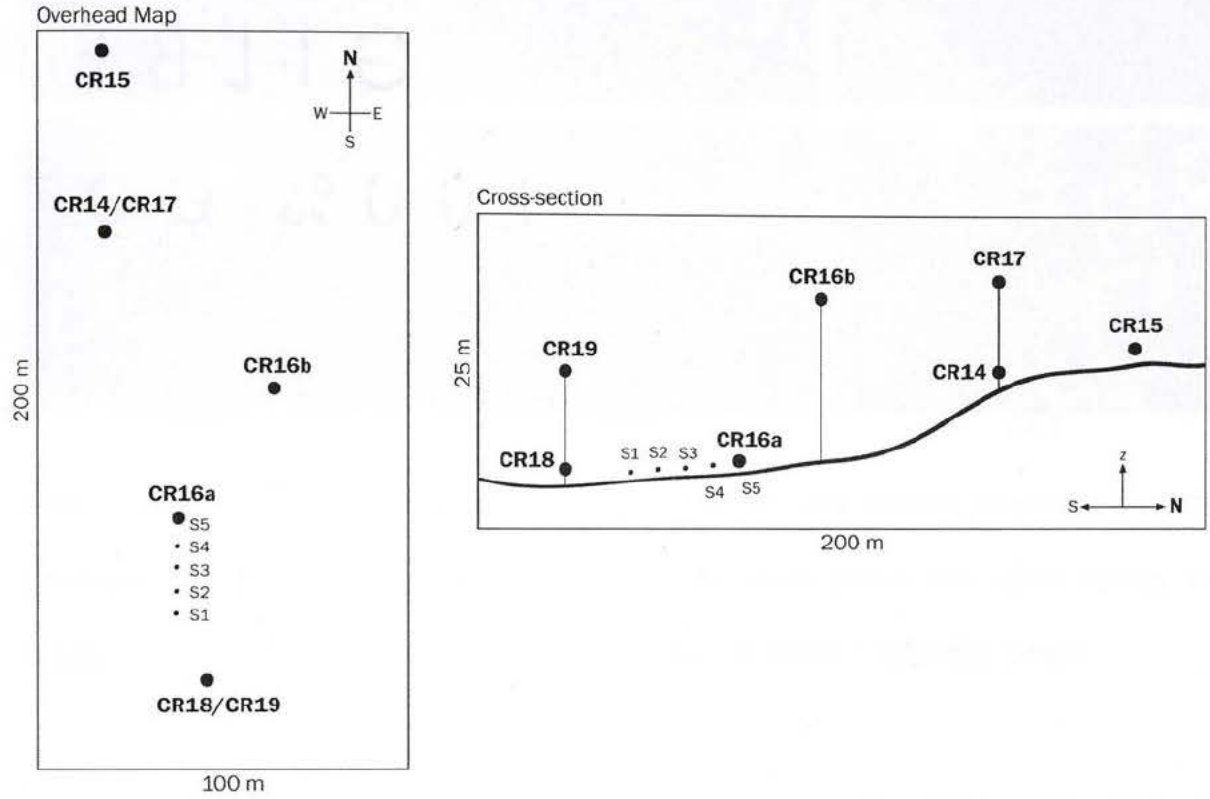

Figure 3.5. Map (overhead and cross-section) showing Crosstimber Micronet sites.

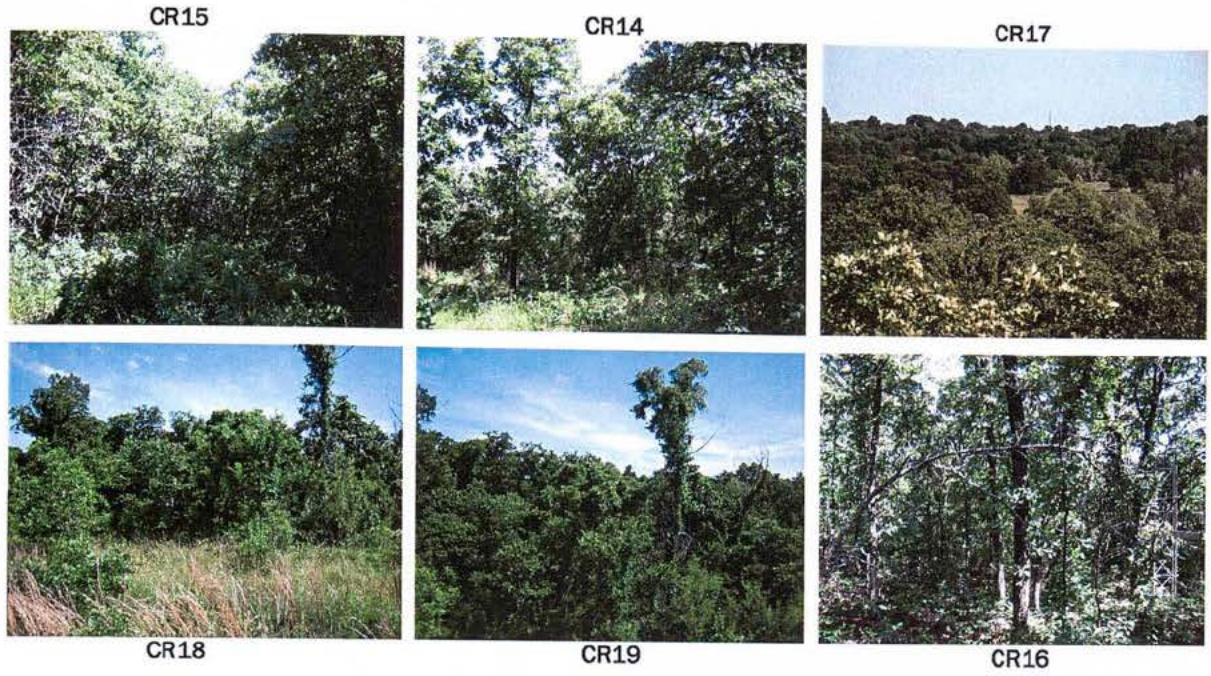

Figure 3.6. Photos at six Crosstimber Micronet sites; the view in each photo is toward the southeast, the prevailing nighttime wind direction. Each photo was taken during the summer from the height of the station's temperature & relative humidity sensor.

The instruments and parameters measured at the Crosstimber Micronet are generally the same as those of the Oklahoma Mesonet (Brock et al. 1995). However, most Micronet stations are not equipped with the full suite of Mesonet sensors, although some stations contain additional instruments and measurement levels that are not used in the Mesonet (Table 3.1; Fig. 3.7).

Station	Parameter	Height (AGL)	Sensor
CR14	Data logging		Campbell Scientific CR10X
	Air temp./humidity	1.5 m	Vaisala HMP45C
	Air temperature	4.5	Thermometrics DC95
	Air pressure	1.0	Vaisala CS105*
CR15	Data logging		Campbell Scientific CR205
	Air temp./humidity	1.5	Vaisala HMP45C

CR16	Data logging		Campbell Scientific CR205, CR10T
	Air temp./humidity	1.5	Vaisala HMP35C
		4.5 +	Vaisala HMP35C
		11 +	Vaisala HMP45C
	Wind speed/direction	14 +	RM Young Wind Monitor
CR17	Data logging		Campbell Scientific CR205
	Air temp./humidity +	9	Vaisala HMP45C
	Wind speed/direction	10	RM Young Wind Monitor
CR18	Data logging		Campbell Scientific CR205, CR10T
	Air temp./humidity	1.5	Vaisala HMP45C
	Air temperature	0.5 +	Thermometrics DC95
	Rainfall	0	MetOne tipping bucket*
	Soil temperature	-0.05	Fenwall NTC Thermistor
	Net radiation	2	REBS net radiometer*
	Wind speed	2	RM Young Wind Sentry
	Ground heat flux	-0.05	REBS HFT-3.1
	CO2 concentration +	2	Vaisala GMP343
CR19	Data logging		Campbell Scientific CR205, CR10T
	Air temp./humidity +	9	Vaisala HMP45C
	Air temperature	2 +	Thermometrics DC95
	Air temperature	3.5 +	Thermometrics DC95
	Air temperature	5 +	Thermometrics DC95
	Air temperature	6.5 +	Thermometrics DC95
	Air temperature	8 +	Thermometrics DC95
	Wind speed/direction	10	RM Young Wind Monitor

* different instrument than its counterpart in the Oklahoma Mesonet
+ not measured by the Oklahoma Mesonet

Table 3.1. Instruments and parameters measured by the Crosstimber Micronet.

Figure 3.7. Photo of the CR18/CR19 site, located in the Micronet's valley.

Like Oklahoma Mesonet sites, the Crosstimber Micronet stations acquire a sample every three seconds and average those samples over a period of five minutes. Each observation is an average of 100 samples over a period of 5 minutes. The five-minute averages of each parameter from each site are transmitted via 900 MHz radio link to CR14 where data from the entire network is stored. The data are later retrieved via phone line from the Crosstimber Micronet office in Norman, Oklahoma.

This study is based on over 3 years of observations from September 2002-January 2006 at the Crosstimber Micronet and five surrounding Oklahoma Mesonet sites. The Oklahoma Mesonet data were quality-assured using the procedures outlined by Shafer et

al. (2000). Quality assurance of data from the Crosstimber Micronet was relatively simple because of the high density of observations there. First, the observations were processed though an automated quality control program that flagged all missing and highly erroneous data (i.e., negative wind speed and RH values, temperatures below –99°C, etc.). Later, the remaining observations were plotted and compared with corresponding observations at nearby Micronet sites and the five surrounding Mesonet sites.

All suspect data were flagged. Finally, the observations were classified into the following categories: good, suspect, missing, instrument error, and radio/transmission error. Only the observations classified as "good" were used in this study. Furthermore, if an observation was classified as "good" at one site but not at other sites, none of the observations for that 5-minute time period were used. Thus, the analysis is limited to time periods when the observations were classified as "good" at each Micronet and Mesonet site. For the period of this study, approximately 300,000 observations were collected. Of those, approximately 98% were classified as "good".

The analysis in this study focuses on observations during clear nights. Approximately 56% of the nights in the dataset were classified as clear. The observed net radiation at the Crosstimber Micronet was used to classify each night as "clear" or "not clear". A night was considered clear if the net radiation was less than –10 W/m^2 for at least 80% of the night. Thus, nights with short periods of cloud cover were classified as clear nights. When net radiation observations were not available, other observations such as the vertical temperature profile and incoming solar radiation near sunset and sunrise were used collectively to determine whether the night was at least 80% clear.

4. Observational Results

Much can be learned about the structure and evolution of the nocturnal boundary layer through a study of observations from the Crosstimber Micronet and surrounding Oklahoma Mesonet sites. Although development of an uncoupled surface layer (USL) is rare at the Mesonet sites in the study domain, USL development is common at the Micronet. Comparing observations from the Micronet with those from the surrounding Mesonet sites can clearly reveal the impact of the USL.

4.1. The Unique Microclimates of the Crosstimber Micronet

The diurnal temperature range at the Micronet is larger than at surrounding Mesonet sites. During most of the year, daytime temperatures across the Micronet are higher than at surrounding Mesonet sites (Fig. 4.1). But during summer months, when the Micronet is greener than surrounding Mesonet sites, daytime temperatures at the Micronet are equal to those at the surrounding Mesonet sites. Throughout the year, nighttime temperatures at the Micronet are significantly lower than at the surrounding Mesonet sites.

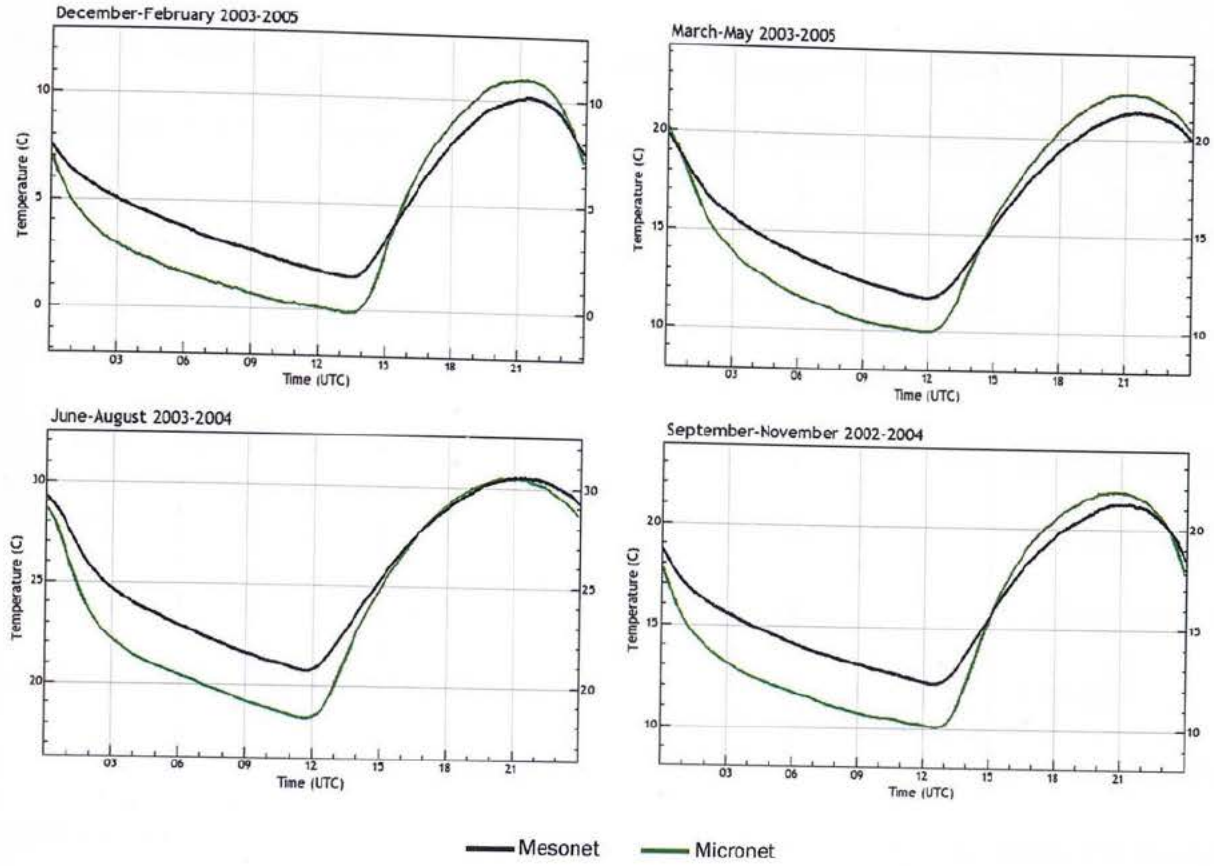

Figure 4.1. Average diurnal cycle of temperature at the Crosstimber Micronet (green) and surrounding Oklahoma Mesonet sites (black).

Average daily minimum air temperatures at 1.5 m across the Crosstimber Micronet are 0.7-4.6°C lower than the average daily minimum at the five surrounding Oklahoma Mesonet sites. This difference in nighttime temperature is not merely a seasonal phenomenon. It occurs during each month of the year (Table 4.1).

Site	Jan	Feb	Mar	Apr	May	Jun	Jul	Aug	Sep	Oct	Nov	Dec	All
All nights (#)	76	85	84	55	62	60	62	62	87	92	84	87	896
CR15 (Ridge)	0.7	1.6	1.7	2.1	1.6	1.7	2.0	2.2	2.8	2.2	1.4	2.2	1.9
CR18 (Valley)	2.2	2.9	3.4	3.7	3.0	2.9	3.5	3.6	4.6	3.9	2.9	4.5	3.4
Micronet Avg.	2.0	2.2	2.4	2.8	2.2	2.3	2.7	2.9	3.6	2.8	2.1	3.2	2.6
Clear nights (#)	44	41	44	31	35	35	44	42	65	51	35	59	526
CR15 (Ridge)	2.6	3.5	2.7	2.7	2.1	2.2	2.3	2.5	3.1	3.3	2.5	2.9	2.7
CR18 (Valley)	4.9	5.8	5.3	4.9	3.9	3.8	4.0	4.1	5.2	5.4	5.4	5.7	4.9
Micronet Avg.	3.7	4.5	3.9	3.7	2.9	2.9	3.1	3.3	4.1	4.3	3.8	4.1	3.7
% Clear nights	58	48	52	56	56	58	71	68	75	55	42	68	59

Table 4.1. Difference between the average daily minimum temperature (°C) at selected Crosstimber Micronet sites and the five surrounding Oklahoma Mesonet sites; the top half represents all nights (excluding those that contained bad or missing observations), while the bottom half represents only those that were classified as "clear".

From 2002-2005, the difference in average daily minimum temperatures between the Micronet and five surrounding Oklahoma Mesonet sites was greatest during September. This difference during September ranged from 2.8°C at CR15 (located near the Micronet's highest point) to 4.6°C at CR18 (located near the Micronet's lowest point). The smallest difference in minimum temperatures occurred during January.

On cloudy nights, nighttime temperatures observed at the Micronet were nearly equal to those observed at the surrounding Mesonet sites (not shown). Thus, the largest differences in the average minimum temperature occurred during months when a high percentage of the nights were clear (e.g., August, September, and December).

However, when only clear nights were considered, the greatest difference in average minimum temperature between a Micronet site and the surrounding Mesonet sites occurred during February (5.8°C at CR18). The smallest occurred during May (2.1°C at CR15). At CR18, the average daily minimum temperature on clear nights was more than 5°C lower than at the surrounding Mesonet sites during 6 of the 12 calendar months.

The nighttime temperature anomaly at a Crosstimber Micronet site is defined as the temperature at that site subtracted from the average temperature observed across the five surrounding Mesonet sites. This anomaly varied substantially across the Micronet. It was largest at the lowest site, CR18 (shown in purple), approximately 2-3 hours after

sunset (Fig. 4.2). At sites located on the Micronet's hill (i.e., CR14 and CR15), the anomaly was relatively constant throughout the night. During the summer months, the anomaly on the hill was strongest at sunrise, while in the valley it was strongest shortly after sunset.

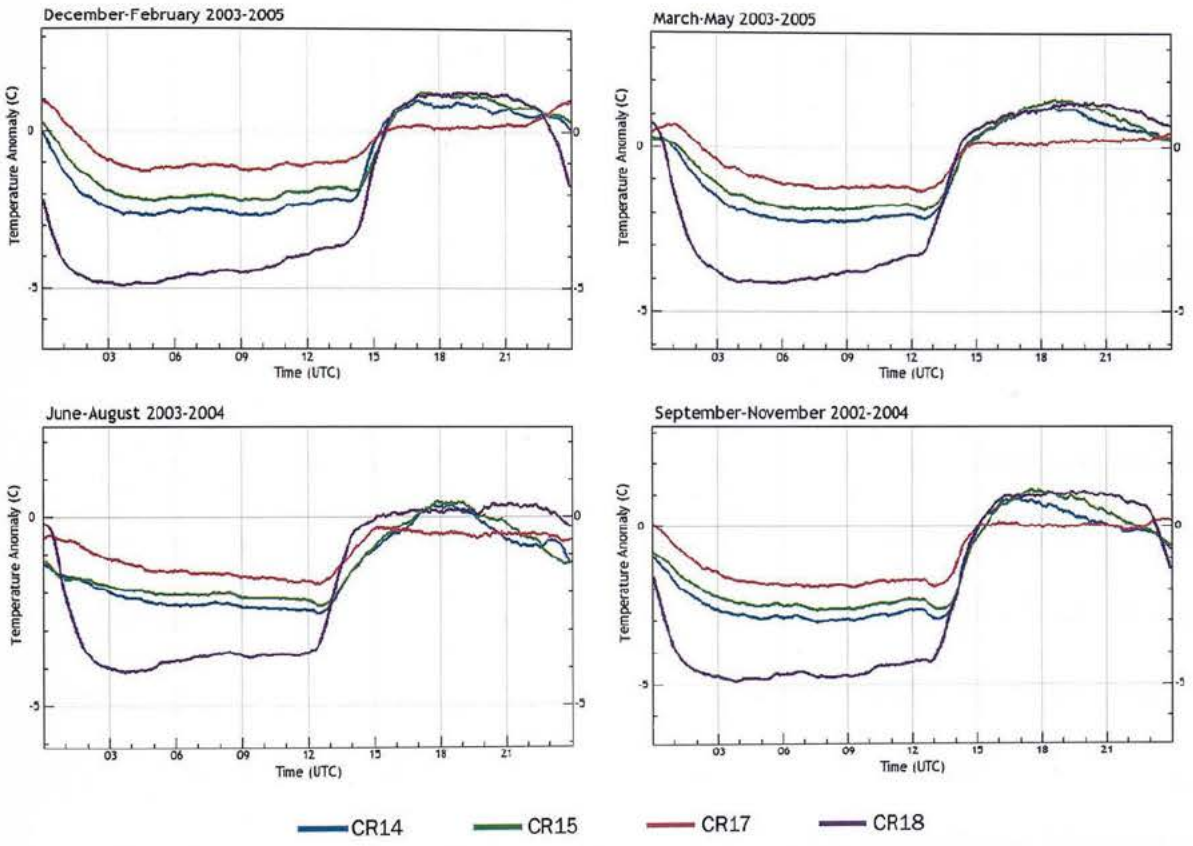

Figure 4.2. Average temperature anomaly (i.e., temperature at the Micronet site subtracted by the average temperature across the five surrounding Mesonet sites) on clear nights at four Micronet sites: CR14 (blue), CR15 (green), CR17 (red), and CR18 (purple).

The largest nightly temperature anomaly (LNTA) is defined as the largest temperature anomaly that is observed at a Micronet site during a particular night. The LNTA can occur at any time between sunset and sunrise. It varies seasonally and

geographically across the Micronet. At CR18, the average LNTA on clear nights ranges from 4.9°C during June to 7.5°C during December (Table 4.2). Thus, during an average clear night, CR18 reaches a temperature that is 4.9-7.5°C lower than the average temperature across the five surrounding Mesonet sites.

Site	Jan	Feb	Mar	Apr	May	Jun	Jul	Aug	Sep	Oct	Nov	Dec
CR14 (Hill)	4.3	5.1	4.3	4.3	3.3	3.7	3.6	4.1	4.6	4.9	4.7	4.9
CR15 (Ridge)	3.7	4.5	3.6	3.8	3.1	3.4	3.4	3.8	4.2	4.4	4.1	4.3
CR17 (Hill 9m)	2.7	3.7	2.7	3.3	2.6	3.2	2.9	3.2	3.6	3.7	3.1	3.1
CR18 (Valley)	6.7	7.0	6.8	6.1	5.0	4.9	5.6	5.6	6.3	6.7	7.4	7.5

Table 4.2. Average largest nightly temperature anomaly (LNTA; °C) on clear nights at the Crosstimber Micronet.

At the top of the Micronet's hill, the average LNTA on clear nights ranged from 3.1°C during May to 4.5°C during February. Even at CR17, which is located 9 meters above the ground and near the top of the Micronet's hill, the average LNTA on clear nights was 2.6-3.7°C. The large LNTA at CR17 suggest that a deep USL, rather than cold air drainage, is responsible for the temperature anomalies on these nights.

Occasionally, nighttime temperature anomalies at the Crosstimber Micronet are substantial. These anomalies have exceeded 8°C on some nights during each calendar month (Table 4.3).

Site	Jan	Feb	Mar	Apr	May	Jun	Jul	Aug	Sep	Oct	Nov	Dec
CR15 (Ridge)	7.8	8.4	8.7	8.6	7.6	7.4	7.2	6.0	7.7	9.5	8.2	9.2
CR18 (Valley)	10.9	11.0	10.9	10.9	10.8	9.6	9.4	8.3	10.3	10.9	12.0	13.3
Micronet Avg.	9.3	9.7	9.7	9.7	8.5	8.5	7.9	7.1	8.9	10.1	9.9	11.2

Table 4.3. Largest monthly nighttime temperature anomaly (°C) at selected Crosstimber Micronet sites and largest anomaly of the average temperature across the Micronet.

The anomaly at CR18 has exceeded 10°C during each month from September-May. The largest anomaly observed at the Micronet between 2002-2005 was an astonishing 13.3°C. At 0425 UTC on December 2003, the temperature at CR18 was −4.8°C while the average temperature across the five surrounding Mesonet sites was 8.5°C.

Large horizontal temperature gradients also have been observed within the Micronet's 0.02 km^2 area. On an average clear night, the temperature at CR18 is up to 1.6-2.9°C lower than that at CR15. Temperature differences of 9°C or greater across the Micronet have been observed during each month from November to April (Table 4.4).

	Jan	Feb	Mar	Apr	May	Jun	Jul	Aug	Sep	Oct	Nov	Dec
All nights	1.5	1.3	1.7	1.6	1.4	1.2	1.5	1.4	1.8	1.7	1.5	2.3
Clear nights	2.3	2.3	2.6	2.2	1.8	1.6	1.7	1.6	2.1	2.1	2.9	2.8
Greatest Temp. Diff.	9.6	9.0	9.7	10.7	7.5	5.0	5.4	6.2	6.0	8.0	11.3	10.4

Table 4.4. Largest average nightly temperature difference (°C) across the Micronet (i.e., between CR18 and CR15) and greatest temperature difference observed across the Micronet.

The largest average temperature differences observed across the Micronet are almost as large as those observed between the Micronet and surrounding Mesonet sites. During November 2003, a temperature difference of 11.3°C (Table 4.4) was observed between CR18 and CR15, a distance of only 180 m. This corresponds to a terrain-following horizontal temperature gradient of approximately 63°C/km.

Cold air drainage at the Micronet can be eliminated as a cause of the temperature difference between CR15 (located on the Micronet's ridge) and the Mesonet. The location of CR15 is extremely unfavorable for cold air drainage, because the surrounding terrain is lower in almost every direction (Fig. 3.4; Elsner et al. 1996). Compared to

CR18, the temperature at CR15 is higher from sunset to sunrise. Thus, it is unlikely that cold air drains from CR15 to CR18. Mobile temperature observations (not shown) suggest that the other ridges near the Micronet also are warmer than CR18. Furthermore, smoke trail observations (not shown), acquired at the Micronet during evenings when large temperature anomalies were occurring, did not reveal downslope flows. On some nights with large temperature anomalies, upslope near-surface flows were detected near CR18 (again based on observations of smoke trails; not shown). The sky view factor (i.e., percentage of the sky that is not obscured by trees) also may be eliminated as a cause, because the sky view factor is significantly greater at the Mesonet sites, where the nighttime temperature is higher.

4.2. Physical Processes

One of the most striking meteorological differences observed between the Crosstimber Micronet and surrounding Mesonet sites occurs in the measurement of wind speed. Average wind speeds at 10 m are approximately twice as strong year round at the Mesonet sites than at the Micronet (Fig. 4.3). On clear nights, the average wind speed is approximately three times stronger at Mesonet sites than across the Micronet.

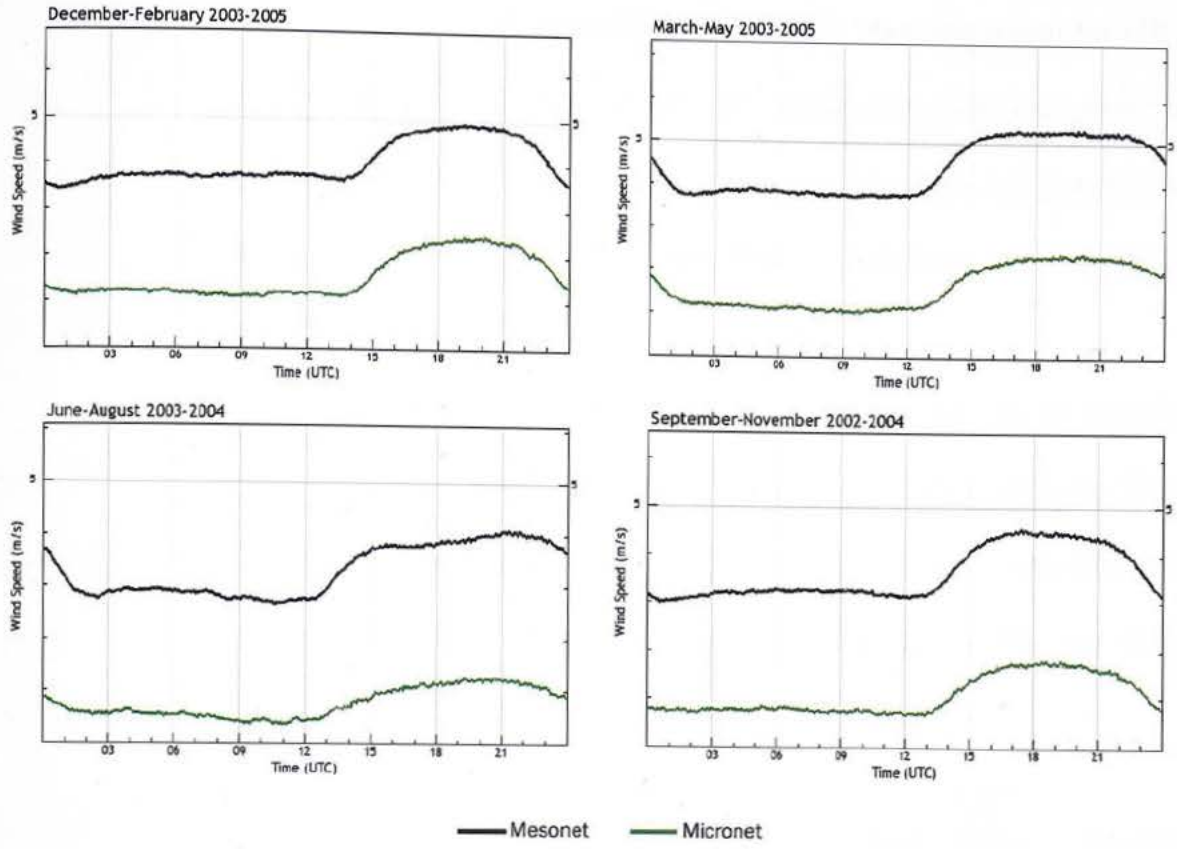

Figure 4.3. Average diurnal cycle of 10 m wind speed at the Crosstimber Micronet (green) and surrounding Oklahoma Mesonet sites (black).

The large wind speed difference occurs because the Micronet is nearly surrounded by trees and hills, while the Mesonet sites are relatively flat and treeless. When the mesoscale wind speed is sufficiently weak, these barriers create calm conditions at the Micronet. Under stable conditions, the absence of turbulent mixing allows the air near the surface to decouple from the ambient stable boundary layer (ASBL) forming an uncoupled surface layer (USL). The calm conditions observed at the Micronet support Proposition 1, which states that the USL develops at the Micronet.

The USL, identified by stable stratification and calm wind (i.e., wind speed below 0.1 m s^{-1}), often develops on clear nights at the Micronet. Within the USL, the nighttime surface energy balance is defined by Eqn. 2.1. As shown in Chapter 2, this energy

balance allows rapid cooling to occur at locations such as the Micronet where the USL is present. However, calm conditions are rare at the surrounding Mesonet sites. The nighttime surface energy balance at those sites is represented by Eqn. 2.2. Sensible and latent heat fluxes help offset radiational cooling. Hence, nighttime temperatures are higher at the Mesonet sites.

The impact of spatial variations in the surface energy balance can be seen on a smaller scale across the Crosstimber Micronet (Table 4.5). Nights with the largest temperature differences across the Micronet are characterized by calm conditions in the valley (CR18) and non-calm conditions at higher locations. In other words, the USL is present at CR18 but not at higher locations.

	Mesonet		CR17		CR18		CR19	
ΔT	Wspd	% calm	Wspd	% calm	Wspd	% calm	Wspd	% calm
0-1	4.41	0	1.77	13.0	0.41	43.3	1.46	6.4
1-2	2.34	0	0.35	66.9	0.02	94.5	0.25	62.2
2-3	2.24	0	0.23	73.3	0.01	98.4	0.12	77.0
3-4	2.57	0	0.37	58.4	0.01	98.1	0.17	65.6
4-5	2.85	0	0.51	43.2	0.01	98.1	0.23	51.7
5-6	3	0	0.63	31.8	0.01	97.9	0.28	42.3
6-7	3.2	0	0.74	24.9	0.01	95.9	0.33	37.4
7-8	3.38	0	0.99	14.7	0.01	96.7	0.37	30.8
8-9	3.41	0	1.09	11.3	0.01	97.3	0.56	12.4
9-10	3.86	0	1.12	18.6	0.01	100	0.43	12.5

Table 4.5. Average wind speeds and percentage of observations that are calm as a function of temperature difference (°C) across the Crosstimber Micronet (ΔT) for all seasons during the study period.

During periods when the temperature difference across the Micronet is small (i.e., less than 1°C), the wind is usually non-calm at all locations. Thus, the USL is not present.

But when the temperature difference is greater than 1°C, the wind is nearly always calm at CR18. On the nights with the largest temperature differences across the Micronet, the USL is present (i.e., the wind speed is below 0.1 m s^{-1}) at CR18 but not at the other sites. It follows that the sensible heat flux is near zero at CR18 but negative at the other sites. Hence, the other sites are warmer than CR18.

When the temperature difference is moderate (i.e., 1-4°C), the USL generally is present across the entire Micronet. Thus, the surface energy balance is assumed to be relatively uniform across the Micronet on those nights.

The USL is defined by a near-zero wind speed. It follows that the presence of the USL is highly dependent on the wind speed across the region and the degree of sheltering at the particular location (Fig. 4.4).

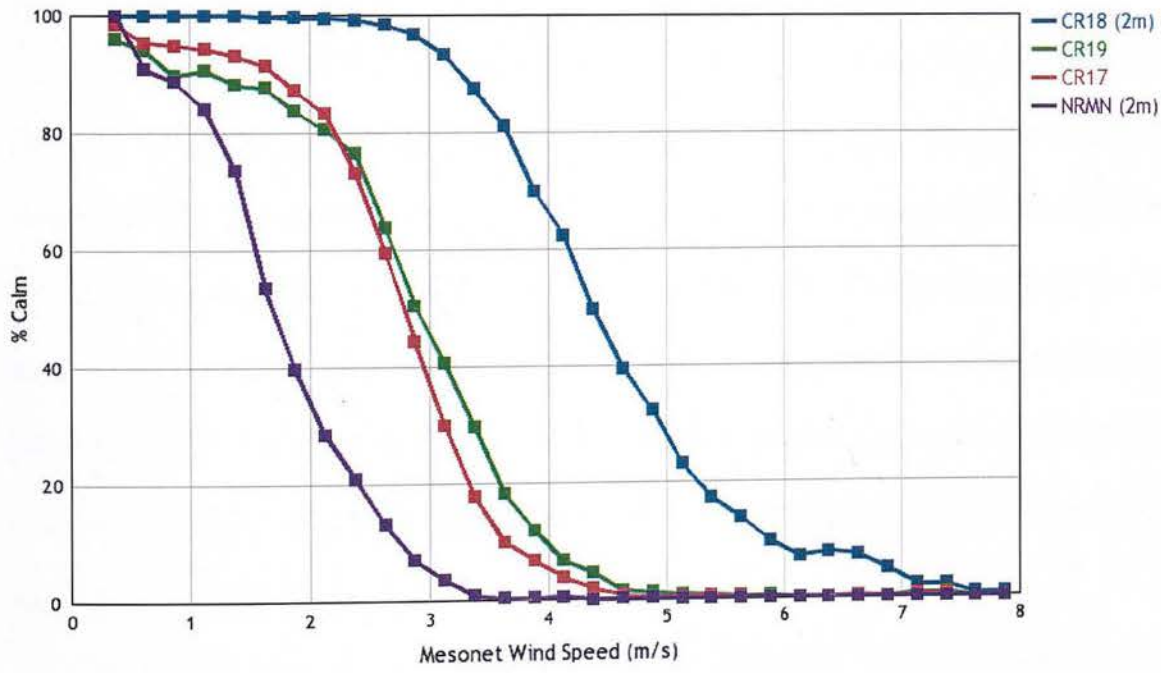

Figure 4.4. Percentage of clear-night observations when a USL is present (i.e., wind speed is less than 0.1 m s^{-1}) as a function of average wind speed across the five Oklahoma Mesonet sites.

The frequency of occurrence of the USL (Fig. 4.4) at a given location is a function of the mesoscale wind speed across the domain, hereafter defined as the average 10-meter wind speed across the five Mesonet sites. When the mesoscale wind speed is less than 0.5 m s^{-1} (Fig. 4.4), the USL is present across the entire Micronet and at 2 m above ground level at NRMN, the Mesonet site that is closest to the Micronet. When the mesoscale wind speed increases to 3 m s^{-1}, the frequency of occurrence of the USL at NRMN decreases to less than 5%, but the frequency remains above 90% at CR18 (Fig. 4.4). The USL becomes rare (i.e., less than 10% of observations) at CR18 when the mesoscale wind speed exceeds 5-6 m s^{-1}; it is absent at all other sites in the Micronet. These results strongly support Proposition 3, which states that the presence and depth of the USL are determined by the wind speed across central Oklahoma.

At 10 meters above ground level, the USL is extremely rare at each of the Mesonet sites. From August 2002-June 2005, there has not been a single 5-minute period when the average 10-meter wind speed across the five Mesonet sites was less than 0.1 m s^{-1}. But across the Micronet at CR19 (in the valley) and CR17 (near the top of the hill), the USL is common unless the mesoscale wind speed exceeds 2.5-3 m s^{-1}. Remarkably, CR19 and CR17 have reported calm winds at 10 m when the mesoscale wind speed was as high as 4.5 m s^{-1} (Fig. 4.4). Similarly, CR18 has reported calm winds with mesoscale wind speeds approaching 7.5 m s^{-1}.

It follows that the nighttime temperature difference across the Micronet and between the Micronet and surrounding Mesonet sites is dependent on the mesoscale wind speed (Fig. 4.5).

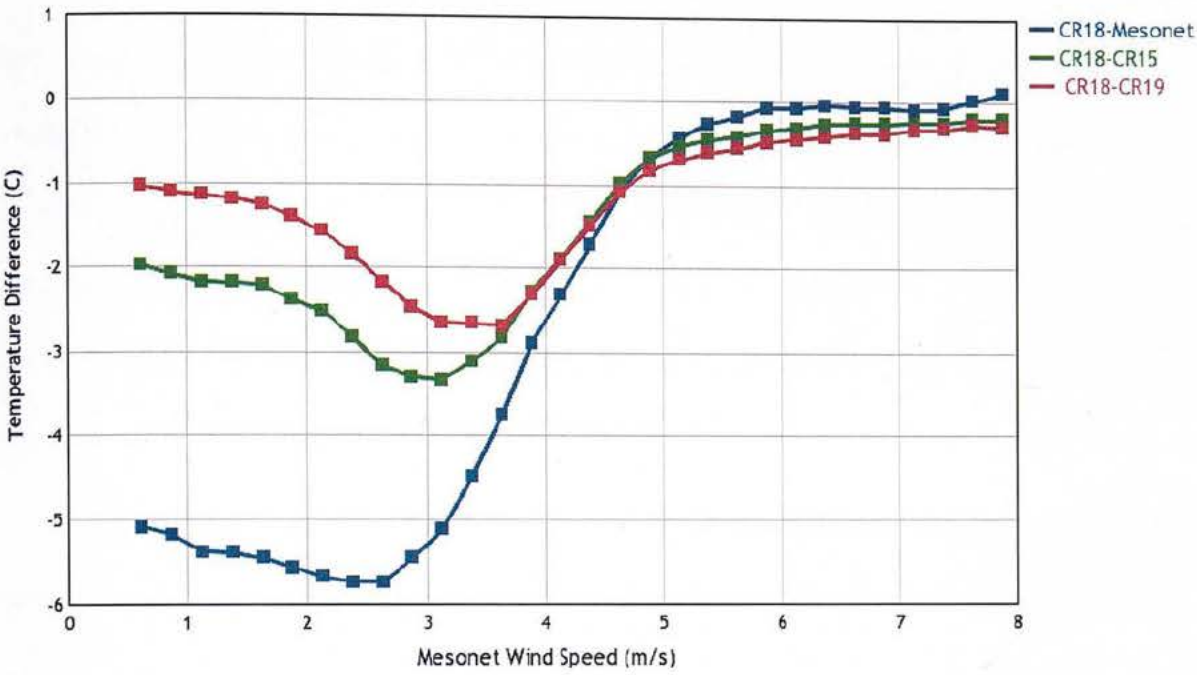

Figure 4.5. Average temperature differences between CR18 and the Mesonet sites (blue), CR18 and CR15 (green), and CR18 and CR19 (red) as a function of the average wind speed observed across the Mesonet sites.

The correspondence between USL frequency and average temperature difference is striking. With mesoscale wind speeds above 5 m s^{-1}, when the USL is not present at CR18, the temperature differences are minimal. The temperature difference between CR18 and the surrounding Mesonet sites is strongest when the mesoscale wind speed is near 2.6 m s^{-1} (Fig. 4.5). This corresponds with a near-100% frequency of USL occurrence at CR18 (Fig. 4.4), 14% at NRMN, and even lower at other Mesonet sites (not shown). Thus, it is clear that the largest temperature difference between CR18 and the surrounding Mesonet sites occurs when the USL is present at CR18 but not at the Mesonet sites, as stated by Proposition 2.

Similarly, the largest temperature difference between CR18 and CR15 occurs with a mesoscale wind speed of 3.1 m s^{-1} (Fig. 4.5). This corresponds with a range in which the USL is usually present at CR18 and usually not present at CR17 (the closest wind observation to CR15; Fig. 4.4). Between CR18 and CR19, the maximum temperature difference occurs at 3.6 m s^{-1} (Fig. 4.5), when the USL is usually present at CR18 but not at CR19 where the frequency of occurrence has dropped below 20% (Fig. 4.4).

The different mesoscale wind speeds at which the maximum average temperature difference occurs is consistent with the degree of sheltering at each location. CR18, located in the Micronet's valley, is the most sheltered. Thus, a higher mesoscale wind speed is required to prevent the USL from developing there. The Mesonet sites are the least sheltered, and thus do not require such a strong mesoscale wind to inhibit USL development.

Not surprisingly, the most extreme temperature differences across the Micronet and between the Micronet and Mesonet occur on nights with a relatively strong mesoscale wind speed, when the USL is present at CR18 and wind is significantly stronger at all other sites.

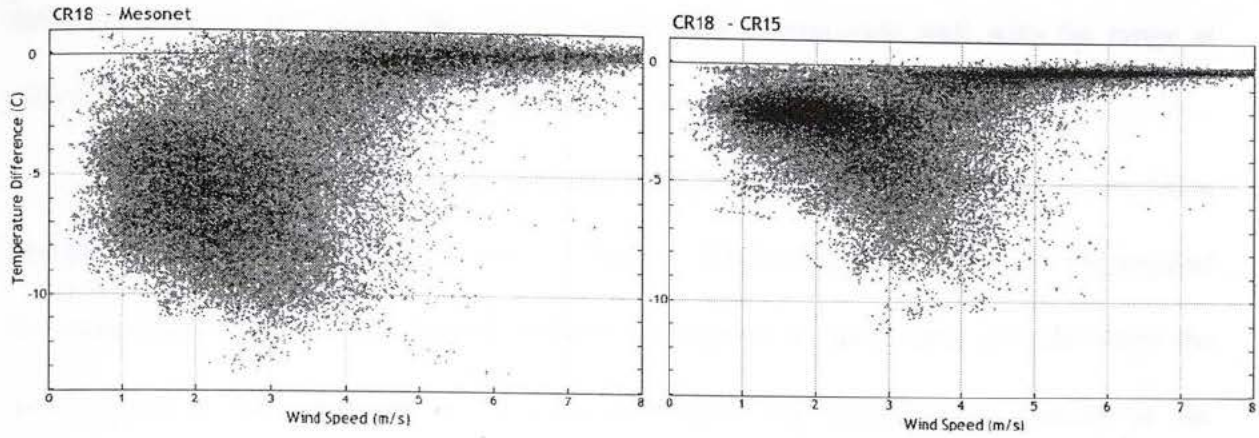

Figure 4.6. Nighttime temperature anomalies at CR18 and temperature differences between CR18 and CR15 as a function of mesoscale wind speed; approximately 75,000 observations were used to generate each plot.

A few of the largest nighttime temperature anomalies at CR18 occurred with mesoscale wind speeds above 5 m s^{-1} (Fig. 4.6). Temperature anomalies greater than 10°C were most common with mesoscale wind speeds of 2.5-4 m s^{-1}. Anomalies of this magnitude did not occur with mesoscale winds below 1.5 m s^{-1}, presumably because the surface energy balance across the domain is relatively uniform on nights with such weak wind. When the mesoscale wind speed was above 6 m s^{-1}, the temperature anomaly at the Micronet was virtually non-existent (Fig. 4.6).

Temperature differences across the Micronet reveal a clearer pattern. When the mesoscale wind speed is less than 2.5 m s^{-1}, this temperature difference is usually 1-3°C. With mesoscale wind speeds above 6 m s^{-1}, there is virtually no temperature difference across the Micronet. But with mesoscale wind speeds of 2.5-4.5 m s^{-1}, the temperature difference can be significantly higher than when the mesoscale wind speed is above or

below that range (Fig. 4.6). The 2.5-4.5 m s^{-1} range corresponds well with the range at which the USL is common at CR18 and relatively rare at CR17 (Fig. 4.4).

Sometimes the temperature gradient across the Micronet is minimal even when the mesoscale wind speed is between 2.5-5 m s^{-1}. Most of these observations correspond to cloudy and partly cloudy nights. Others correspond to short time periods when the wind speed at the surrounding Mesonet sites does not represent the forcing at the Crosstimber Micronet (e.g., when a substantial change in wind speed is occurring across central Oklahoma).

Large temperature differences across the Micronet (i.e., greater than 7°C) have not been observed with mesoscale wind speeds less than 2 m s^{-1}; yet the largest temperature differences occurred when the mesoscale wind speed was near 3 m s^{-1}. Thus, a slight change in mesoscale wind speed from 2 m s^{-1} to 3 m s^{-1} can have a strong impact on the temperature gradient across the Micronet.

Anomalies created by cold air drainage or most forms of in-situ cooling are expected to be strongest at the lowest wind speeds. Thus, the absence of large temperature anomalies at the Micronet on nights with relatively weak wind is not consistent with these processes as the origin of the temperature anomalies. However, the mesoscale wind speeds at which the largest temperature differences do occur (i.e., 2.5-4.5 m s^{-1}) support Proposition 2, which states that temperature anomalies at the Micronet are primarily created by the presence of the USL at the Micronet and absence of the USL at the surrounding Mesonet sites.

4.3. Case Studies

a) Nights when the USL is not present

On clear nights when the mesoscale wind speed is greater than 5 m s^{-1}, the USL does not develop at the Crosstimber Micronet (Figs. 4.7-4.8).

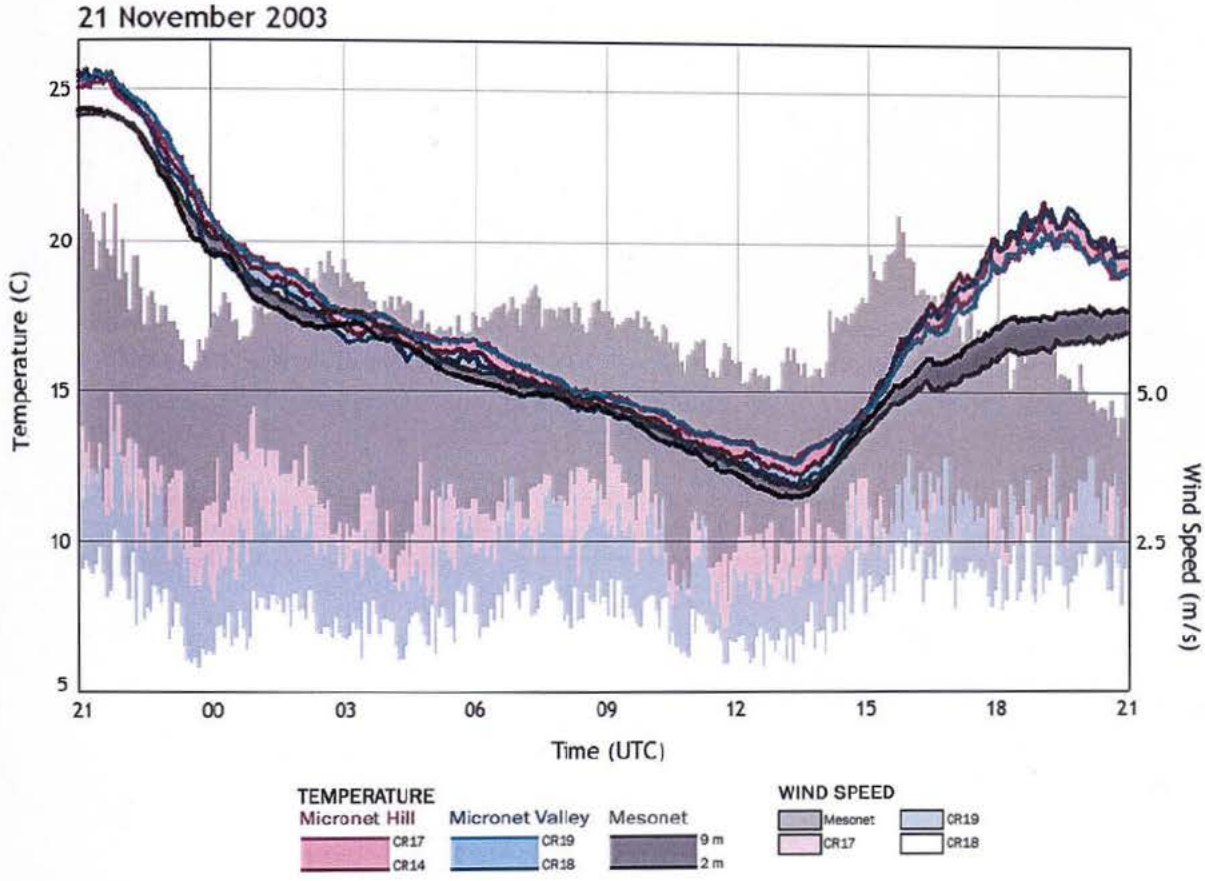

Figure 4.7. Temperature and wind speed at Micronet and Mesonet sites on 12 November 2003.

On these nights, temperatures were nearly uniform across the domain. Larger vertical and horizontal temperature gradients were observed during the afternoon than at night, especially on 21 November 2003 (Fig. 4.7). Shortly after sunset on 24 August 2004 (Fig. 4.8), when the mesoscale wind speed dropped below 5 m s^{-1}, the USL began to

develop at CR18. But when the mesoscale wind speed increased, the USL at CR18 was destroyed. Thus, only the ASBL was present at all locations in the domain.

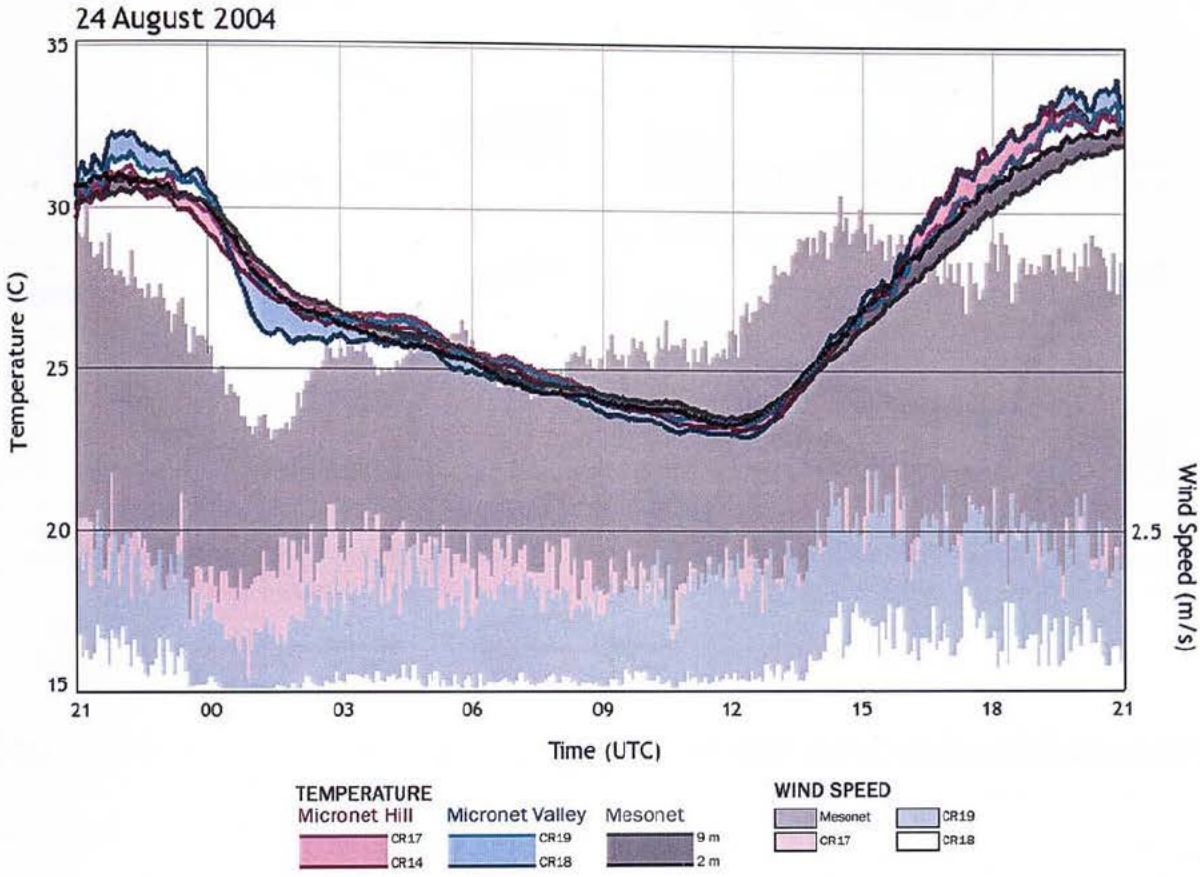

Figure 4.8. Temperature and wind speed at Micronet and Mesonet sites on 24 August 2004.

b) Nights when the USL is present across the entire Micronet

On nights with sufficiently weak mesoscale winds (i.e., less than 2.5 m s^{-1}), the USL developed across the entire Micronet (i.e., observed wind speeds across the Micronet were less than 0.1 m s^{-1}), including CR17 which is located at a height of 9 m above ground level near the top of the hill (Fig. 4.9). Temperature differences between the Micronet and surrounding Mesonet sites were large (i.e., greater than 5°C), but temperature differences across the Micronet were relatively small.

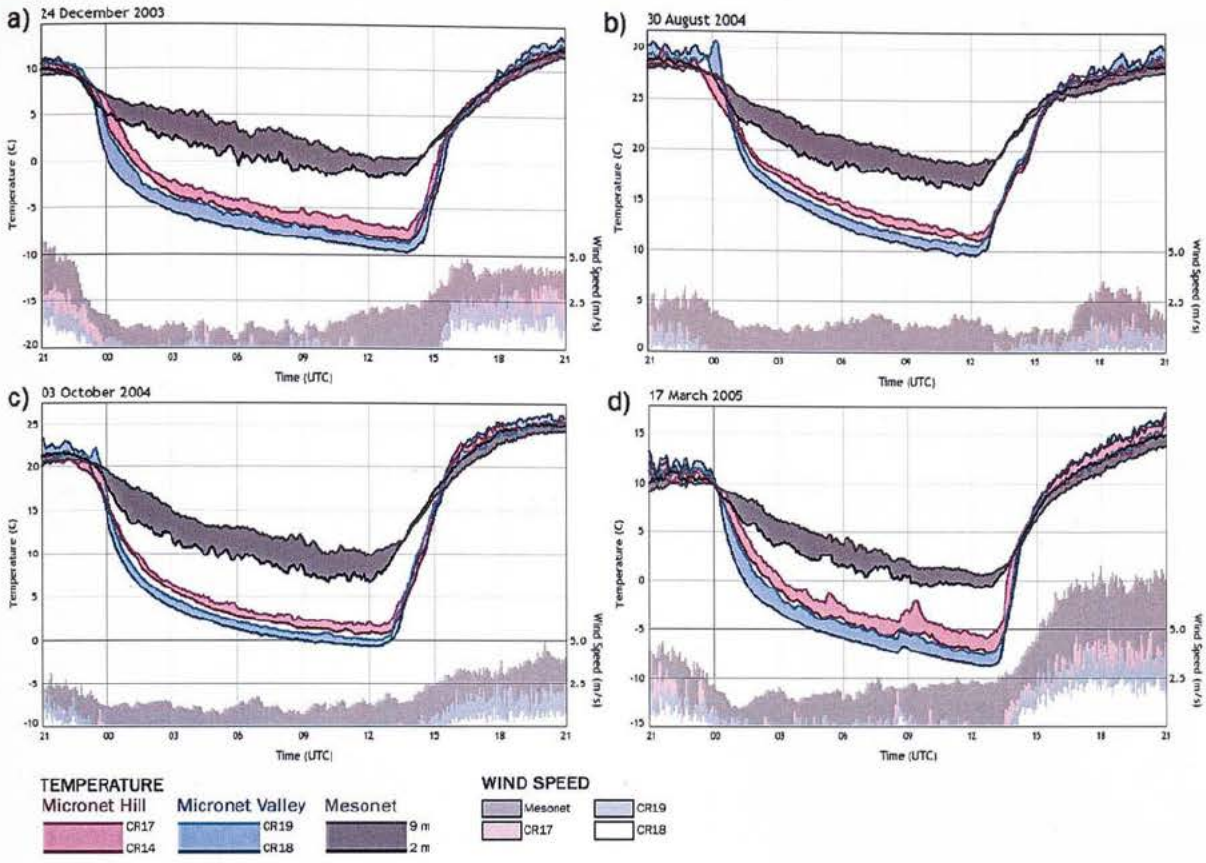

Figure 4.9. Temperature and wind speed on selected clear nights when a USL developed across the entire Micronet.

On these nights, wind speeds were less than 0.1 m s^{-1} at CR18, CR19, and CR17, while wind speeds generally were between 1-2.5 m s^{-1} at the surrounding Mesonet sites. Thus, the USL was present at the Micronet sites but not at the Mesonet sites. The impact of the unique energy balance of the USL is very clear. With the absence of sensible and latent heat fluxes, temperatures at the Micronet sites were significantly (i.e., more than 5°C) lower than at the surrounding Mesonet sites. However, the 2-9 m inversions were stronger at the Mesonet sites (dark gray shading in Fig. 4.9) than at the Micronet sites (pink and blue shading), except on 17 March 2005 when the mesoscale wind was slightly

stronger than during the other three nights (Fig. 4.9d). Thus, the observations from these four cases strongly support Propositions 1-2.

c) Nights when the USL is present only across part of the Micronet

On nights with mesoscale wind speeds between 2.5-5 m s^{-1}, the USL developed across the lower elevations of the Micronet but not at the higher elevations (Fig. 4.10). Very large temperature anomalies and strong near-surface temperature gradients were observed at the Micronet on these nights.

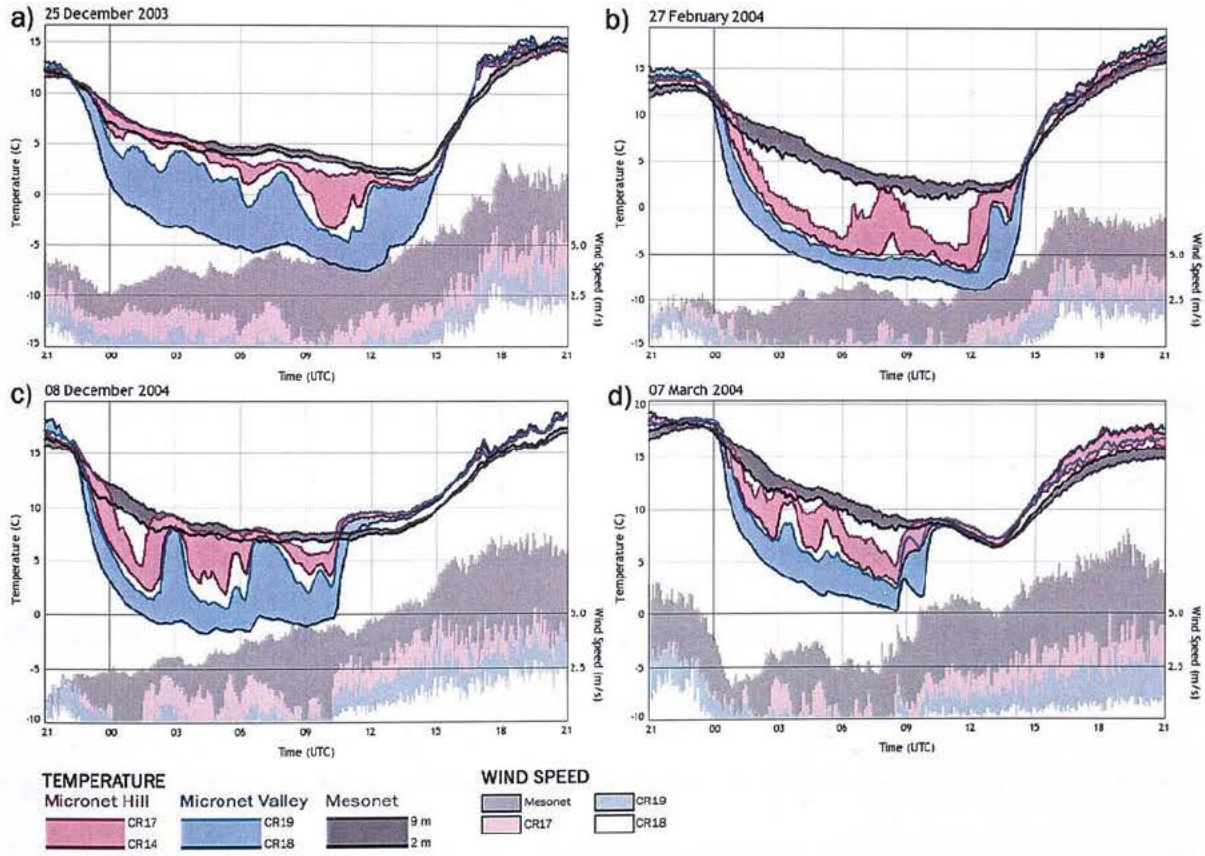

Figure 4.10. Temperature and wind speed on clear nights when a USL developed across only part of the Micronet.

On 27 February 2004 (Fig. 4.10b), the mesoscale wind speed was weaker than on the other three nights shown in Fig. 4.10. From 0000 UTC to 0600 UTC, the USL was present across the entire Micronet. But after 0600 UTC, the mesoscale wind speed increased above 2.5 m s^{-1}. During the next three hours, the enhanced wind shear eroded the USL at the highest elevations of the Micronet. The temperature at CR17 was significantly (i.e., more than 5°C) higher than at CR18, and nearly equal to the temperature at the surrounding Mesonet sites where the USL was not present.

On 8 December 2004 and 7 March 2004, at approximately 1100 UTC, the mesoscale wind speed increased above 4-5 m s^{-1} and the wind speed observed at CR18 became nonzero (Fig. 4.10c-d). Thus, the USL dissipated at the Micronet after 1100 UTC on those nights. The critical mesoscale wind speed (i.e., the wind speed at which the USL could no longer exist at the Micronet) was approximately 5 m s^{-1}. The results are consistent with Fig. 4.4, which suggests that the optimal mesoscale wind speed for a partial USL at the Micronet is between 2.5-5 m s^{-1}. Furthermore, the results support Proposition 3.

On 25 December 2003, the mesoscale wind speed was between 2.5-5 m s^{-1} during the entire night (Fig. 4.10a). The USL developed at CR18, but not at CR17. Consequently, the temperature at CR18 was approximately 10°C cooler than at the surrounding Mesonet sites, while the temperature at CR17 was nearly equal to the temperature at the Mesonet sites. At intermediate heights, such as at CR19 (light blue line) and CR14 (dark red line), the temperature oscillated throughout the night.

The oscillation was similar to that observed by Van der Wiel et al. (2003). For short periods of time on 25 December 2003, the USL grew sufficiently deep to impact

CR19 and CR14, but shortly thereafter, its depth was reduced by strong vertical wind shear. This process was repeated throughout the night. Similar temperature oscillations were observed on 8 December 2004 and 7 March 2004 (Fig. 4.10c-d). The local oscillations suggest that the vertical and horizontal gradients of temperature and wind speed were very high near CR19 and CR14. Furthermore, the relatively moderate temperatures observed at those sites indicate that a mixture of air from the USL and ASBL was present. Thus, one can conclude that CR19 and CR14 were located in the capping inversion layer (CIL), which is defined to contain a mixture of air from the USL and ASBL.

Oscillations at CR18 (Fig. 4.11) are common on nights with slightly stronger mesoscale winds than observed in the previous cases. On these nights, the CIL was located near 2 m above ground level at CR18. The vertical wind shear was too strong to allow the USL to exist for several hours, but too weak to prevent the USL from developing.

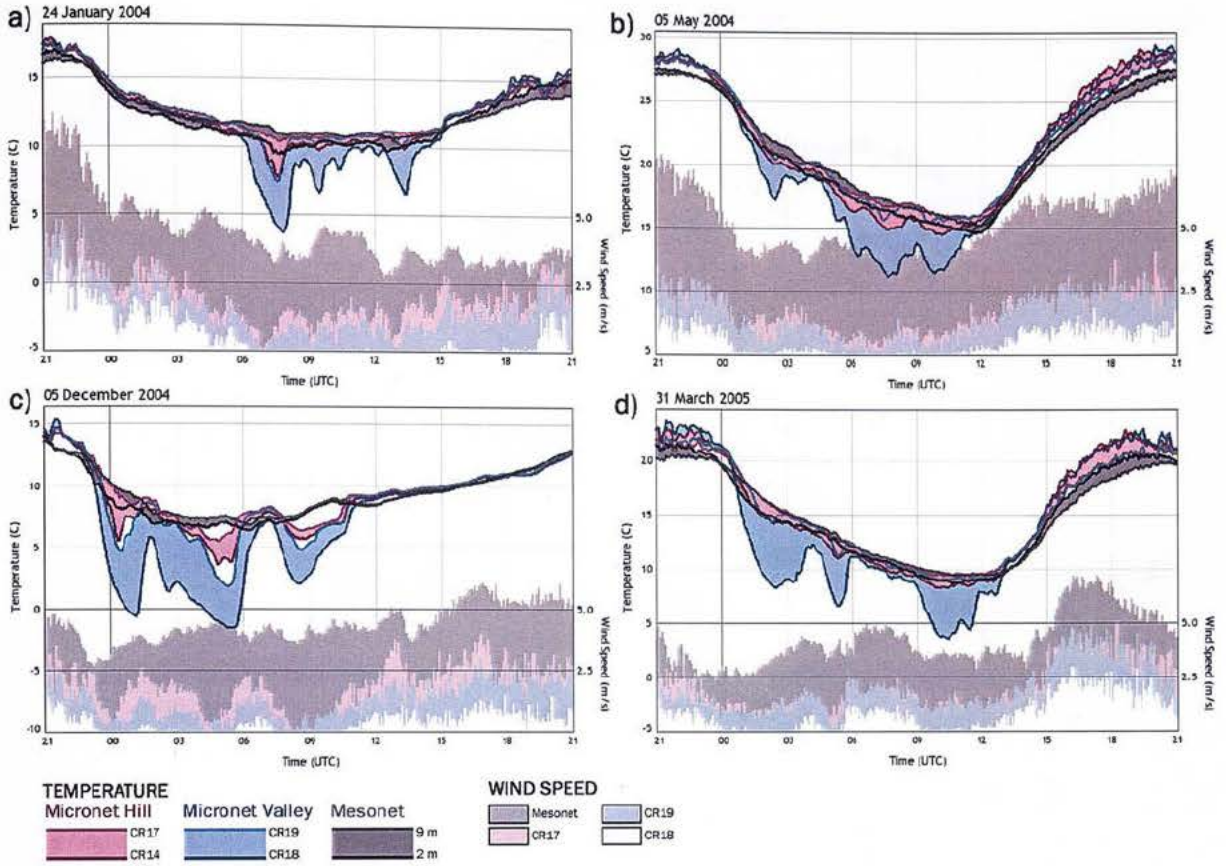

Figure 4.11. Temperature and wind speed on selected clear nights when a USL developed intermittently at CR18.

On nights when the mesoscale wind speed changed substantially, dramatic changes occurred within the near-surface boundary layer at the Micronet (Fig. 4.12).

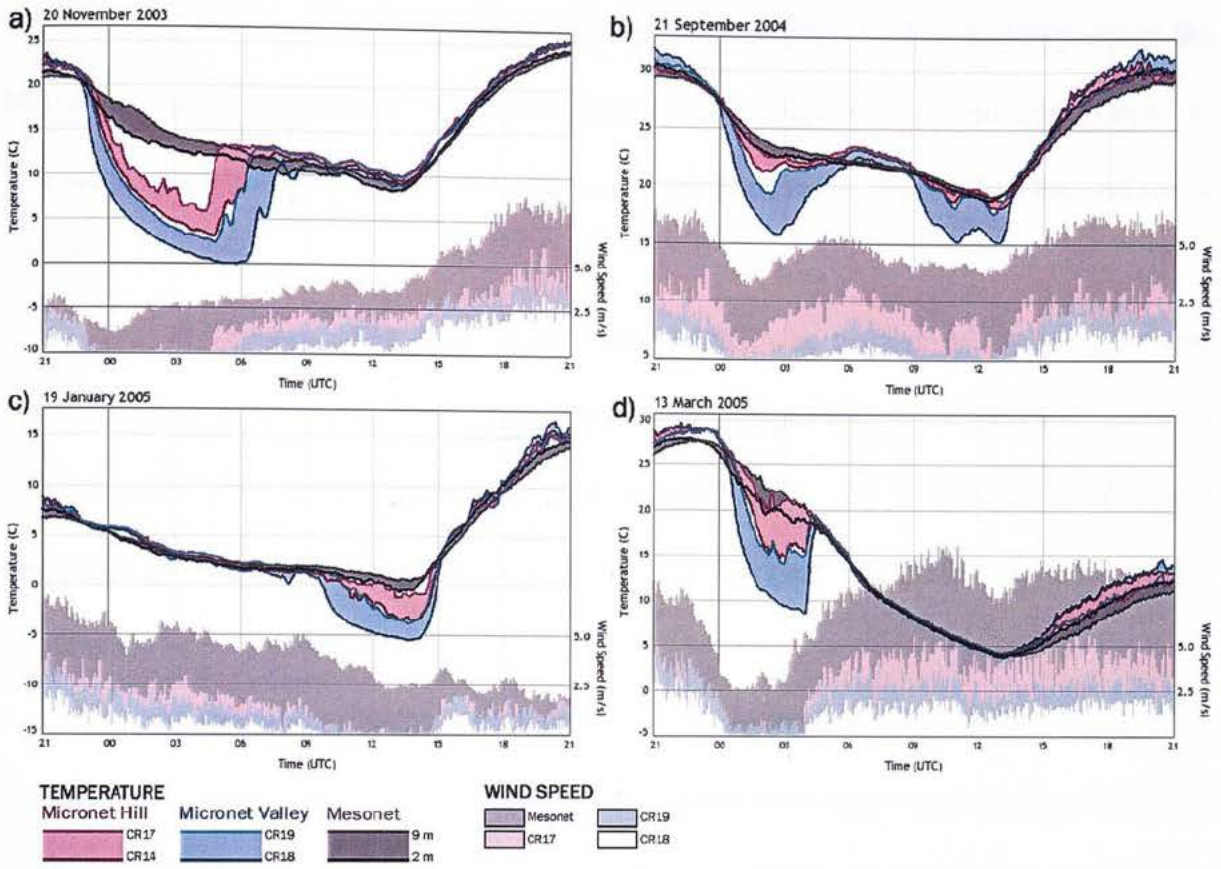

Figure 4.12. Temperature and wind speed on selected clear nights when substantial changes occurred in the mesoscale wind speed.

On 20 November 2003 (Fig. 4.12a), the mesoscale wind speed slowly increased throughout the night. From 2300-0400 UTC, the USL was present across the entire Micronet but not at the Mesonet sites. The Micronet was nearly 10°C cooler than the surrounding Mesonet sites, but the temperature variation across the Micronet was relatively small (i.e., less than 5°C). At 0430 UTC, when the mesoscale wind speed increased above 2.5 m s^{-1}, the USL became limited to the lower elevations of the Micronet, and the temperature variation across the Micronet increased significantly. At 0600 UTC, the temperature difference between CR18 and CR14 (approximately 150 m apart) was an astonishing 10°C.

On 13 March 2005 (Fig. 4.12d), the USL existed over the lower elevations of the Micronet. Between 0300-0500 UTC, the mesoscale wind speed increased from 3 m s^{-1} to 7 m s^{-1}. During that period, the USL dissipated and the ASBL approached the surface at CR18.

On 19 January 2005 (Fig. 4.12c), the ASBL was present at all Mesonet and Micronet sites during most of the night. Thus, temperature differences between Micronet and Mesonet sites were minimal. But after 0900 UTC, the mesoscale wind speed decreased to less than 4 m s^{-1}, which allowed the USL (and relatively large temperature gradients) to develop at the Micronet.

On 21 September 2004 (Fig. 4.12b), the mesoscale wind was strongest during the middle of the night (i.e., 0400-0900 UTC) and weaker near sunset and sunrise. Thus, the USL was present at the Micronet near sunrise and sunset but not during the middle of the night.

4.4. Other Impacts of the USL

The presence of the USL and CIL also impacts other near-surface atmospheric parameters such as dewpoint and carbon dioxide (CO_2) concentrations. Gasses such as water vapor and CO_2 are released from the surface through the soil and vegetation. At exposed locations such as the Mesonet sites, these gasses are transported to higher levels by turbulence in the ASBL. Air with lower concentrations of these gases is transported to the surface. But in the USL, the lack of turbulence prevents the vertical mixing of gasses to higher levels of the nocturnal boundary layer. The capping inversion layer (CIL) also inhibits vertical transport. Thus, gasses released near the surface are trapped in the USL.

Compared to the surrounding Mesonet sites, the diurnal range of dewpoint is larger at the Micronet (Fig. 4.13).

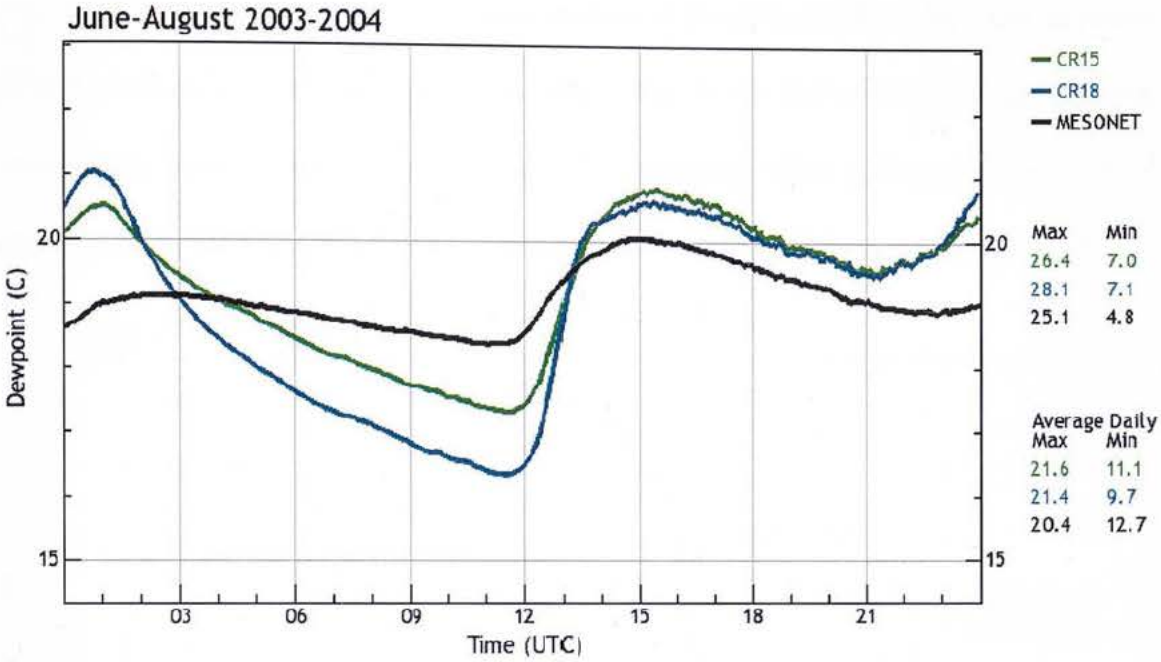

Figure 4.13. Average diurnal cycle of dewpoint on clear days at CR15 (green), CR18 (blue), and the five surrounding Mesonet sites (black; June-August 2003-2004).

During June-August, when the Micronet is greener than the surrounding Mesonet sites, the average afternoon dewpoint is 0.5-1°C higher at the Micronet than at the surrounding Mesonet sites. But near sunset, the average dewpoint is 1.5-2°C higher at the Micronet. The large increase of the dewpoint near sunset at the Micronet indicates that water vapor is being trapped in the USL. This increase of the dewpoint supports Proposition 4.

During the night, the average dewpoint at the Micronet decreases to become 1-2°C lower than observed at surrounding Mesonet sites. The relatively sharp decrease of the dewpoint during the night at the Micronet is caused by condensation (Haugland and

Crawford 2005). More condensation occurs at the Micronet than at surrounding Mesonet sites because of the relatively low temperature at the Micronet.

Like water vapor, the CO_2 concentration at the Crosstimber Micronet increases significantly near sunset as the USL develops (Fig. 4.14). But unlike the concentration of water vapor (represented by the dewpoint temperature), which is strongly impacted by condensation, the CO_2 concentration remains relatively high throughout the night.

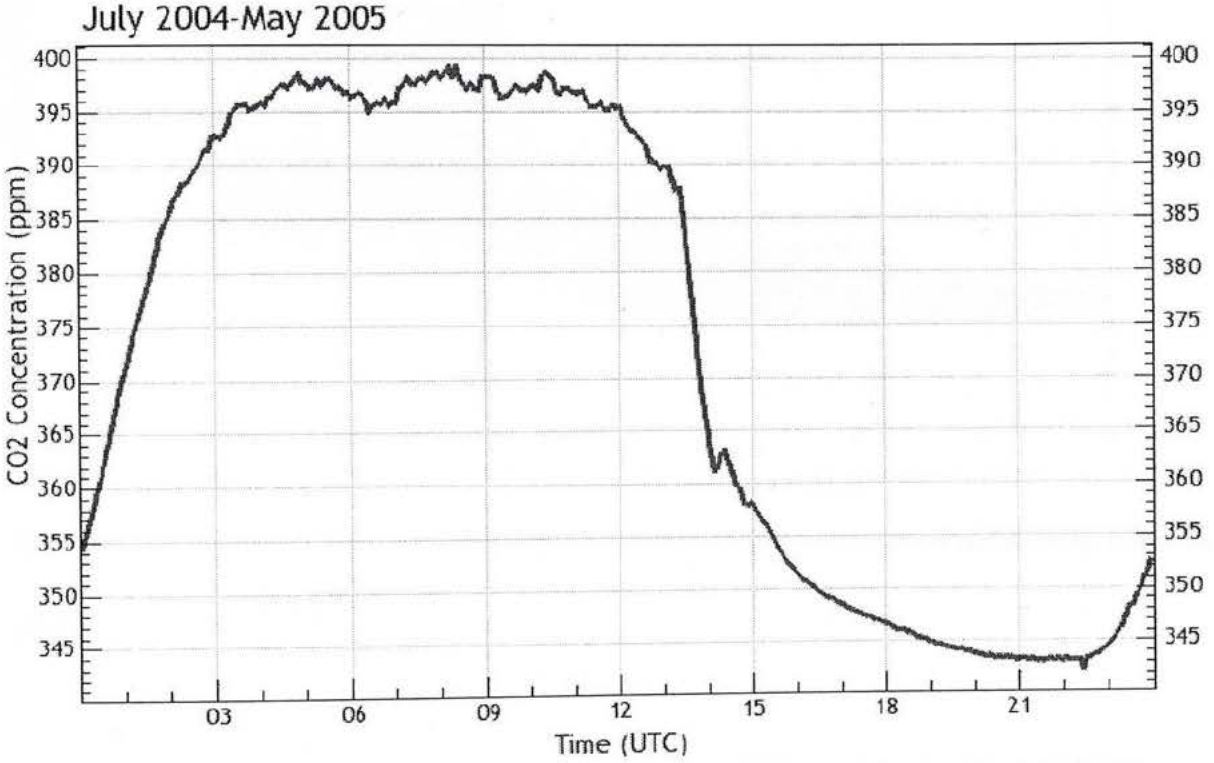

Figure 4.14. Average diurnal cycle of CO_2 concentration on clear days at CR18 (July 2004-May 2005).

As with the nighttime temperature, the CO_2 concentration at CR18 on clear nights is strongly related to the mesoscale wind speed (Fig. 4.15). When the mesoscale wind speed is above 4 m s^{-1}, the nighttime CO_2 concentration at CR18 usually is between 340-380 ppm. But when the mesoscale wind speed is less than 4 m s^{-1}, the nighttime CO_2

concentration at CR18 becomes much more variable and generally much higher (i.e., it ranges between 380-550 ppm).

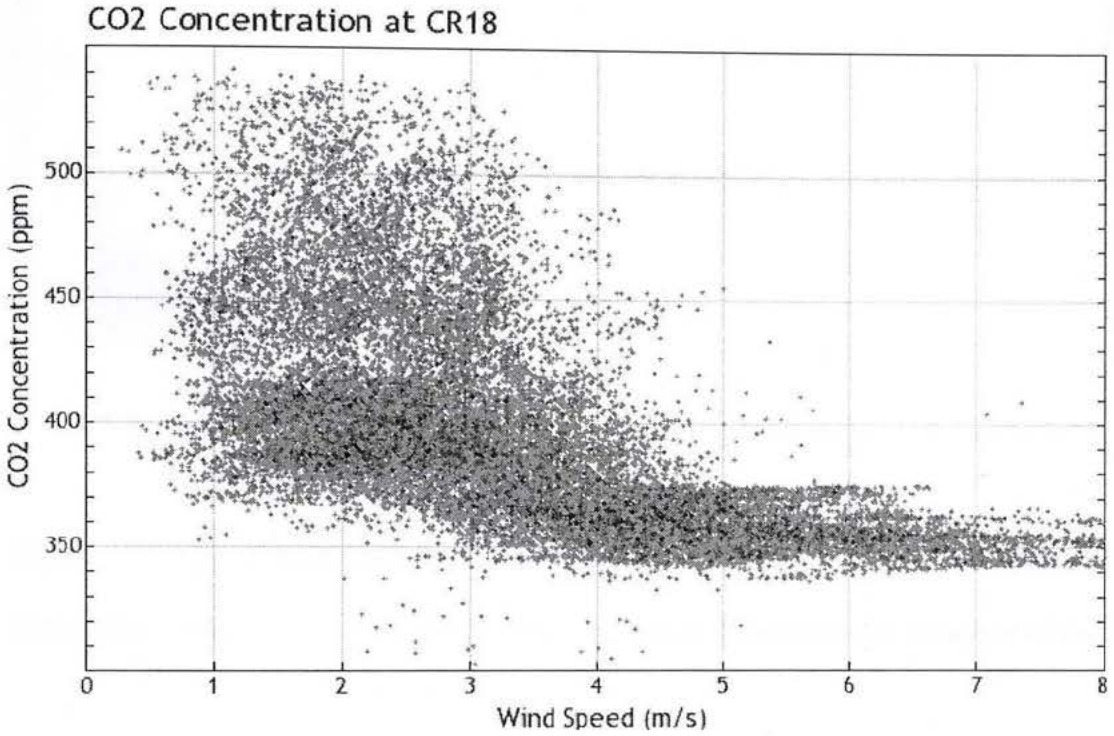

Figure 4.15. Nighttime concentration of CO_2 at CR18 as a function of mesoscale wind speed (July 2004-May 2005).

High concentrations of CO_2 (i.e., greater than 380 ppm) during the nighttime hours at CR18 correspond nearly perfectly with the presence of the USL (Fig. 4.16).

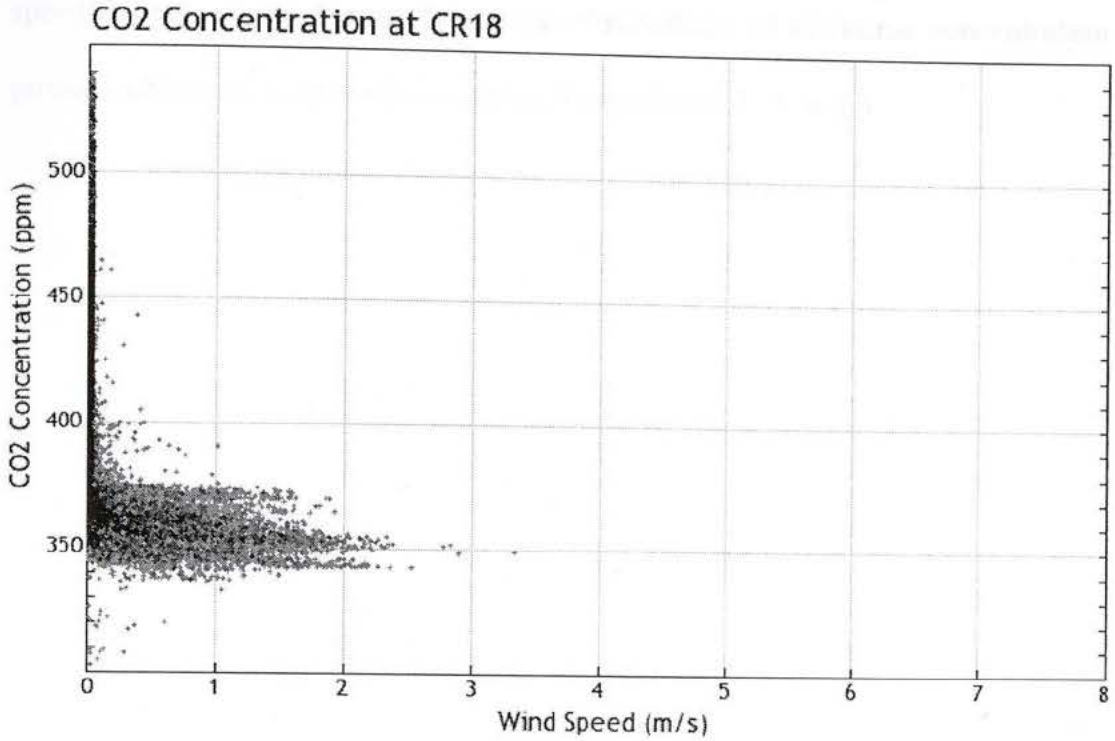

Figure 4.16. CO_2 concentration on clear nights at CR18 as a function of wind speed at CR18 (July 2004-May 2005). Wind speed values of 0 indicate the presence of the USL.

When the USL is not present at CR18 (i.e., when the wind speed observed at CR18 is greater than 0.1 m s^{-1}), the nighttime concentrations of CO_2 are usually between 340-380 ppm (Fig. 4.16). The CO_2 concentration at CR18 rarely exceeds 380 ppm unless the USL is present. However, if the USL is periodically present, huge variations in the concentrations of CO_2 are observed (a range between 340-550 ppm shown in Fig. 4.15).

Though CO_2 is not measured at the surrounding Mesonet sites, it is likely that the CO_2 concentration on clear nights at the surrounding Mesonet sites is similar to that observed at CR18 when the USL is not present (i.e., between 340-380 ppm). The strong relationship between CO_2 and the USL presence suggests that large CO_2 gradients of the CO_2 concentration exist across the Micronet on clear nights when the mesoscale wind

speed is between 2.5-5 m s^{-1}. Thus, the observations of nighttime concentration of CO_2 provide additional support for accepting Propositions 1, 3, and 4.

5. Model Description

The Uncoupled Surface Layer (USL) model is designed to predict near-surface temperatures between sunset and sunrise on clear nights. It is a physical model based on the surface energy budget. The key difference between the USL model and other surface energy budget models is that it represents the three-layer framework of the near-surface nocturnal boundary layer described in Chapters 1-4.

Unlike most models presented in the scientific literature (i.e., those based on Monin-Obukhov similarity theory), the USL model recognizes the distinct impacts of the non-turbulent uncoupled surface layer (USL), the quasi-turbulent capping inversion layer (CIL), and the turbulent ambient stable boundary layer (ASBL).

The primary function of the USL model is to predict temperatures within the non-turbulent USL. Thus, the model is primarily thermodynamic rather than dynamic. Dynamic processes, such as entrainment of relatively warm air from the ASBL, are parameterized. These parameterizations are based on observations from the Crosstimber Micronet.

For this study, the model will output temperature forecasts at 1.5 m above ground level (AGL) at three forecast sites: CR18 at the Micronet, the El Reno Mesonet station in west-central Oklahoma, and an agricultural station in Madera, California (Fig. 5.1).

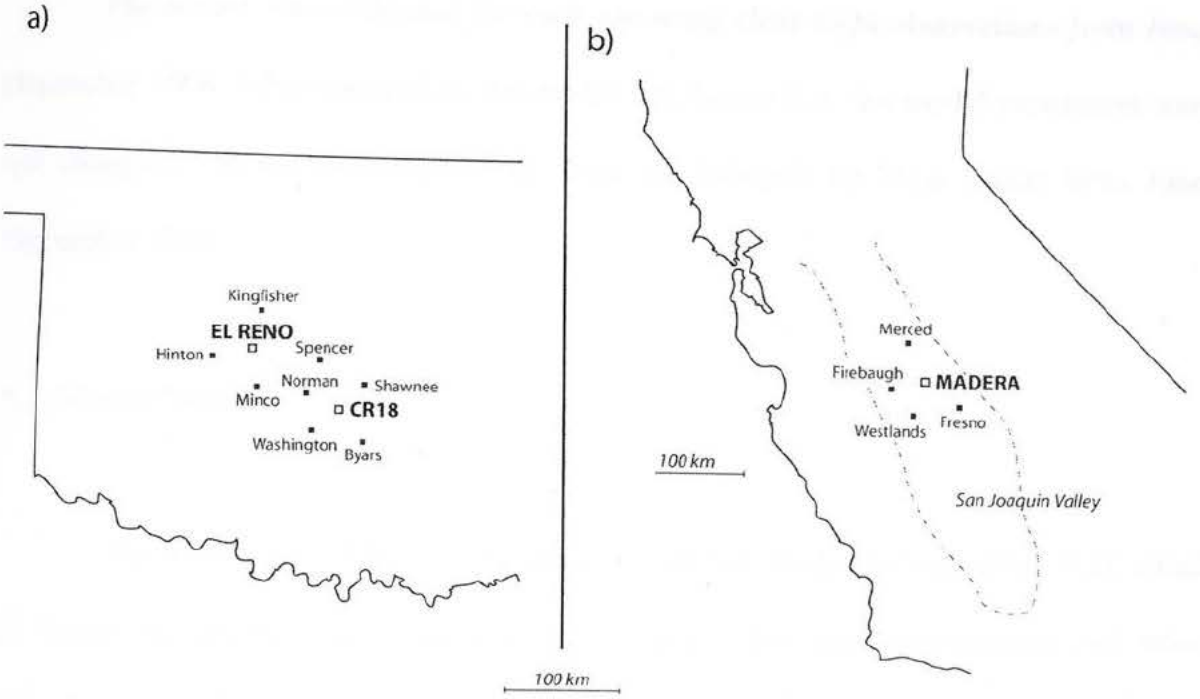

Figure 5.1. Maps of forecast sites and surrounding stations for (a) CR18 and El Reno, Oklahoma and (b) Madera, California.

The El Reno Mesonet site is located in central Oklahoma, approximately 40 km west of Oklahoma City. The terrain around the site is flatter than at the Crosstimber Micronet, yet has sufficient terrain relief to reduce turbulent mixing on some clear nights (Hunt et al. 2005). The Madera site is part of a surface observation network known as the California Irrigation Management Information Systems (CIMIS) network, which uses instruments similar to those within the Oklahoma Mesonet and Crosstimber Micronet (CIMIS 2005). Madera is located near the center of the San Joaquin Valley in central California, approximately 40 km northwest of Fresno. The San Joaquin Valley is extremely flat compared to central Oklahoma. The Madera CIMIS site is situated on a relatively low flood plain, but otherwise, the vegetation and terrain around the site are typical of the region.

The model was calibrated for each site using clear-night observations from June-December 2004. After calibration, the model was frozen (i.e., the model parameters were not changed). Model performance is based on forecasts for clear nights from June-December 2005.

5.1. Model Physics

The foundation of the USL model is the surface energy balance (Eqn. 5.1), which is based on the law of conservation of energy. The parameterizations and other calculations performed by the model are designed to estimate the terms in this equation.

$$R_{net} + H + LE + G + \Delta Q = 0\,, \tag{5.1}$$

where R_{net} is net radiation, H is sensible heat flux, LE is latent heat flux, G is ground heat flux, and ΔQ is the net heat storage within the "surface" interface layer.

The model regards the "surface" as an interface layer that spans the ground/air interface and includes soil, vegetation, and air. This definition of the surface has been used successfully in other modeling studies (e.g., Blackadar 1976; Deardorff 1978; Wetzel 1978; Tremback and Kessler 1985; Sellers et al. 1986). The interface layer as represented in the USL model extends from 0.02 m below ground level (BGL) to 0.5 m above ground level (AGL). The depth below ground was selected such that the average temperature across the below-ground portion of the interface layer is approximately equal to the average temperature across the above-ground portion. The average temperature across the entire interface layer (i.e., "surface temperature"; T_{sfc}) is calculated from the following formula:

$$\frac{\partial T_{sfc}}{\partial t} = \frac{1}{\rho c \Delta z}\left[R_{net} - (H + LE + G)\right], \tag{5.2}$$

where:

$\frac{\partial T_{sfc}}{\partial t}$ is the time rate of change of the "surface" temperature.

ρ is the mean density of the "surface" (interface layer).

c is the mean specific heat of the "surface" (interface layer).

Δz is the depth of the "surface" (interface layer).

The density, specific heat, and depth of the interface are prescribed in the model. The density of the interface layer, which is composed of approximately 4% soil and 96% air by volume, is regarded as a constant (i.e., 50 kg m^{-3}) at each site. The specific heat of the interface layer depends on the forecast site and is derived from temperature observations (i.e., estimated from the cooling rate shortly after sunset) during the calibration period. This value was regarded as a constant (i.e., 1100 J kg^{-1} K^{-1}) throughout the year. A sensitivity analysis confirmed that this was an acceptable simplification (Chapter 6.2; Table 6.6).

With these values prescribed, the USL model predicts the temperature by estimating the remaining terms (i.e., the components of the surface energy balance). Because the model is designed to predict only nighttime temperatures, shortwave radiation is neglected. The net radiation at the surface is determined by the incoming and outgoing longwave radiation components. Incoming longwave radiation is emitted by the ASBL and also by the CIL and USL if the wind speed is sufficiently weak to allow those

layers to develop. Thus, the individual contribution by each layer to the net radiation at the surface is calculated. The equation for net radiation is expanded to:

$$R_{net} = \omega_{ASBL} LW_{\downarrow ASBL} + \omega_{CIL} LW_{\downarrow CIL} + \omega_{USL} LW_{\downarrow USL} - LW_{\uparrow sfc}, \quad (5.3)$$

where:

ω_{ASBL} is the longwave contribution parameter of the ASBL.

ω_{CIL} is the longwave contribution parameter of the CIL.

ω_{USL} is the longwave contribution parameter of the USL.

σ is the Steffan-Boltzmann constant, 5.67 x 10^{-8} W m^{-2} K^{-4}.

$LW_{\downarrow ASBL} = \varepsilon_{ASBL} \sigma T_{ASBL}^4$ is the incoming longwave radiation from the ASBL. T_{ASBL} is the temperature at the bottom of the ASBL and ε_{ASBL} is the emissivity of air in the ASBL.

$LW_{\downarrow CIL} = \varepsilon_{CIL} \sigma T_{CIL}^4$ is the incoming longwave radiation from the CIL. T_{CIL} is the mean temperature within the CIL, which is taken as the mean of the ASBL and USL temperatures.

$LW_{\downarrow USL} = \varepsilon_{USL} \sigma T_{USL}^4$ is the incoming longwave radiation from the USL.

$LW_{\uparrow sfc} = \varepsilon_{sfc} \sigma T_{sfc}^4$ is the outgoing longwave radiation from the surface.

The longwave contribution parameters ($\omega_{ASBL}, \omega_{CIL}, \omega_{USL}$) determine how much each layer contributes to the net radiation at the surface. Under windy conditions when the USL is not present, ω_{USL} has a value of 0 and ω_{CIL} has a value that is inversely proportional to the wind speed. The value of ω_{ASBL} depends on the temperature and mixing ratio, which affect the depth from which radiation is received at the surface. The

values are scaled such that the total contribution from the three layers (i.e., $\omega_{ASBL} + \omega_{CIL} + \omega_{USL}$) is always equal to 1.

The emissivity of each layer is regarded as a function of the mean temperature and dewpoint within the layer. This assumption has been incorporated in numerous modeling studies. Several empirical emissivity functions were tested (e.g., Berdahl and Fromberg 1982; Martin and Berdahl 1984; Clark and Allen 1985; Walton et al. 1985; Chen et al. 1991; Prata 1996). An average of the functions obtained by Clark and Allen (1985) and Chen et al. (1991) was selected because it produced the most accurate forecasts with the USL model.

Because the model is not designed to predict vertical profiles of temperature near the ground and net radiation is only observed at one height by the Micronet and Mesonet, net radiation is simplified as constant with height within the interface layer. Divergence of net radiation, which can be a significant source of cooling near the ground (Funk 1960; Grant and Brost 1981), is implicitly represented via the ΔQ term.

The wind speed at the forecast site is determined by the initial mesoscale wind speed (i.e., the observed wind speed shortly before sunset at the stations that surround the forecast site). Observations from across the country have shown that the wind speed at most locations decreases after sunset (National Diurnal Climatology 2004). Thus, the wind speed observed shortly before sunset, which is used as an initial condition in the USL model, generally is too strong to represent the mesoscale wind speed during the night.

To correct this problem, the nighttime wind reduction parameter (λ) was introduced. This parameter represents the reduction of the near-surface wind speed by

stable stratification of the boundary layer. It is regarded as a constant with a value of 0.67. This value was derived from observations of wind speed on clear nights at the Crosstimber Micronet and surrounding Mesonet sites. These observations showed that the mean overnight wind speed was approximately 33% weaker than the wind speed observed shortly before sunset. Hence, λ was determined to be 0.67.

Crosstimber Micronet observations have shown that the wind at a sheltered location can be substantially weaker than the mesoscale wind speed across the region (Fig. 4.3). Thus, the mesoscale wind speed may not accurately represent the wind speed at the forecast site. To address this problem, the sheltering parameter (ζ) was introduced.

$$\zeta = \frac{u_{meso}}{u_{site}}, \tag{5.4}$$

where u_{meso} is the (climatological) average nighttime mesoscale wind speed and u_{site} is the average nighttime wind speed at the forecast site. The sheltering parameter is analogous to the efficiency of a windbreak (Rosenberg 1974; Skidmore 1986). The value of ζ is equal to 1 at flat, open locations where the wind speed is approximately equal to the mesoscale wind speed. At elevated locations, where the local wind is relatively strong, the value of ζ is less than 1. At sheltered locations such as CR18, ζ is greater than 1. The sheltering parameter is expected to depend on the surrounding terrain, height of surrounding vegetation or other obstructions, wind speed, and wind direction. In the USL model, it is regarded as a constant at each forecast site. A sensitivity analysis suggested that this was an acceptable simplification (Chapter 6.2; Table 6.5).

Using these corrections, the overnight wind speed at the forecast site is calculated from:

$$u = \frac{\lambda u_{meso}}{\zeta}, \tag{5.5}$$

where u is the wind speed at the forecast site, u_{meso} is the initial mesoscale wind speed, λ is the nighttime wind reduction parameter, and ζ is the sheltering parameter. The sheltering parameter was placed in the denominator to maintain the physical interpretation of the parameter (i.e., that larger values represent stronger sheltering).

Ground Heat Flux is calculated from:

$$G = k_{soil} \frac{\partial T_{soil}}{\partial z}, \tag{5.6}$$

where k_{soil} is the thermal conductivity of the soil. A simple one-layer soil scheme is used to represent the sub-surface conditions. The vertical temperature gradient within the soil is determined by the temperature difference between the surface and the soil at 0.1 m BGL (0.15 m BGL for the Madera site). The initial ground heat flux is calculated from the initial observations of soil and surface temperatures. Then the soil temperature for the next time step is calculated from:

$$\frac{\partial T_{soil}}{\partial t} = \frac{1}{\rho c} \frac{\partial G}{\partial z}, \tag{5.7}$$

where ρ, c are the density and specific heat of the soil layer, respectively. For this study, the three forecast sites were considered to have identical soil properties. A sensitivity analysis confirmed that this was an acceptable simplification (Chapter 6.2; Table 6.7).

Because the model is intended to forecast temperature only, fluxes of sensible and latent heat are not considered individually. Both are assumed to be zero within the USL because turbulence within this layer is negligible. When entrainment of air from the ASBL occurs, the combined flux is calculated from:

$$H + LE = \mu\alpha\left(T_{ASBL} - T_{sfc}\right), \tag{5.8}$$

where μ is the ASBL mixing parameter and α is an empirical constant that represents the energy required to heat the USL by entrainment of relatively warm air from the ASBL. The value of α is taken as 45 W m^{-2} K^{-1}, which was determined from Crosstimber Micronet observations (i.e., estimated from the rate of change in observed surface temperature when air from the ASBL penetrated into the USL).

One of the key parameters in the USL model is the ASBL mixing parameter (μ). This parameter determines whether the USL, CIL, or ASBL is present at the surface. It is defined as the proportion of air at a given height (e.g., 1.5 m AGL) that is entrained from the ASBL. The value of μ is 1 within the ASBL, 0 within the USL, and varies between 0-1 within the CIL. The ASBL mixing parameter is a function of the wind speed at the forecast site. This function is based on observations at the Crosstimber Micronet (Fig. 4.4; Fig. 4.5).

It follows from Equation 5.7 that fluxes of latent and sensible heat are zero when the USL is present (i.e., when $\mu = 0$). If the near-surface air becomes fully turbulent (i.e., μ reaches 1), turbulence heats the surface until it reaches the temperature of the ASBL. These properties of Equation 5.7 are consistent with the observations presented in Chapter 4.

The initial temperature of the ASBL is set equal to the initial temperature observed at 1.5 m AGL. It is assumed that the rate of change of the ASBL temperature is proportional to the net radiation at the surface and is inversely proportional to the heat capacity of air in the ASBL. The constant of proportionality is called the ASBL cooling efficiency (η).

The ASBL cooling efficiency is the proportion of net radiation that is partitioned to cool the ASBL (i.e., sensible heat flux at the bottom of the ASBL). The net radiation at the bottom of the ASBL is approximated as equal to the net radiation at the surface. Thus, the temperature of the ASBL is approximated by:

$$\frac{\partial T_{ASBL}}{\partial t} = \frac{\eta R_{net}}{\rho c}, \tag{5.9}$$

where η is the ASBL cooling efficiency, ρ is the density of air in the ASBL, and c is the specific heat of air in the ASBL.

At the forecast sites used in this study, the values of η were less than 0.4. These values were determined from observations of net radiation and surface temperature on clear nights when the wind speed was above 5 m s^{-1} (i.e., when the ASBL was present at the surface). The values of η obtained from these observations did not vary substantially between seasons. Thus, η is regarded as a constant at each site. The value of η was found to be identical (i.e., 0.23) at both CR18 and El Reno. Thus, it can be assumed that sub-mesoscale variations of η are negligible.

The near-linear nature of Equation 5.8 is qualitatively consistent with the linear cooling rates observed within the ASBL (e.g., Fig. 4.7; Fig. 4.8; Fig. 4.11; Fig. 4.12). Thus, it can be concluded that Equation 5.8 provides an acceptable approximation of the ASBL temperature.

The model assumes that the temperature of the ASBL is constant with height. Within the USL, it is assumed that heat is transferred only by radiation and conduction. Initial model runs and comparison of modeled net radiation with observed net radiation at the Micronet suggest this is a valid assumption. It follows that the modeled lapse rate

within the USL is nearly linear, which is consistent with Micronet observations (not shown).

The temperature within the CIL is a function of the ASBL mixing parameter (μ), which ranges from 0 at the top of the USL to 1 at the bottom of the ASBL. If the USL is present at the surface, the variation of μ within the CIL is unknown and is complicated by the horizontally inhomogeneous nature of the CIL (Chapter 2). The model's prediction in this case is limited to the average temperature within the CIL, which is only used in the calculation of net radiation (Eqn. 5.3). Though the model does not explicitly predict temperature profiles, a schematic profile may be constructed from the model output (Fig. 5.2).

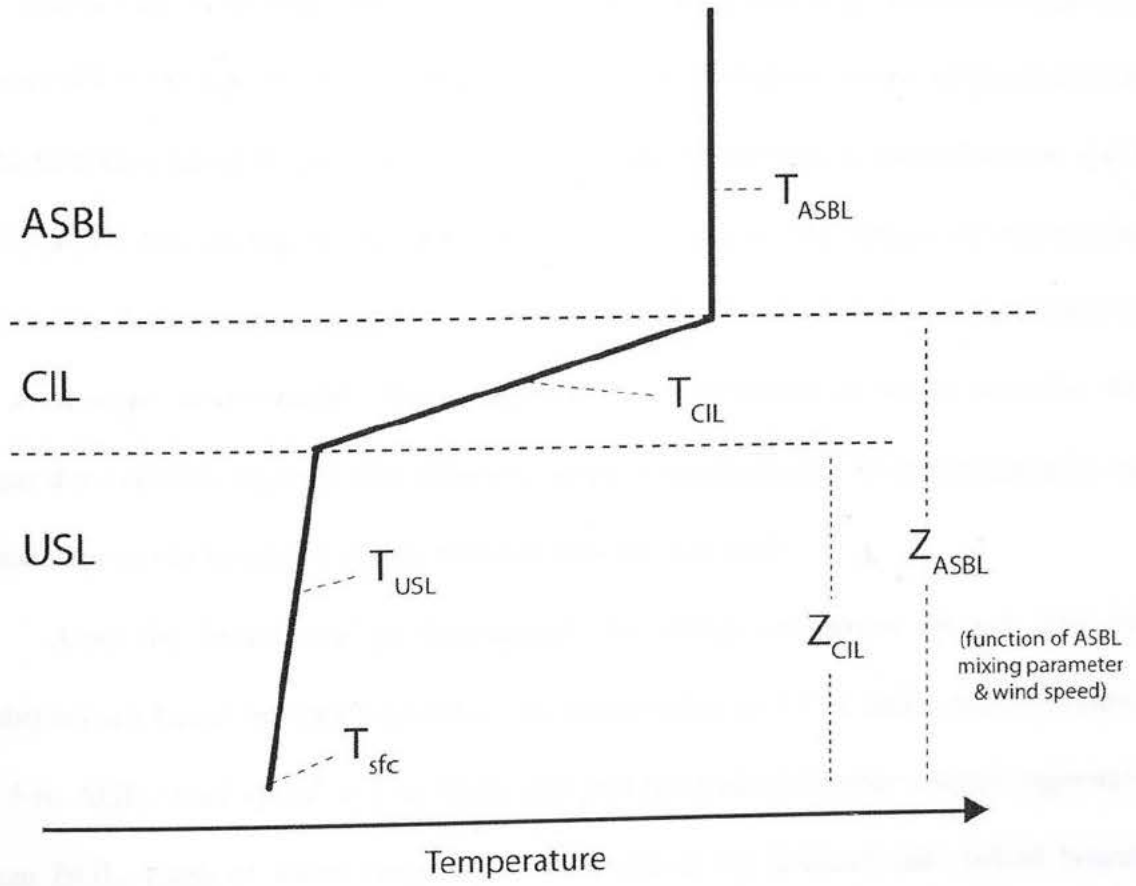

Figure 5.2. Schematic temperature profile based on model output.

A disadvantage to this approach is that the model's usefulness is limited at heights more than 10 m above the ground. However, this disadvantage is eliminated when forecasts are confined to the temperature at 1.5 m AGL. To forecast temperature profiles well above the surface (i.e., within the ASBL), the model may be coupled with a conventional turbulence-based boundary layer model using the ASBL temperature as a lower boundary condition.

5.2. Model Procedure

The first step of the model procedure is to determine the model's initial time (Fig. 5.3). Rather than beginning the first time step at a fixed time (e.g., 0000 UTC) as occurs in most NWP models, the initial time is set to be shortly before sunset when stratification of the boundary layer is approximately neutral. The sunset time is determined by the date and location. Initializing the model at this time minimizes the impact of microclimatic features on the initial observations to help ensure the observations are representative of the mesoscale environment. This approach also provides a more realistic initial temperature profile, because the observed surface temperatures are approximately equal to those above the height at which observations are acquired.

After the initial time is determined, the initial conditions are set. The initial conditions are based on four variables: air temperature at 1.5 m AGL, relative humidity at 1.5 m AGL, wind speed at 2 m AGL, and soil temperature under natural vegetation at 10 cm BGL. Each of these variables is observed at the forecast site. Initial boundary conditions are provided by observations of the mesoscale environment. These

observations include air temperature at 1.5 m AGL, relative humidity at 1.5 m AGL, and wind speed at 2 m AGL at stations that surround the forecast site. The mesoscale environment is assumed to remain constant throughout the night (i.e., constant wind speed and no advection of relatively warm or cool air).

After the model is initialized, net radiation is calculated from the initial conditions (Fig. 5.2) using Equation 5.3. Ground heat flux is then calculated using equations 5.6 and 5.7. Next, the ASBL mixing parameter and ASBL temperature are calculated, which are used to determine sensible heat flux at the surface. The ASBL mixing parameter is calculated from the initial wind speed (Eqn. 5.6), while the sensible heat flux is estimated using equations 5.8 and 5.9. Finally, a new surface temperature is calculated using Equation 5.2. If the new surface temperature is lower than the surface dewpoint, the surface dewpoint is set to equal the surface temperature. The next time step begins by calculating net radiation and the process is repeated. The duration of each time step is 300 seconds (5 minutes).

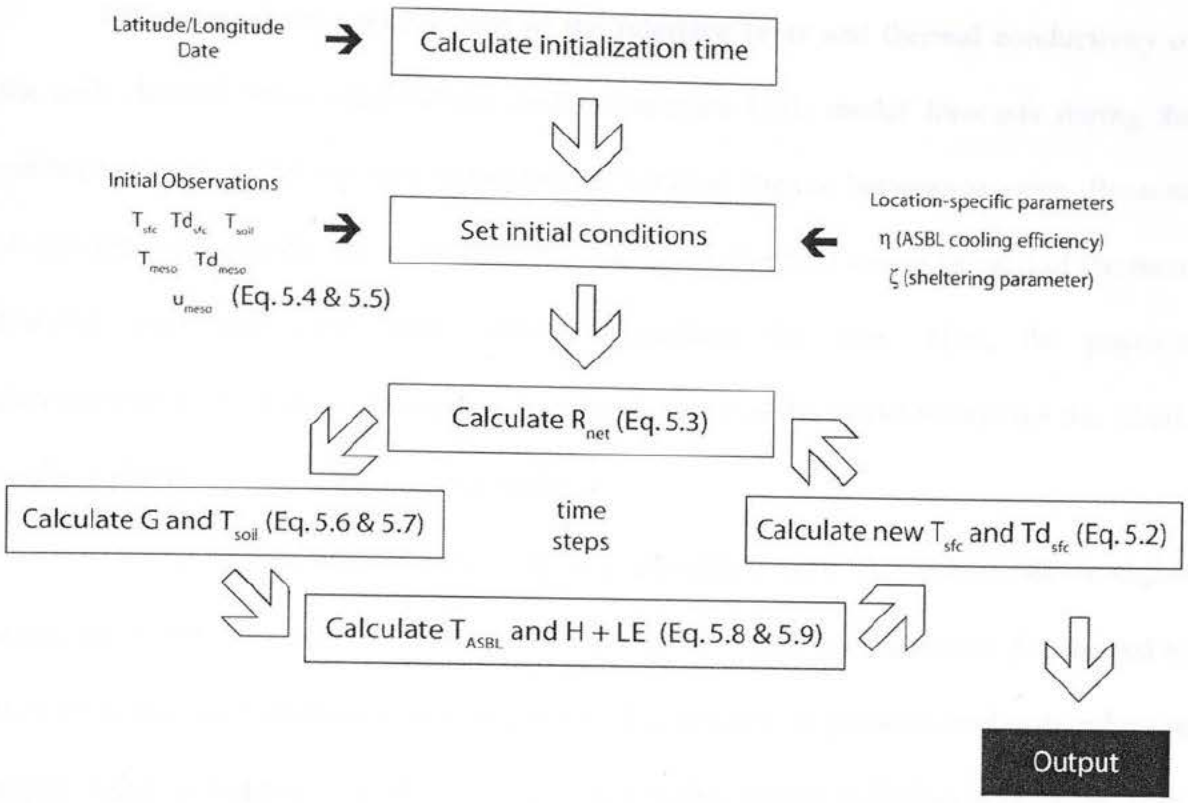

Figure 5.3. Flowchart of model procedure

5.3. Location-specific Parameters

The model initially was designed to forecast for the Crosstimber Micronet. However, adjustment of a few parameters allows it to forecast for other locations as well. These location-specific parameters include latitude and longitude, specific heat of the surface, thermal conductivity of the soil, ASBL cooling efficiency, sheltering parameter, and initial mesoscale conditions.

The location-specific parameters for each site were determined when the model was calibrated using observations from June-December 2004. During the calibration process, the parameters were adjusted (i.e., incrementally changed) to minimize the root-mean-square (RMS) forecast error.

Estimates of the specific heat of the interface layer and thermal conductivity of the soil, derived from observations and preliminary USL model forecasts during the calibration period, did not vary substantially between sites or between seasons. Because of this lack of variation, these parameters were given identical values at each of the three forecast sites and were held constant throughout the year. Thus, the physical characteristics of the three forecast sites were identical in the model except for the ASBL cooling efficiency and sheltering parameter.

The ASBL cooling efficiency (η) was calculated from the cooling rate on nights when the ASBL was present (i.e., nights with strong wind). Its value was determined to be 0.23 at the two Oklahoma locations and 0.38 at Madera. A possible explanation for the higher value at Madera is its location in a large valley, where radiation is expected to be more effective at cooling the ASBL than across central Oklahoma.

The sheltering parameter was determined to be 10.0 at CR18, 1.6 at El Reno, and 1.1 at Madera. These values were determined by comparing overnight wind speeds at the forecasts sites with corresponding wind observations from surrounding stations, then adjusting the observation-derived values to minimize the forecast error.

The initial mesoscale conditions were provided by stations that surround each forecast site. At CR18, these conditions were given as the mean across the five surrounding Mesonet sites: Byars, Norman, Shawnee, Spencer, and Washington (Fig. 5.1a). At El Reno, they were given as the mean across four surrounding Mesonet sites: Hinton, Kingfisher, Minco, and Spencer. At Madera, they were given as the mean across four surrounding CIMIS sites: Firebaugh, Fresno, Merced, and Westlands (Fig. 5.1b).

6. Modeling Results

Proposition 5 states that a forecast model which represents the uncoupled surface layer (i.e., the USL model described in Chapter 5) will produce on clear nights better temperature forecasts than concurrent forecasts from operational Model Output Statistics (MOS). To test this proposition, forecasts by the USL model were compared with corresponding forecasts by MOS generated from output by the Aviation (AVN) model. AVN MOS is an established forecasting tool that has been used successfully for decades and is widely used today (Taylor and Leslie 2005). Thus, it serves as an excellent benchmark to evaluate the skill of the USL model.

The AVN MOS forecasts used for the comparison were generated from the model cycle at 0000 UTC. They included 6-, 9-, and 12-hour forecasts valid at 0600, 0900, and 1200 UTC, respectively. These forecasts were compared with USL model forecasts valid at the same times. The USL model forecasts were generated from initial conditions shortly before sunset.

The forecast error is defined as the root-mean-square (RMS) difference between the model forecasts and observed temperatures at 0600, 0900, and 1200 UTC. The RMS difference was chosen because it "penalizes" large errors more than does the mean absolute difference.

The forecast bias is defined as the mean difference between the model forecasts and observed temperatures at 0600, 0900, and 1200 UTC. On days when sunrise occurred before 1200 UTC at the two Oklahoma stations, only forecasts valid at 0600 and 0900 UTC were used to calculate the forecast error at those stations.

USL model forecasts for each forecast site were compared with AVN MOS forecasts valid at airports nearest to the three forecast sites. For CR18, the nearest AVN MOS site was Max Westheimer Airport (KOUN) in Norman, located 28 km west-northwest of CR18. Forecasts for El Reno were compared with MOS forecasts for Wiley Post Airport (KPWA) in Bethany, which is located 36 km east of El Reno. AVN MOS forecasts for Madera were generated for the Madera Municipal Airport (KMAE), which is located 9 km southeast of the Madera CIMIS site.

6.1. Calibration period

Observations on clear nights from June-December 2004 were used to calibrate the USL model. The model's forecast output was compared with the archived observations. Then the parameters of the model, which initially were "first guess" estimates, were adjusted to minimize the forecast error and bias.

After the parameter values were determined empirically, the model was frozen (i.e., parameter values were permanently fixed). The model was then used to forecast temperatures for clear nights during the calibration period of June-December 2004. The results were recorded and compared with AVN MOS forecasts for the same nights.

During the calibration period, forecasts by the USL model were (on average) 59% more accurate than those by AVN MOS at CR18 (Table 6.1).

	AVN MOS (KOUN)		USL model (CR18)		Error difference	
Month	Error	Bias	Error	Bias	°C	%
June	2.61°C	+2.57°C	1.32°C	-1.07°C	-1.29	-49.4
July	3.70	+3.70	0.72	-0.41	-2.98	-80.5
August	3.05	+3.05	1.15	-0.38	-1.9	-62.3

September	5.34	+5.34	1.60	+0.39	-3.74	-70.0
October	6.34	+5.51	1.69	-0.20	-4.65	-73.3
November	3.36	+2.79	1.51	+0.16	-1.85	-55.1
December	5.06	+4.81	3.85	+1.5	-1.21	-23.9
Total	4.25	+4.12	1.74	+0.06	-2.51	-59.1

Table 6.1. Forecast error and bias (°C) for forecasts by AVN MOS and the USL model for the Crosstimber Micronet site CR18. Forecasts were valid at 0600, 0900, and 1200 UTC on clear nights from June-December 2004.

A slight cool bias was observed in the USL model forecasts during warm season months and a slight warm bias was observed during cool season months. These biases may be a result of the model's assumption that the surface properties remained constant throughout the year. The large (i.e., > 4°C) warm bias by AVN MOS reflected the unique location of CR18. Because CR18 was consistently cooler than KOUN on clear nights, AVN MOS forecasts designed for KOUN were consistently too warm.

A similar result occurred at El Reno, which is more sheltered than KPWA (Table 6.2). AVN MOS forecasts were approximately 2°C too warm. The forecast error of the USL model was 1.15°C, approximately 1°C better than AVN MOS.

	AVN MOS (KPWA)		USL model (ELRE)		Error difference	
Month	Error	Bias	Error	Bias	°C	%
June	1.47°C	+1.42°C	0.96°C	-0.01°C	-0.51	-34.7
July	1.43	+1.43	0.60	-0.16	-0.83	-58.0
August	1.65	+1.55	0.58	0.17	-1.07	-64.8
September	2.48	+2.47	1.04	+0.01	-1.44	-58.1
October	3.78	+3.59	1.99	+0.37	-1.79	-47.4
November	0.90	+0.90	1.09	+0.53	+0.19	+21.1
December	2.61	+2.51	2.15	+0.22	-0.46	-17.6
Total	2.11	+2.05	1.15	+0.08	-0.96	-45.5

Table 6.2. Forecast error and bias (°C) for forecasts by AVN MOS and the USL model for the Oklahoma Mesonet station at El Reno, Oklahoma. Forecasts were valid at 0600, 0900, and 1200 UTC on clear nights from June-December 2004.

AVN MOS forecasts for the Madera Municipal Airport were 1.31°C too warm at the nearby Madera CIMIS site (Table 6.3). The USL model produced a 39.4% improvement in accuracy with a mean forecast error of 0.86°C.

	AVN MOS (KMAE)		USL model (Madera)		Error difference	
Month	Error	Bias	Error	Bias	°C	%
June	1.12°C	+0.97°C	0.81°C	-0.31°C	-0.31	-27.7
July	1.25	+1.14	1.08	-0.42	-0.17	-13.6
August	1.43	+1.41	0.70	+0.23	-0.73	-51.0
September	1.70	+1.46	0.87	-0.17	-0.83	-48.8
October	1.54	+1.36	0.78	-0.04	-0.76	-49.4
November	1.77	+1.76	0.78	+0.28	-0.99	-55.9
December	1.94	+1.91	1.07	+0.5	-0.87	-44.8
Total	1.42	+1.31	0.86	-0.09	-0.56	-39.4

Table 6.3. Forecast error and bias (°C) for forecasts by AVN MOS and the USL model for the CIMIS station at Madera, California. Forecasts were valid at 0600, 0900, and 1200 UTC on clear nights from June-December 2004.

6.2. Sensitivity to Parameters

To determine the sensitivity of the USL model to various parameters, the parameters were perturbed by given percentages (e.g., +/- 25%) or by given values (e.g., +/- 0.01). New temperature forecasts were generated for the calibration period to determine the impact of the perturbations. The sensitivity of the model to the following

parameters was tested: ASBL cooling efficiency (η), sheltering parameter (ζ), specific heat of the surface (c), and thermal conductivity of the soil (k_{soil}).

Forecasts for El Reno and Madera were more sensitive to the ASBL cooling efficiency than for CR18 (Table 6.4). This result is consistent with observations of the presence of the ASBL at these sites. At El Reno and Madera the ASBL is commonly observed at 1.5 m above ground level (AGL) because these sites are exposed to the wind. Thus, changes to the cooling rate of the ASBL (via the ASBL cooling efficiency) have a relatively large impact on the near-surface temperature at those sites. But at CR18, the presence of the ASBL at 1.5 m AGL is relatively rare. Thus, changes to the ASBL cooling rate have a relatively small impact on the near-surface temperature forecasts at CR18.

ASBL cooling efficiency (η)

	CR18 ΔError		El Reno ΔError		Madera ΔError	
$\Delta\eta$	°C	%	°C	%	°C	%
+ 0.01	0.00	0.0	0.00	0.0	0.01	1.2
+ 0.05	0.01	0.6	0.07	6.1	0.21	24.4
+ 0.10	0.04	2.3	0.28	24.3	0.69	80.2
+ 0.20	0.21	12.1	1.01	87.8	1.95	226.7
- 0.01	0.01	0.6	0.01	0.9	0.01	1.2
- 0.05	0.05	2.9	0.12	10.4	0.19	22.1
- 0.10	0.13	7.5	0.41	35.7	0.64	74.4
- 0.20	0.40	23.0	1.26	109.6	1.94	225.6

Table 6.4. Sensitivity of the USL model forecast error to perturbations of the ASBL cooling efficiency (η) on clear nights from June-December 2004.

The model was less sensitive to the sheltering parameter than to the ASBL cooling efficiency (Table 6.5).

Sheltering parameter (ζ)

	CR18 ΔError		El Reno ΔError		Madera ΔError	
$\Delta\zeta$	°C	%	°C	%	°C	%
+ 2.0	0.01	0.6	0.05	4.3	0.02	2.3
+ 5.0	0.09	5.2	0.21	18.3	0.22	25.6
+ 100%	0.30	17.2	0.03	2.6	0.00	0.0
+ 200%	0.48	27.6	0.09	7.8	0.03	3.5
- 1.0	0.01	0.6	0.01	0.9	0.02	2.3
- 2.0	0.06	3.4	0.37	32.2	0.34	39.5
- 50%	0.23	13.2	0.01	0.9	0.01	1.2
- 90%	0.66	37.9	0.02	1.7	0.02	2.3

Table 6.5. Sensitivity of the USL model forecast error to perturbations of the sheltering parameter (ζ) on clear nights from June-December 2004.

Perturbations to the sheltering parameter simulated the impact of increased or reduced wind speed at the forecast site. Increases to the sheltering parameter reduced the wind speed, which resulted in temperature forecasts that were too cold. These forecasts were too cold because the model underestimated the impact of entrainment of relatively warm air from the ASBL (i.e., sensible heat flux). Decreases to the sheltering parameter increased the wind speed, which created a warm bias in the USL model.

The forecast error was not substantially affected by decreases to the specific heat of the "surface" (where the "surface" is defined as a layer containing soil and air; Table 6.6). These decreases mostly affected the temperature within the first few hours after sunset, because the temperature during those hours is especially sensitive to the properties of the surface (Gustavsson et al. 1988; Simonsen 2001). The error at 0600, 0900, and 1200 UTC was more sensitive to increases to the specific heat of the surface. These increases created a warm bias because the modeled cooling occurred too slowly. In other words, the modeled surface was 'retaining' its warmth longer into the night. This

was especially true of CR18 and Madera, which have a larger diurnal temperature range than El Reno (not shown). A high specific heat of the surface reduces the diurnal temperature range by raising the minimum temperatures. Hence, the errors created by these perturbations were highest at CR18 and Madera.

Specific heat of "surface" (c)

	CR18 ΔError		El Reno ΔError		Madera ΔError	
Δc	°C	%	°C	%	°C	%
+ 10%	0.02	1.1	0.00	0.0	0.00	0.0
+ 50%	0.16	9.2	0.00	0.0	0.06	7.0
+ 100%	0.39	22.4	0.03	2.6	0.24	27.9
+ 200%	0.86	49.4	0.16	13.9	0.80	93.0
- 10%	0.00	0.0	0.00	0.0	0.00	0.0
- 25%	-0.01	-0.6	0.00	0.0	0.02	2.3
- 50%	0.01	0.6	0.00	0.0	0.04	4.7
- 90%	0.03	1.7	0.00	0.0	0.08	9.3

Table 6.6. Sensitivity of the USL model forecast error to perturbations of the specific heat of the "surface" (c) on clear nights from June-December 2004.

Perturbations to the thermal conductivity of the soil (k_{soil}) had a minimal impact on the forecast error (Table 6.7). In the USL model, k_{soil} is only used for the calculation of ground heat flux. Ground heat flux is a relatively minor factor in the surface energy balance (i.e., compared to sensible heat flux). Thus, it is not surprising that perturbations to k_{soil} and their associated impact on ground heat flux had a relatively small impact on near-surface air temperature forecasts.

Thermal conductivity of soil (k_{soil})

	CR18 ΔError		El Reno ΔError		Madera ΔError	
Δk_{soil}	°C	%	°C	%	°C	%

+ 10%	0.01	0.6	0.00	0.0	0.00	0.0
+ 50%	0.02	1.1	0.00	0.0	0.00	0.0
+ 100%	0.03	1.7	0.00	0.0	0.00	0.0
+ 200%	0.04	2.3	0.00	0.0	0.00	0.0
- 10%	0.00	0.0	0.00	0.0	0.00	0.0
- 25%	-0.01	-0.6	0.00	0.0	0.00	0.0
- 50%	-0.02	-1.1	0.01	0.9	0.01	1.2
- 90%	0.07	4.0	0.07	6.1	0.07	8.1

Table 6.7. Sensitivity of the USL model forecast error to perturbations of the thermal conductivity of the soil on clear nights from June-December 2004.

This result suggests that soil properties such as soil moisture have a relatively small impact on nighttime temperatures. It has been shown that nighttime cooling occurs more rapidly at locations with dry soils than at locations with moist soils (Oke 1978, 43-45; Elsner et al. 1996). But because the impact of soil properties is relatively small compared to other factors (e.g., sheltering), it is not surprising that such rapid cooling occurs (contrary to intuition) at CR18 where the soil is extremely moist during the entire year (not shown). The lower cooling rates observed at adjacent Mesonet sites, where the soil usually is drier than at CR18, confirms that the impact of soil moisture is relatively small.

The result is encouraging from a larger perspective, because soil moisture is not observed at many meteorological stations and is difficult to estimate accurately. However, it should be noted that mesoscale soil properties likely have an impact on the ASBL cooling efficiency, a parameter to which the USL model is more sensitive. Thus, mesoscale soil properties should be considered even though microscale variations of these properties can be neglected in the USL model.

The sensitivity analysis revealed that the most important site-specific parameters were the ASBL cooling efficiency (η) and the sheltering parameter (ζ). These parameters also were the easiest to estimate. The identical values of η found at CR18 and El Reno (i.e., 0.23) suggest that its microscale variation is minimal. The value of ζ, which can vary substantially on the microscale, can easily be estimated from knowledge of the mean wind speed at the forecast site and surrounding sites. For areas that lack meteorological observations, high-resolution maps of vegetation and terrain may be used to estimate ζ. These estimates can be achieved by analyzing the impact of similar land features at sites that do have wind observations. It can be assumed that hills and trees of a particular height and density have a consistent, measurable impact on the wind speed that is independent of the geographic region. Portable anemometers also could be used as an alternative method or to supplement the estimates from high-resolution maps. The moderate sensitivity of the USL model to the sheltering parameter suggests that rough estimates (i.e., within 50% of the actual value) of this parameter are sufficient to produce nighttime temperature forecasts that are more accurate than MOS (Tables 6.1-6.3; Table 6.5).

6.3. Sensitivity to Initial Conditions

A similar process was used to determine the model's sensitivity to the initial conditions. Sensitivity to the following initial conditions was tested: mesoscale wind speed at 2 m AGL, soil temperature at 0.1 m BGL, air temperature at 1.5 m AGL, and dewpoint at 1.5 m AGL.

The sensitivity of the model's forecast accuracy to the initial mesoscale wind speed illustrates the importance of the model's discrimination between the energy balances of the ASBL, CIL, and USL (Table 6.8). The El Reno and Madera sites were more sensitive to negative perturbations of the initial mesoscale wind speed (i.e., reduced wind speed) than to positive perturbations (i.e., increased wind speed). This finding reflects the relative dominance of the ASBL at those sites. In other words, the ABSL usually is a dominant feature at El Reno and Madera. A reduction of the wind speed in simulated model conditions allows the USL or CIL to develop near the surface in the model. The resulting surface energy balance creates conditions that are too cold near the surface. But with an increased wind speed at these sites, the modeled ASBL remains at the surface. Thus, the surface energy balance does not change enough to significantly affect the near-surface temperature.

Initial mesoscale wind speed (u_{meso})

	CR18 ΔError		El Reno ΔError		Madera ΔError	
Δu_{meso}	°C	%	°C	%	°C	%
+ 10%	0.01	0.6	0.01	0.9	0.01	1.2
+ 50%	0.17	9.9	0.06	5.2	0.06	7.0
+ 100%	0.32	18.4	0.12	10.4	0.13	15.1
+ 200%	0.57	32.8	0.22	19.1	0.24	27.9
- 10%	0.01	0.6	-0.01	-0.9	0.00	0.0
- 25%	0.06	3.4	0.00	0.0	0.02	2.3
- 50%	0.32	18.4	0.13	11.3	0.18	20.9
- 90%	0.57	32.8	1.66	144.3	1.98	230.2

Table 6.8. Sensitivity of the USL model forecast error to perturbations of the initial mesoscale wind speed (u_{meso}) at 2 m AGL on clear nights from June-December 2004.

At El Reno, a 10% reduction to the initial mesoscale wind speed decreased the error. This suggests that the value of the sheltering parameter at El Reno derived from observations during June-December 2004 may be too small. Hence, a decreased wind speed, which could be accomplished by an increase to the sheltering parameter, led to a slight improvement in forecast accuracy. However, this improvement was extremely small (i.e., less than 1%).

The impact of perturbations to the initial soil temperature was minimal (Table 6.7). Perturbations of +/- 5°C increased the forecast error by only 0.04-0.24°C (1.7-13.8%).

Initial soil temperature (T_{soil})

	CR18 ΔError		El Reno ΔError		Madera ΔError	
ΔT_{soil} (°C)	°C	%	°C	%	°C	%
+ 1.0	0.03	1.7	0.00	0.0	0.01	1.2
+ 2.0	0.07	4.0	0.01	0.9	0.02	2.3
+ 3.0	0.11	6.3	0.02	1.7	0.03	3.5
+ 5.0	0.24	13.8	0.04	3.5	0.06	7.0
- 1.00	0.00	0.0	0.00	0.0	0.00	0.0
- 2.0	0.00	0.0	0.00	0.0	0.00	0.0
- 3.0	0.03	0.0	0.00	0.0	0.01	1.2
- 5.0	0.13	1.7	0.02	1.7	0.04	4.7

Table 6.9. Sensitivity of the USL model forecast error to perturbations of the initial soil temperature (T_{soil}) at 0.1 m BGL on clear nights from June-December 2004.

The low sensitivity to initial soil temperature is encouraging because soil temperature varies significantly on the microscale (not shown) and is not measured by some meteorological stations. This result appears to contradict other studies that suggest forecast models require accurate soil temperature conditions to properly partition the

surface heat fluxes (e.g., Godfrey 2006). However, those studies generally are not focused on nighttime conditions.

The sensitivity of the forecast error to the initial air temperature (at both the forecast site and the surrounding sites) was relatively large, especially at El Reno and Madera (Table 6.10). This sensitivity is not surprising because the initial temperature determines the initial net radiation, which is a key component in the calculation of temperature at the next time step. If the initial temperature is too warm, the model overestimates the incoming (i.e., from the air to the ground) longwave radiation. Thus, the value of net radiation at 1.5 m is too small and the associated cooling rate is too low. The result is an overestimate of the near-surface temperature. If the initial temperature is too cool, the model underestimates the incoming longwave radiation at the ground, which creates a cool bias in the temperature forecast.

Initial air temperature (at forecast site and surrounding sites)

	CR18 ΔError		El Reno ΔError		Madera ΔError	
ΔT_0 (°C)	°C	%	°C	%	°C	%
+ 0.5	0.03	1.7	0.05	4.3	0.07	8.1
+ 1.0	0.10	5.7	0.18	15.7	0.26	30.2
+ 2.0	0.32	18.4	0.59	51.3	0.87	101.2
+ 3.0	0.63	36.2	1.15	100.0	1.63	189.5
- 0.5	0.03	1.7	0.02	1.7	0.07	8.1
- 1.0	0.11	6.3	0.11	9.6	0.29	33.7
- 2.0	0.38	21.8	0.48	41.7	0.97	112.8
- 3.0	0.77	44.3	1.02	88.7	1.80	209.3

Table 6.10. Sensitivity of the USL model forecast error to perturbations of the initial temperature at 1.5 m AGL on clear nights from June-December 2004.

The largest increases in the error were observed at Madera, while relatively small increases were observed at CR18 and El Reno. This result reflects the relatively high ASBL cooling efficiency (i.e., 0.38) at Madera, which makes the ASBL temperature more sensitive to changes in net radiation than at CR18 and El Reno (which have an ASBL cooling efficiency of 0.23).

The initial dewpoint impacts net radiation by determining the emissivity of air. If the initial dewpoint is too high, the emissivity (and thus, the incoming longwave radiation from the air to the ground) is overestimated, which creates a warm bias in the temperature forecast. Likewise, if the initial dewpoint is too low, the temperature forecast by the USL model is too cold.

The sensitivity of the USL model to perturbations to the initial dewpoint was relatively small (Table 6.11). A +/- 2°C perturbation to the initial dewpoint increased the forecast error by only 0.00-0.03°C (0-4%). Even with initial dewpoint perturbations of +/- 5°C, the USL model's forecast error only increased by 0.04-0.17°C (2-20%).

Initial dewpoint (at forecast site and surrounding sites)

	CR18 ΔError		El Reno ΔError		Madera ΔError	
ΔT_d (°C)	°C	%	°C	%	°C	%
+ 1.0	0.01	0.6	0.00	0.0	0.01	1.2
+ 2.0	0.03	1.7	0.01	0.9	0.03	3.5
+ 3.0	0.05	2.9	0.03	2.6	0.06	7.0
+ 5.0	0.07	4.0	0.06	5.2	0.16	18.6
- 1.0	0.00	0.0	0.00	0.0	0.01	1.2
- 2.0	0.00	0.0	0.00	0.0	0.02	2.3
- 3.0	0.01	0.6	0.01	0.9	0.06	7.0
- 5.0	0.04	2.3	0.05	4.3	0.17	19.8

Table 6.11. Sensitivity of the USL model forecast error to perturbations of the initial dewpoint at 1.5 m AGL on clear nights from June-December 2004.

The largest increases in forecast error were observed at Madera, which is consistent with the relatively high ASBL cooling efficiency there. Like the initial temperature, the initial dewpoint primarily impacts the net radiation at the surface, to which the ASBL cooling rate (regulated by the ASBL cooling efficiency) is especially sensitive (Eqn. 5.8).

To forecast for areas that lack meteorological observations, the initial conditions must be estimated. Thus, the sensitivity of the USL model to errors in these initial conditions is extremely important to the potential accuracy of the model in these areas.

To forecast temperatures more than 12 hours in advance, the conditions at sunset must be forecasted using another model and supplied to the USL model as initial conditions. If the larger-model forecasts are perfect, the accuracy of the USL model would be the same as for the 12-hour forecasts documented in this study. In practice, perfect forecasts of the conditions at sunset are not possible. Thus, errors will exist in the initial conditions supplied to the USL model. It follows that the sensitivity of the USL model to these errors (especially those of temperature) determines the model's ability to predict temperatures more than 12 hours in advance.

6.4. Forecasts for the June-December 2005 Test Period

A completely independent dataset, June-December 2005, was used to test the USL model's real forecast skill. During the test period from June-December 2005, 104 nights (49%) were classified as clear at CR18 and El Reno, and 154 (72%) were

classified as clear at Madera. Observations from these nights were used to verify the model forecasts. Because the USL model was frozen after its calibration using observations from 2004, the test represented real forecast situations during 2005.

Like during the 2004 calibration period, a seasonal bias at CR18 was observed for the test period (Table 6.12). The forecasts were too cool from June-September and too warm from October-December. However, the mean bias across the entire period was near-zero. Forecasts by the USL model were approximately 4°C (72%) better than those by AVN MOS at CR18.

	AVN MOS (KOUN)		USL model (CR18)		Error difference	
Month	Error	Bias	Error	Bias	°C	%
June	4.68°C	+4.68°C	0.92°C	-0.77°C	-3.72	-80.3
July	4.07	+4.07	0.88	-0.85	-3.19	-78.4
August	3.91	+3.91	1.15	-0.78	-2.76	-70.6
September	5.66	+5.66	1.14	-0.05	-4.52	-79.9
October	7.29	+7.29	1.97	+0.54	-5.32	-73.0
November	8.34	+8.25	3.67	+1.46	-4.67	-56.0
December	8.03	+8.03	2.61	+1.89	-5.42	-67.5
Total	5.71	5.70	1.59	+0.02	-4.12	-72.2

Table 6.12. Forecast error and bias (°C) for forecasts by AVN MOS and the USL model for the Crosstimber Micronet site CR18. Forecasts were valid at 0600, 0900, and 1200 UTC on clear nights from June-December 2005.

Forecasts by the USL model were more accurate at El Reno than at CR18, but the improvement over AVN MOS was smaller (Table 6.13). This result reflects the relatively small error by AVN MOS at El Reno compared to that at CR18. It also suggests that El Reno is an easier site for which to forecast, probably because of the relatively infrequent

presence of the USL and CIL at El Reno (not shown). The forecast error by the USL model was 1.19°C, which was 1.5°C (56%) lower than that by AVN MOS.

	AVN MOS (KPWA)		USL model (ELRE)		Error difference	
Month	Error	Bias	Error	Bias	°C	%
June	2.24°C	+2.24°C	0.63°C	-0.46°C	-1.61	-71.9
July	2.55	+2.55	0.90	-0.07	-1.65	-64.7
August	2.01	+2.01	0.64	-0.07	-1.37	-68.2
September	2.61	+2.61	0.69	-0.11	-1.92	-73.6
October	3.52	+3.52	1.53	-0.72	-1.99	-56.5
November	3.27	+2.88	2.28	-1.22	-0.99	-30.3
December	2.61	+2.39	2.30	-1.42	-0.31	-11.9
Total	2.69	+2.62	1.19	-0.50	-1.50	-55.8

Table 6.13. Forecast error and bias (°C) for forecasts by AVN MOS and the USL model for the Oklahoma Mesonet station at El Reno, Oklahoma. Forecasts were valid at 0600, 0900, and 1200 UTC on clear nights from June-December 2005.

The forecast error by the USL model at Madera was less than 1°C, and was 46% better than that by AVN MOS (Table 6.14). During July-August, when most nights were clear at Madera, the USL model error was less than 0.7°C.

	AVN MOS (KMAE)		USL model (Madera)		Error difference	
Month	Error	Bias	Error	Bias	°C	%
June	1.43°C	+0.76°C	0.94°C	-0.68	-0.49	-34.3
July	1.54	+1.21	0.62	-0.04	-0.92	-59.7
August	1.75	+1.41	0.66	+0.12	-1.09	-62.3
September	1.39	+0.72	0.79	-0.31	-0.60	-43.2
October	1.77	+1.46	1.14	-0.12	-0.63	-35.6
November	2.68	+2.44	1.78	+1.32	-0.90	-33.6
December	2.32	+2.08	1.21	-0.33	-1.11	-47.8
Total	1.73	+1.30	0.93	-0.06	-0.80	-46.2

Table 6.14. Forecast error and bias (°C) for forecasts by AVN MOS and the USL model for the CIMIS station at Madera, California. Forecasts were valid at 0600, 0900, and 1200 UTC on clear nights from June-December 2005.

The relatively high accuracy of USL model forecasts at Madera compared to those at CR18 and El Reno can be attributed to synoptic-scale weather conditions. Overnight advection of warm or cool air is known to be much more substantial across central Oklahoma than across central California. Neglecting advection in the USL model makes the model less accurate in areas where advection is significant (i.e., CR18 and El Reno). Furthermore, wind observations (not shown) suggest that the USL model's assumption of a constant overnight wind speed is most valid at Madera (where the smallest forecast errors were observed) and least valid at CR18 (where the largest forecast errors were observed).

Surprisingly, the USL model demonstrated greater improvements over AVN MOS during 2005 than during the 2004 calibration period. During each calendar month from June-December of 2005, the USL model forecasts for each of the forecast sites were more accurate than those by AVN MOS by 12-80%. The consistent accuracy of the USL model during 2004 and 2005 suggests that seasonal and annual weather variations have a minimal impact on the accuracy of USL model forecasts on clear nights. Thus, similar results can be expected during other seasons and years.

6.5. Lack of Mesoscale Observations

Unlike CR18, El Reno, and Madera, some areas are not surrounded by meteorological stations. In coastal areas (e.g., Santa Barbara and Santa Monica, CA), meteorological observations generally are not available offshore. In narrow valleys (e.g., Bishop, Cuyama and Morgan Hill, CA), the available mesoscale observations may not be representative of the valley floor. In remote desert areas (e.g., Barstow and Bishop, CA), only synoptic-scale meteorological observations may be available.

Because these observational limitations are so common, the USL model was tested at other sites without initializing the model with observations from surrounding sites. Instead, it was assumed that the initial conditions (i.e., the conditions observed shortly before sunset) at each forecast site were representative of the mesoscale environment. Using only these observations at the forecast site as initial conditions, the USL model was tested for the following forecast sites (i.e., CIMIS stations) during the period June-December of 2005: Barstow, Bishop, Cuyama, Morgan Hill, Santa Barbara, and Santa Monica, California (Fig. 6.1; Table 6.15). This diverse selection of sites includes coastal locations, desert locations, flat locations, and narrow valleys.

Figure 6.1. Map of central and southern California showing forecast sites: Barstow, Bishop, Cuyama, Morgan Hill, Santa Barbara, and Santa Monica.

Forecast Site	Description	AVN MOS	Clear Nights
Barstow	Desert. Relatively flat land.	Dagget (KDAG) 21 km E of CIMIS site	145 (68%)
Bishop	Desert. Deep, narrow valley.	Bishop (KBIH) 4 km NE	115 (54%)
Cuyama	Agricultural. Narrow inland valley.	Santa Maria (KSMX) 93 km W	131 (61%)
Morgan Hill	Suburban. Narrow coastal valley.	*San Jose (KSJC) 39 km NW	65 (30%)
Santa Barbara	Coastal. Mountains toward the north.	Santa Barbara (KSBA) 11 km W	75 (35%)
Santa Monica	Coastal, urban, relatively flat. Hills toward the north.	Santa Monica (KSMO) 4 km SE	53 (25%)

* Though coastal Watsonville (KWVI) is slightly closer, the climate of San Jose (KSJC) is more representative of that at Morgan Hill.

Table 6.15. Description of forecasts sites for USL model runs without use of observations at surrounding stations.

Like the previous cases, the USL model was calibrated using observations from June-December 2004. Then the model was frozen and tested using CIMIS observations from clear nights during June-December 2005.

At the six forecast sites, the average forecast error by the USL model was 1.24°C, which was 0.79°C (36.9%) lower than that by AVN MOS (Table 6.16).

Site	AVN MOS		USL model		Error difference	
	Error	Bias	Error	Bias	°C	%
Barstow	2.03°C	+1.63°C	1.12°C	+0.28	-0.91	-44.9
Bishop	2.38	+1.83	1.87	-0.14	-0.51	-21.4
Cuyama	2.74	-1.26	0.91	-0.35	-1.83	-66.8
Morgan Hill	1.72	+1.14	1.34	-0.23	-0.38	-22.2
Santa Barbara	1.72	-0.94	1.06	-0.43	-0.66	-38.4
Santa Monica	1.62	-0.03	1.16	-0.50	-0.46	-27.9
Average	2.04	+0.40	1.24	-0.29	-0.79	-36.9

Table 6.16. Forecast error and bias (°C) for forecasts by AVN MOS and the USL model for six CIMIS stations across central and southern California. Forecasts were valid at 0600, 0900, and 1200 UTC on clear nights from June-December 2005.

Of the six forecast sites, the most accurate forecasts by the USL model (and largest improvement over AVN MOS) were observed at Cuyama. Cuyama is located in the Cuyama Valley, an isolated valley between the Caliente and Sierra Madre mountain ranges. The terrain of the Cuyama Valley is considered very favorable for development of the USL. Thus, the accuracy of USL model forecasts there is not surprising.

The most surprising result was from Santa Monica, a relatively flat coastal location that is not particularly favorable for development of the USL. The forecast bias by AVN MOS was near-zero, which suggests that conditions at the Santa Monica airport

(KSMO) are well-representative of conditions at the nearby CIMIS site. Despite a relatively large (i.e., 0.5°C) bias by the USL model, its forecasts were approximately 0.5°C (28%) more accurate than those by AVN MOS. This result suggests that even at airports for which MOS was designed, including those in areas considered unfavorable for development of the USL, the USL model is likely to produce better clear-night temperature forecasts than does MOS.

The 9 sites used in this study represent an extremely wide variety of vegetation and terrain. The consistent results of the USL model across such diverse regions suggest that the model is likely to yield forecasts of similar accuracy in other parts of the world.

6.6. Unsteady Mesoscale Environment

The previous results were based on model runs that assumed the wind speed was constant throughout the night and advection did not occur. The forecasts can be improved if the mesoscale conditions during the night are forecast via an operational mesoscale NWP model or MOS guidance.

The USL model was adjusted to incorporate observations of the wind speed throughout the night. This technique approximates the performance of the USL model if given a perfect wind speed forecast. The results of this "perfect prog" approach can be used to estimate the potential accuracy of the USL model when given wind speed forecasts from an operational model or MOS.

When the mesoscale wind speed was known throughout the night, the forecast error by the USL model at CR18 was reduced from 1.59°C (Table 6.12) to 1.20°C. When

the wind speed at CR19 (located at 10 m AGL above CR18) was known, the error was reduced to 1.06°C, which was 4.65°C (81.4 %) lower than that by AVN MOS and 0.53°C (33.3%) lower than the USL model with the assumption of constant overnight wind speed

With this modification, the USL model appears to accurately represent the phenomena that create the nighttime temperature fluctuations observed at the Crosstimber Micronet (Fig. 6.2).

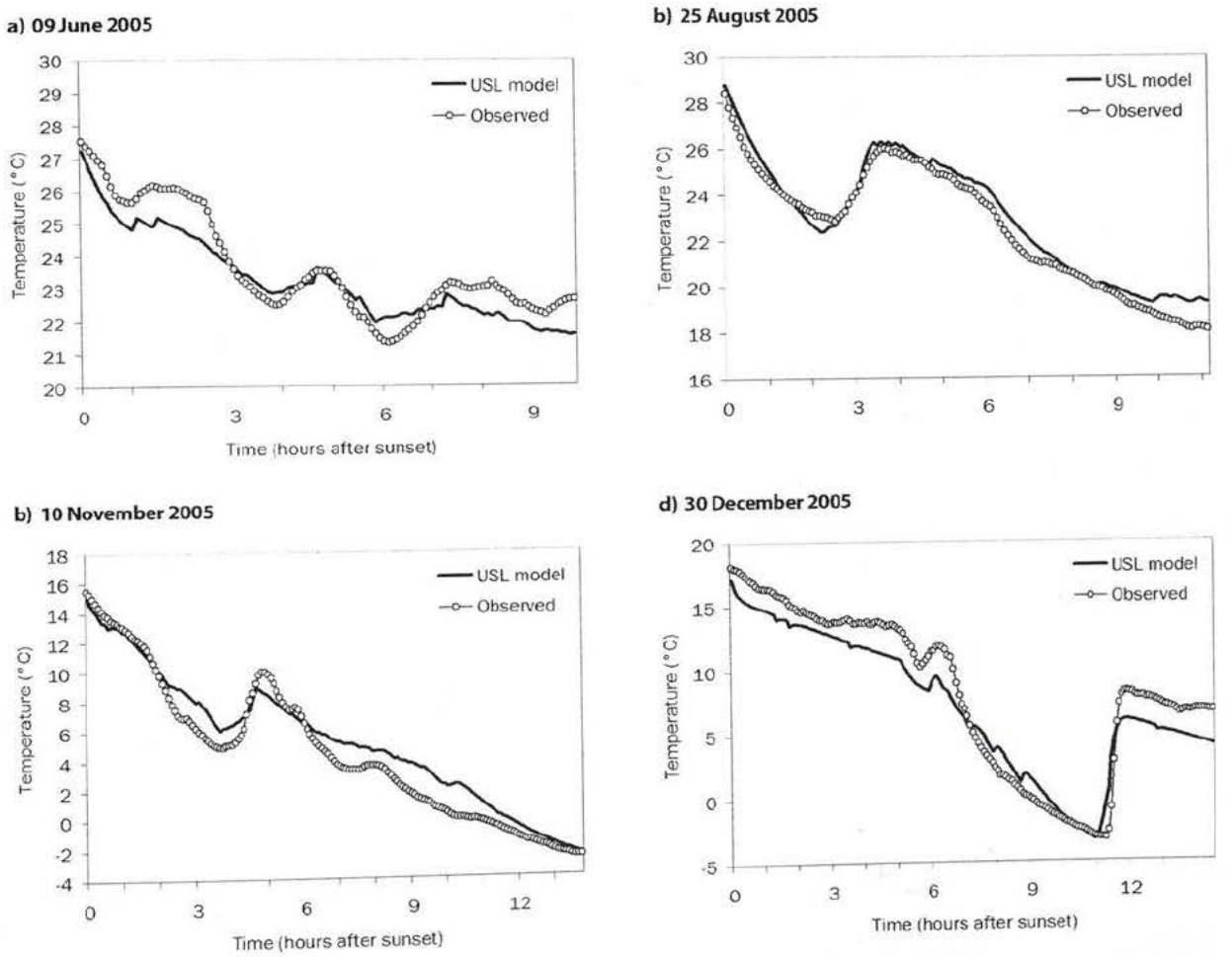

Figure 6.2. USL model forecasts and observations of the temperature (°C) at CR18 on selected clear nights.

Therefore, based on these model results, it appears that all propositions of this work have been validated by the model's ability to improve substantially on the best operational forecasts available.

7. Conclusions

Using observations from the Crosstimber Micronet, it was shown that an uncoupled turbulence-free layer of air (i.e., the uncoupled surface layer; USL) develops near the ground on clear nights. The unique surface energy balance within the USL was shown to create cool nighttime temperature anomalies at the Micronet. The surrounding Oklahoma Mesonet sites, where the USL usually did not develop, were considerably (i.e., up to 13°C) warmer.

The presence and depth of the USL at the Micronet were shown to be closely related to the wind speed across central Oklahoma. On clear nights with mesoscale wind speeds below 2.5 m s^{-1}, the USL usually developed across the entire Micronet. Thus, temperatures across the Micronet were substantially cooler than at the surrounding Mesonet sites, but the temperature variation within the Micronet was relatively small.

At mesoscale wind speeds between 2.5-5 m s^{-1}, the USL developed across the lower elevations of the Micronet but not across the higher elevations. It was on these nights that the largest microscale temperature gradients (i.e., > 10°C across less than 200 m of land) were observed. When the mesoscale wind speed was above 5 m s^{-1}, the USL generally did not develop at the Micronet. Thus, on those windy nights, spatial temperature variations across the Micronet and between the Micronet and surrounding Mesonet sites were virtually non-existent.

The impact of the USL also was evidenced by observations of dewpoint and CO_2 concentration. The thermodynamic stability and lack of turbulence within the USL allowed water vapor and CO_2 to accumulate near the surface shortly after sunset. Along

with the observations of wind speed, these secondary observations helped confirm that the USL, rather than other processes such as cold air drainage, is responsible for the unique phenomena observed at the Crosstimber Micronet.

The Uncoupled Surface Layer (USL) model was developed according to the framework for the nocturnal boundary layer described in Chapter 2. The physical basis of the USL model is the surface energy budget. Temperatures are predicted via calculations involving components of the surface energy budget. These components are calculated using empirical parameterizations derived from Crosstimber Micronet observations. Based on the scientific literature, it appears the USL model is a 'first of its kind'.

The USL model was designed to forecast temperatures at 1.5 m above ground level from sunset to sunrise on clear nights. Forecasts were generated for the CR18 Micronet site, the El Reno, Oklahoma Mesonet site, and the Madera, California CIMIS site. Similar forecasts were generated for six other CIMIS sites across diverse regions of central and southern California.

The model was calibrated using observations from June-December 2004 and was tested and verified using observations from clear nights during June-December 2005 (104 nights at CR18 and El Reno and 154 nights at Madera). Forecasts by the USL model were compared with forecasts by MOS, a forecasting technique that has been well-respected and widely used for decades. The MOS forecasts were generated from AVN model output for airports nearest to the Micronet, Mesonet, and CIMIS sites.

At CR18, the average (root-mean-square) forecast error by the USL model was 1.59°C, which was 4.12°C lower than that by AVN MOS for Norman, Oklahoma (KOUN). This corresponds to a 72% improvement in forecast accuracy.

At El Reno and Madera, the average forecast error was even smaller (i.e., 1.19°C at El Reno and 0.93°C at Madera). These errors were 56% lower than those by AVN MOS at El Reno and 46% lower at Madera. The result at Madera is noteworthy because the Madera CIMIS site is located on relatively flat terrain and only 9 km from the airport for which the MOS forecasts were generated. This spatial relationship suggests that the improvements by the USL model over AVN MOS were not strictly the result of MOS failing to be representative of the area surrounding Madera.

The USL model also generated more accurate forecasts for sites in California that were not surrounded by meteorological stations. At these sites, which included two coastal locations, two desert locations, and two inland valley locations, the USL model's forecasts were 21-67% more accurate than those by AVN MOS. Two of these forecast sites were less than 5 km from the airport for which the MOS forecasts were generated. The consistent accuracy of the USL model in these diverse areas suggests that it would likely produce forecasts of similar accuracy across the United States and in other parts of the world.

The results are remarkable considering that the USL model did not account for advection or changes in the mesoscale wind speed throughout the night. When the current wind speed at CR18 was known by the model (i.e., in a 'perfect prog' scenario), its forecast error was reduced by 33%. Though perfect forecasts of the overnight wind speed are not possible, even rough estimates would likely improve the accuracy of the USL model's temperature forecasts. The inclusion of advection in the model also would likely improve its accuracy. These improvements could be achieved by coupling the USL model with a mesoscale NWP model or MOS guidance.

Unlike statistical forecasting techniques (e.g., MOS), the USL model is physically-based. The physically-based technique is immune to many of the disadvantages of MOS. For example, MOS forecasts are partly based on observations from airports or other standard observing sites. As the results of this study illustrate, the MOS locations may not represent the broader areas for which the MOS forecasts are applied. On the other hand, forecasts by the USL model are not limited to airports or standard observing sites.

While MOS requires a long-term archive of observations (i.e., several years or more), the USL model was calibrated using only 7 months of observations. The calibration was primarily used to determine two parameters: the ASBL cooling efficiency and the sheltering factor. If these parameters are estimated from high-resolution maps of vegetation and terrain, the USL model could forecast for virtually anywhere. In addition to the improved accuracy, the resolution of these forecasts could be orders of magnitude finer than that of today's operational forecasting techniques.

The simplicity of the USL model is a major advantage. A 12-hour temperature forecast for a single site requires less than one second of computational time by a personal computer. Thus, large forecast domains with extremely high spatial and temporal resolution are possible.

Another advantage of the USL model is that it may be coupled with any model that can provide mesoscale boundary conditions. Unlike MOS, which requires a frozen model (e.g., AVN and NGM) for consistent forecasts, the USL model can generate near-surface temperature forecasts based on output by evolving operational models (e.g., ETA), mesoscale research models (e.g., MM5, WRF, ARPS, and RAMS), ensemble

models, or models designed for other countries. Such a coupling could significantly improve the accuracy of short and medium-range near-surface nighttime temperature forecasts around the world.

The applications and benefits of improved nighttime temperature forecasts are broad. These improvements would be of considerable value to the energy industry, especially natural gas utilities (Roebber and Bosart 1996). The agriculture industry would benefit from improved frost and freeze forecasts, which would help mitigate damage to crops.

Public safety also would benefit through improved warnings and response to hazardous travel conditions such as fog and black ice on roadways. Nighttime temperature forecasts are critical to road salting operations (Collins and Roulston 2004). Forecasts of radiation fog, which is closely related to the temperature on clear nights, also could be improved by better temperature forecasts. Increased resolution of these forecasts could help alert motorists about areas where roadways will be particularly foggy or icy.

The largest benefits of the USL model would likely be in sheltered areas where the climate differs significantly from that of the nearest airport (e.g., the Crosstimber Micronet, El Reno, and Cuyama). Large benefits also are likely in countries that lack MOS forecasts or dedicated meteorological forecast offices.

The challenge of forecasting temperatures on clear nights may not be as difficult as once believed. Observations from the Crosstimber Micronet have provided considerable insight into the structure and dynamics of the near-surface nocturnal boundary layer. The results of this study suggest that the USL model, based on these

microscale observations, has the potential to revolutionize and dramatically improve forecasting of near-surface temperatures on clear nights.

Therefore, the five propositions of Chapter 1 are confirmed. In addition, the USL model represents a new approach to generalized temperature forecasting that, heretofore, has not been documented in the scientific literature.

References

Acevedo, O. C., and D. R. Fitzjarrald, 2001: The early evening surface-layer transition: Temporal and spatial variability. *J. Atmos. Sci.*, **58**, 2650–2667.

Beljaars, A. C. M. and A. M. Holtslag, 1991. Flux parameterization over land surfaces for atmospheric models. *J. Appl. Met.*, **30**, 327-341.

Berdahl, P., and R. Fromberg, 1982. "The Thermal Radiance of Clear Skies" Solar Energy, **29**(4), pp 299-314.

Blackadar, A. K., 1976: Modeling the nocturnal boundary layer. Preprints, *Third Symp. on Atmospheric Turbulence, Diffusion, and Air Quality,* Raleigh, NC, Amer. Meteor. Soc., 46-49.

Brock, F. V., K. C. Crawford, R. L. Elliott, G. W. Cuperus, S. J. Stadler, H. L. Johnson, and M. D. Eilts, 1995: The Oklahoma Mesonet: a technical overview. *J. Atmos. Oceanic. Technol.*, **12** , 5-19.

Busch, N. E., Chang, S. C., and Anthes, R. A. (1976). A multi-level model of the planetary boundary layer suitable for use with mesoscale dynamic models. *J. Appl. Met.*, **15**(9), 909-919.

Businger, J. A., J. C. Wyngaard, Y. Izumi, and E. F. Bradley, 1971: Flux profile relationships in the atmospheric surface layer. *J. Atmos. Sci.*, **28,** 181–189.

Businger, J. A., 1973: Turbulent transfer in the atmospheric surface layer. *Workshop on Micrometeorology,* D. H. Haugen, Ed., Amer. Meteor. Soc., 67–100.

Chen, B. et al., 1991. Determination of the Clear Sky Emissivity For Use In Cool Storage Roof and Roof Pond Applications, ASES proceedings, Denver, CO.

CIMIS, 2005: California irrigation management and information system—Data reports. California Department of Water Resources. [Available online at www.cimis.water.ca.gov].

Clark and Allen, 1985. Assessment of Passive Cooling Rates and Application in the U.S., DOE Contract DE-AC03-TIC31600.

Clements, C. B., C. D. Whiteman and J. D. Horel. 2003: Cold-Air-Pool Structure and Evolution in a Mountain Basin: Peter Sinks, Utah. *J. Appl. Meteorol.*: **42**, 752–768.

Deardorff, J. W., 1978: Efficient prediction of ground surface temperature and moisture with inclusion of a layer of vegetation. *J. Geophys. Res.*, **93,** 1889-1903.

Derbyshire, S. H., 1990: Nieuwstadt's stable boundary layers revisited. *Quart. J. Roy. Meteor. Soc.*, **116**, 127–158.

Derbyshire, S. H., 1994: A "balance" approach to stable boundary layer dynamics. *J. Atmos. Sci.*, **51**, 3486–3504.

Elsner, J. B., H. E. Fuelberg, R. L. Deal, J. A. Orrock, G. S. Lehmiller, and P. H. 1996: Tallahassee, Florida, minimum temperature anomaly: Description and speculations. *Bull. Amer. Meteor. Soc.*: **77**, 721–728.

Fiebrich, C. A. and K. C. Crawford, 2001: The impact of unique meteorological phenomena detected by the Oklahoma Mesonet and ARS Micronet on automated quality control. *Bull. Amer. Meteor. Soc.*: **82**, 2173-2187.

Fleagle, R. G., 1950: A theory of air drainage. *J. Meteor.*, **7**, 227–232.

Funk, J. P., 1960: Measured radiative flux divergence near the ground at night. *Quart. J. Roy. Meteor. Soc.*, **86**, 382-389.

Garratt, J. R., 1992: *The Atmospheric Boundary Layer*. Cambridge University Press, 316 pp.

Garratt, J. R. and R. A. Brost, 1981. Radiative Cooling Effects within and above the Nocturnal Boundary Layer. *J. Atmos. Sci.*, **38**, 2730-2746.

Geiger, R., 1965: *The Climate Near the Ground.* Harvard University Press, 482 pp.

Godfrey, C. M., 2006: Soil temperature and moisture errors in Eta model analyses. Preprints, *18th Conf. on Clim. Var. and Change,* Atlanta, GA, Amer. Meteor. Soc.

Gross, G., 1987: Some effects of deforestation on nocturnal drainage flow and local climate—A numerical study. *Bound.-Layer Meteor.*, **38,** 315–337.

Gustavsson, T., M. Karlsson, J. Bogren and S. Lindqvist. 1998: Development of temperature patterns during clear nights. *J. Appl. Meteorol.*: **37**, 559–571.

Harrison, A. A., 1971: A discussion of the temperatures of inland Kent with particular reference to night minima in the lowlands. *Meteor. Mag.*, **100**, 97–110.

Haugland, M. J. and K. C. Crawford: The diurnal cycle of land-atmosphere interactions across Oklahoma's Winter Wheat Belt. *Mon. Wea. Rev.*, **133**(1), 120-130.

Hobbs, B. F., et al., 1999. *Analysis of the Value for Unit Commitment Decisions of Improved Load Forecasts*. IEEE Transactions on Power Systems, **14**(4), 1342-1348.

Holden, J. J., S. H. Derbyshire, and S. E. Belcher, 2000: Tethered balloon observations of the nocturnal stable boundary layer in a valley. *Bound.-Layer Meteor.*, **97**, 1–24.

Holtslag, A. A. M., and Nieuwstadt F. T. M., 1986: Scaling the atmospheric boundary layer. *Bound.-Layer Meteor.*, **36**, 201–209.

Hunt, E., J. B. Basara, and C. Morgan, 2005: Significant Inversions and Rapid In-Situ Cooling at a Well-Sited Oklahoma Mesonet Station. *J. Appl. Meteor.*, in review.

Kalma, J. D., G. P. Laughlin, A. A. Green, and M. T. O'Brien, 1986: Minimum temperature surveys based on near-surface air-temperature measurements and airborne thermal scanner data. *J. Climatol.*, **6,** 413–430.

Kara, A. Birol, J. B. Elsner and P. H. Ruscher. 1998: Physical Mechanism for the Tallahassee, Florida, Minimum Temperature Anomaly. *J. Appl. Meteorol.*: **37**, 101–113.

Klein, R. and R. A. Pielke Jr., 2002: Bad Weather? Then Sue the Weatherman! *Bull. Amer. Met. Soc.*: **83**(12), 1801-1807.

Kondo, J., O. Kanechika and N. Yasuda. 1978: Heat and Momentum Transfers under Strong Stability in the Atmospheric Surface Layer. *J. Atmos. Sci.*: **35**, 1012–1021.

Kondo, J., Kuwagata T., and Haginoya S., 1989: Heat budget analysis of nocturnal cooling and daytime heating in a basin. *J. Atmos. Sci.*, **46**, 2917–2933.

Laughlin, G. P. amd J. D. Kalma, 1987. Frost hazard assessment from local weather and terrain data. *Agric. For. Meteorol.*: **40**: 1–16.

Laughlin, G. P. and J. D. Kalma, 1990. Frost risk mapping for landscape planning: a methodology. *Theor. & Appl. Clim.*: 42: 41-51.

LeMone, M. A., K. Ikeda, R. L. Grossman, and M. W. Rotach. 2003: Horizontal Variability of 2-m Temperature at Night during CASES-97. *J. Atmos. Sci.s*: **60**, 2431–2449.

Louis, J. F., 1979: A parametric model of vertical eddy fluxes in the atmosphere. *Bound.-Layer Meteor.*, **17**, 187–202.

Lyons, R., H. A. Panofsky and S. Wollaston. 1964: The Critical Richardson Number and Its Implications for Forecast Problems. *J. Appl. Meteorol.*: **3**, 136–142.

Mahrt, L., J. Sun, W. Blumen, A. Delany, G. McClean and S. Oncley, 1998: Nocturnal boundary-layer regimes. *Bound.-Layer Meteor.*, **88**, 255-278.

Mahrt, L., D. Vickers, R. Nakamura, J. Sun, S. Burns, D. Lenschow *and* M. Soler, 2001. Shallow drainage and gully flows. *Boundary-Layer Meteorol.*, **101**, 243-260.

Maki, M., Harimaya T., and Kikuchi K., 1986: Heat budget studies on nocturnal cooling in a basin. *J. Meteor. Soc. Japan.*, **64**, 727–740.

Maki, M., and T. Harimaya, 1988: The effect of advection and accumulation of downslope cold air on nocturnal cooling in basins. *J. Meteor. Soc. Japan.*, **66**, 581–597.

Malhi, Y. S., 1995: The significance of the dual solutions for heat fluxes measured by the temperature fluctuation method in stable conditions. *Bound.-Layer Meteor.*, **74**, 389–396.

Martin, M. and P. Berdahl. 1984. "Characteristics of Infrared Sky Radiation in the United States," Solar Energy, Vol. 33, pp. 321-326.

Mason, P. J., 1987: Diurnal variations in flow over a succession of ridges and valleys. *Quart. J. Roy. Meteor. Soc.*, **113**, 1117–1140.

Monin, A. S., and A. M. Obukhov, 1954: Basic laws of turbulent mixing in the surface layer of the atmosphere (in Russian). *Tr. Geofiz. Inst., Akad. Nauk SSSR*, **24**, 1963-1967.

National Diurnal Climatology, The, 2004: Haugland, M. J. [Available online at www.microclimates.org/diurnal].

Norwine, J. R., 1973: Heat Island Properties of an Enclosed Multi-Level Suburban Shopping Center. *Bull. Amer. Meteor. Soc.*: **54**, 637–641.

NRC, 1998: *The Atmospheric Sciences: Entering the Twenty-First Century*. National Academy Press, 364 pp.

Ohya, Y. D., Tatuno, M., Nakamura, Y., and Ueda, H.: 1996, A Thermally Stratified Wind Tunnel for Environmental Flow Studies, *Atmos. Environ.* **30**, 2881–2887.

Ohya, Y. D., E. Neff, and R. N. Merone, 1997: Turbulence structure in a stratified boundary layer under stable conditions. *Bound.-Layer Meteor.*, **83**, 139–161.

Oke, T. R., 1978: *Boundary Layer Climates*. Methuen (Halsted Press), 372 pp.

Poulos, G. S., W. Blumen, D. C. Fritts, J. K. Lundquist, J. Sun, S. P. Burns, C. Nappo, R. Banta, R. Newsom, J. Cuxart, E. Terradellas, B. Balsley and M. Jensen. 2002: CASES-99: A Comprehensive Investigation of the Stable Nocturnal Boundary Layer. *Bull. Amer. Meteor. Soc.*: **83**, 555–581.

Prata, A. J., 1996: A new long-wave formula estimating downward clear-sky radiation at the surface. Quart.J. R. Meteor. Soc., 122, 1127-1151.

Revelle, D. O., 1993: Chaos and "bursting" in the planetary boundary layer. *J. Appl. Meteor.*, **32**, 1169–1180.

Roebber, P. J., and L. F. Bosart, 1996: The contributions of education and experience to forecast skill. *Wea. Forecasting.*, **11**, 21-40.

Rosenberg, N. J., 1974. Microclimate: The biological environment. John Wiley & Sons. New York.

Sellers, P. J., Y. Mintz, Y. C. Sud, and A. Dalcher, 1986: A simple biosphere model (SiB) for sure within general circulation models. *J. Atmos. Sci.*, **43**, 505-531.

Shafer, M. A., C. A. Fiebrich, D. S. Arndt, S. E. Fredrickson and T. W. Hughes. 2000: Quality Assurance Procedures in the Oklahoma Mesonetwork. *J. Atmos. Oceanic Technol.*: **17**, 474–494.

Simonsen, Troy K., 2001: The meso-scale influence of terrain on the nocturnal variation of temperature in the Little Washita Watershed. M.S. Thesis, University of Oklahoma, 95 pp.

Skidmore, E.L. (1986). Wind erosion control. Climatic Change, **9**, 209-218.

Smedman, A. S., 1988: Observations of a multi-level turbulence structure in a very stable atmospheric boundary layer. *Bound.-Layer Meteor.*, **44**, 231–253.

Stull, R. B., 1988: *An Introduction to Boundary Layer Meteorology*. Kluwer, 670 pp.

Taylor, A. A. and L. M. Leslie. 2005: A Single-Station Approach to Model Output Statistics Temperature Forecast Error Assessment. *Weather and Forecasting,* **20**(6), 1006–1020.

The Ancient Cross Timbers Consortium, 2005: University of Arkansas. [Available online at www.uark.edu/misc/xtimber].

Thompson, B. W., 1986: Small-scale katabatics and cold hollows. *Weather,* **41,** 146–153.

Tremback, C. J., and R. Kessler, 1985: A surface temperature and moisture parameterization for use in mesoscale numerical models. Preprints, *Seventh Conf. on Numerical Weather Prediction,* Montreal, PQ, Canada, Amer. Meteor. Soc., 355-358.

Tribble, A., 2003: The relationship between weather variables and electricity demand to improve short-term load forecasting. *Ph.D. Dissertation*, University of Oklahoma, 221 pp.

Van de Wiel, B. J. H., R. J. Ronda, A. F. Moene, H. A. R. De Bruin, and A. A. M. Holtslag, 2002a: Intermittent turbulence and oscillations in the stable boundary layer over land. Part I: A bulk model. *J. Atmos. Sci.*, **59**, 942–958.

Van de Wiel, B. J. H., A. F. Moene, R. J. Ronda, H. A. R. De Bruin and A. A. M. Holtslag. 2002b: Intermittent Turbulence and Oscillations in the Stable Boundary Layer over Land. Part II: A System Dynamics Approach. *J. Atmos. Sci.*: **59**, 2567–2581.

Van de Wiel, B. J. H., A. F. Moene, O. K. Hartogensis, H. A. R. De Bruin and A. A. M. Holtslag. 2003: Intermittent Turbulence in the Stable Boundary Layer over Land. Part III: A Classification for Observations during CASES-99. *J. Atmos. Sci.*: **60**, 2509–2522.

Walton, G.N., *Thermal Analysis Research Program- Reference Manual*, NBSIR **83-2655**, U.S. Department of Commerce, March 1983, Update 1985.

Webb, E. K., 1970: Profile relationships, the log linear range, and extension to strong stability. *Quart. J. Roy. Meteor. Soc.*, **96,** 67–90.

Wetzel, P. J., 1978: A detailed parameterization of the atmospheric boundary layer. Ph.D. dissertation, Colorado State University, 195 pp. [Available from Dept. of Atmospheric Science, Colorado State University, Fort Collins, CO 80523.].

Whiffen, B., P. Delannoy, and S. Siok, 2002: Fog: Impact on Road Transportation & Mitigation Options. *National Highway Visibility Conference*.

Whiteman, C. D., 1990: Observations of thermally developed wind systems in mountainous terrain. *Atmospheric Processes over Complex Terrain, Meteor. Monogr.*, No. 45, Amer. Meteor. Soc., 5–42.

Whiteman, C. D., McKee T. B., and Doran J. C., 1996: Boundary layer evolution within a canyonland basin. Part I: Mass, heat, and moisture budgets from observations. *J. Appl. Meteor.*, **35**, 2145–2161.

Whiteman, C. D., Haiden, T., Pospichal, B., Eisenbach, S., Steinacker, R. 2004: Minimum Temperatures, Diurnal Temperature Ranges, and Temperature Inversions in Limestone Sinkholes of Different Sizes and Shapes. *J. Appl. Meteorol.*: **43**, No. 8, pp. 1224–1236.

Wong, Raymond K. W., K. D. Hage, and L. D. Phillips. 1987: The Numerical Simulation of Drainage Winds in a Small Urban Valley under Conditions with Supercritical Richardson Numbers. *J. Appl. Meteorol.*: **26**, 1447–1463.

Zdunkowski, Wilford G. and D. C. Trask. 1971: Application of a Radiative–Conductive Model to the Simulation of Nocturnal Temperature Changes over Different Soil Types. *J. Appl. Meteorol.*: **10**, 937–948.

Zilitinkevich, S. S., E. E. Fedorovich, and M. V. Shabalova, 1992: Numerical model of a nonsteady atmospheric planetary boundary layer, based on similarity theory. *Bound. Layer Meteor.*, **59**, 387-411